JAERI 1181
INDC-345

Evaluation of Thermal Neutron Scattering Cross Sections for Reactor Moderators

(Summary Report)

September 1969

日本原子力研究所

Japan Atomic Energy Research Institute

日本原子力研究所は，研究成果，調査結果などを JAERI レポートとして，つぎの4種に分けそれぞれの通し番号を付し，不定期に刊行しております．

1. 研究報告	まとまった研究の成果あるいはその一部における重要な結果の報告	JAERI 1001-
2. 調査報告	総説・展望・調査の結果などをまとめたもの	JAERI 4001-
3. 年　　報	研究・開発その他の活動状況などの報告	JAERI 5001-
4. 資　　料	施設の概要や手引きなど	JAERI 6001-

このうち既刊分については「JAERI レポート一覧」にタイトル・要旨をまとめて掲載し，また新刊レポートは「研究成果要旨集」（隔月刊）で逐次紹介しています．

これらのリスト・研究報告書の入手および複写・翻訳などのご要求は，日本原子力研究所技術情報部（茨城県那珂郡東海村）に申しこんでください．

Japan Atomic Energy Research Institute publishes the nonperiodical reports with the following classification numbers:

1. JAERI 1001-	Research reports
2. JAERI 4001-	Survey reports and reviews
3. JAERI 5001-	Annual reports
4. JAERI 6001-	Manuals etc.

Requests for the above publications, and reproduction and translation should be addressed to Division of Technical Information, Japan Atomic Energy Research Insitute, Tokai-mura,Naka-gun, Ibaraki-ken, Japan

編集兼発行　日本原子力研究所
印　　刷　学術図書印刷株式会社

Evaluation of Thermal Neutron Scattering Cross Sections for Reactor Moderators

Summary

This is a summary report of the evaluation work of thermal neutron scattering cross sections, which has been performed during the years from 1965 to 1968 by members of the thermalization group of Japanese Nuclear Data Committee. The report consists of three parts: general description, evaluation, and basic research works. The evaluation was aimed to be complete within the incoherent approximation. The studies and evaluations of the coherent effect, the multiple scattering correction, and other related problems are also included in the report as supplement.

December 1968

Thermalization Group*
Japanese Nuclear Data Committee
Japan Atomic Energy Research Institute

減速物質の熱中性子散乱断面積の評価

要　旨

本報告は日本原子力研究所シグマ研究委員会熱化グループにおいて，1965年～1968年に行なった熱中性子散乱断面積の評価作業の総合報告である．報告は一般的記述，評価，基礎的研究の３つの部分に分かれている．評価は非干渉近似の範囲で完全であることを目指している．干渉効果，多重散乱補正，その他の関連した諸問題についての研究，評価は補足として加えた．

1968年12月

日本原子力研究所
シグマ研究委員会
熱化グループ*

* Group Members: S. Iijima (Nippon Atomic Industry Group Co., Ltd.), Y. Nakahara (Japan Atomic Energy Research Institute), M. Izumi (Japan Atomic Energy Research Institute), I. Otake (Fuji Electric Co. Ltd.), T. Sekiya (Osaka University), M. Sakamoto (Japan Atomic Energy Research Institute), H. Kadotani (Tokyo Institute of Technology), N. Haga (Hitachi Ltd.), S. Ayao (Japan Atomic Energy Research Institute), T. Nishigori (Osaka University), A. Sugawara (Mitsubishi Atomic Power Industries Inc.)

Former Members: H. Takahashi (Brookhaven National Laboratory), Y. Goto (Japan Atomic Energy Research Institute, now at Brookhaven National Laboratory), K. Matsuoka (Hitachi Ltd.), S. Shimada (Mitsubishi Atomic Power Industries Inc.), H. Yamakoshi (Ship Research Institute), T. Maejima (Nippon Electric Co. Ltd.)

熱化グループ・メンバー：飯島俊吾（日本原子力事業），中原康明（日本原子力研究所），飯泉仁（日本原子力研究所），大竹巌（富士電機），関谷全（阪大），坂本正誠（日本原子力研究所），角谷浩亨（東工大），芳賀暢（日立），綾尾貞治（日本原子力研究所），錦織毅夫（阪大），菅原彬（三菱原子力）

旧メンバー：高橋博（ブルックヘブン国立研究所），後藤敏男（日本原子力研究所），松岡謙一（日立），嶋田昭一郎（三菱原子力），山越寿夫（船舶技研），前島享（日本電気）

Contents

目　次

- D_2O の酸素に対する σ_0 $(E_0 \rightarrow E)$
- D_2O の酸素に対する σ_1 $(E_0 \rightarrow E)$
- THERMOS 散乱核
  - H_2O
  - D_2O の D に対する TERMOS 散乱核
  - D_2O の O に対する TERMOS 散乱核
- UNCLE散乱核
  - グラファイト (1800°K)
  - グラファイト (室温)
  - ベリリウム (室温)

1. Introduction

The evaluation of thermal neutron scattering cross sections for neutron moderating materials has been the main research program organized by the Thermalization Group of Japanese Nuclear Data Committee. A number of codes have been made available for the evaluation purpose. Some of them have been programmed originally by members of the Thermalization Group and the others were kindly offered by several foreign authors.

One of the main purposes of the numerical analysis of thermal neutron scattering cross sections is to find the most appropriate frequency distribution or spectral density for lattice vibrations of crystals, molecular vibrations and rotations in solids and liquids, i.e., to determine the frequency distribution in the generalized sense which gives scattering laws, kernels, total scattering cross sections and other parameters related to the thermal neutron scattering in good agreement with experimental values. The other purpose is to provide standard sets of kernels and cross sections for reactor analysis.

Phenomenological frequency distributions for practical purposes have been determined from measured scattering laws by means of the well-known extrapolation and iteration technique on the scattering law. Physical quantities which can be calculated directly from frequency distributions given as input data for codes are listed below.

(1) Scattering law $S(\alpha, \beta)$
(2) Scattering kernel and its Legendre moments $\sigma_l(E_0 \to E)$, $(l=0, 1, 2, 3)$
(3) Total scattering cross section $\sigma_s(E)$
(4) Transport cross section $\sigma_{t,r}(E)$ and the mean cosine of scattering angle $\bar{\mu}(E)$
(5) Others (second moments, etc.)

Evaluated values of these quantities are given in Chapter 3. Frequency distributions are shown in the form of tables and figures. Some typical kernels are illustrated graphically and numerical values of full kernels are given in the form of the list of output cards from the codes. Scattering laws are shown in figures and compared with experimental values. The total scattering cross section, the transport cross section and $\bar{\mu}$ are given in tables and figures and are discussed in comparison with measurements.

Materials for which these quantities have been evaluated are light water, heavy water, graphite, beryllium, beryllium oxide and organic moderators. For light water and heavy water 30 energy point kernels for THERMOS, source spectrum and thermal neutron diffusion parameters have been calculated in addition to the quantities (1)—(5) listed above. The evaluation which was partially completed but not to the extent to cover the whole items of (1)-(5) is also included in the present report as the supplement to the evaluation of individual scattering materials.

Most of the experimental data on the scattering law or the double differential scattering cross section ever published contain some errors, resulting from the resolution and multiple scattering. The method of multiple scattering correction is explained in Section 2.3 and some applications are illustrated in Chapter 3. Numerical analysis based on the properly corrected experimental values has to be done and this work is certainly the next step in our evaluation program.

In Chapter 4 research works on thermal neutron scattering by our members which have not been introduced in Chapter 3 are presented as progress reports. These works are now in progress or almost completed. Their full descriptions will be published in journals.

2. General Description

2.1 Theoretical Consideration

Generalities

We write for the double differential scattering cross section of neutrons from monatomic substance,[1]

$$\frac{d^2\sigma}{d\Omega d\omega}=\frac{k}{k_0}\left[<a^2>S_s(\vec{\kappa},\omega)+<a>^2S_d(\vec{\kappa},\omega)\right] \tag{1}$$

$S(\vec{\kappa},\omega)$ and $\chi(\vec{\kappa},t)$ are, the scattering law and time correlation function (or the intermediate scattering function) respectively, defined by

$$S_s(\vec{\kappa},\omega)=\frac{1}{2\pi}\int_{-\infty}^{\infty}dte^{-i\omega t}\chi_s(\vec{\kappa},t) \tag{2}$$

$$S_d(\vec{\kappa},\omega)=\frac{1}{2\pi}\int_{-\infty}^{\infty}dte^{-i\omega t}\chi_d(\vec{\kappa},t) \tag{3}$$

$$\chi_s(\vec{\kappa},t)=<\frac{1}{N}\sum_i e^{-i\vec{\kappa}\cdot\vec{r}_i(0)}e^{i\vec{\kappa}\vec{r}_i(t)}>_T \tag{4}$$

$$\chi_d(\vec{\kappa},t)=<\frac{1}{N}\sum_{i\neq j}e^{-i\vec{\kappa}\vec{r}_i(0)}e^{i\vec{\kappa}\vec{r}_i(t)}>_T \tag{5}$$

The symbols used above and in the following are summarized below.

N=number of atoms or unit cells in the system,
$\vec{k}_0$, $\vec{k}$ =wave vectors of incident and scattered neutrons, respectively,
E_0, E=energies of incident and scattered neutrons, respectively,
$\vec{\kappa}=\vec{k}_0-\vec{k}$ =momentum transfer,
$\hbar\omega=E_0-E=\varepsilon$, energy transfer,
T=temperature of the system in energy unit,
$\alpha=\hbar^2\kappa^2/2MT$,
$\beta=(E_0-E)/T$,
M=the mass of scatterer atom,
$\sigma_b=4\pi<a^2>$; bound atom scattering cross section,
$\sigma_f=\sigma_b/\left(1+\frac{m}{M}\right)^2$; free atom scattering cross section,
$<a>$=bound atom coherent scattering amplitude,
$S_s(\vec{\kappa},\omega)$=self term of the scattering law,
$S_d(\vec{\kappa},\omega)$=distinct term of scattering law,
$\chi(\vec{\kappa},t)$=time correlation function or intermediated scattering function,
$r_i(t)$=position of the i-th atom of the system,
$<\cdots>_T$=thermal average over the states of scatterer system,
$\rho(\omega)$=the spectral density function or the generalized frequency distribution.

When molecules in the system are randomly oriented, $S(\vec{\kappa},\omega)$ is averaged over the direction $\vec{\kappa}$. In this case, $S(\alpha,\beta)$ defined by

$$S(\alpha,\beta)=\frac{T}{\hbar}e^{-\frac{\beta}{2}}S(|\vec{\kappa}|,\omega) \tag{6}$$

is used often. The conventional use of $S(\alpha,\beta)$ instead of $S(|\vec{\kappa}|,\omega)$ does not seem to be particularly convenient except for the case of free gas, since $S(\alpha,\beta)$ changes in rather complexed manner when temperature

varies.

Eq. (1) is applicable only to the nuclear part of the scattering. The assumptions underlying Eq. (1) are that (1) the two-body scattering in the center of mass system is independent of energy and isotropic, (2) Fermi's pseudo-potential and the first Born approximation can be used, and (3) nuclear spins are randomly oriented. These assumptions restrict the range of validity of Eq. (1). The second assumption above was investigated by NISHIGORI *et al.*[2]. They studied neutron propagation in a scatterer system quantum mechanically and showed that the correction to the use of the first Born approximation is of the order of magnitude of (nuclear scattering amplitude)/(atomic distance). So the correction will be quite negligible.

Main scattering quantities evaluated in the present report are, besides the scattering law, the total cross section, the transport cross section (or the average cosine of scattering angle) and the Legendre components of scattering kernel for $l=0$, 1, 2 and 3.

$$\sigma_t(E_0)=\int\sigma_0(E_0\to E)\,dE, \tag{7}$$

$$\sigma_{tr}(E_0)=\sigma_t(E_0)\,(1-\bar{\mu}(E_0)) \tag{8}$$

$$\bar{\mu}(E_0)=\int\sigma_1(E_0\to E)\,dE/\sigma_t(E_0) \tag{9}$$

$$\sigma_l(E_0\to E)=\int\frac{d^2\sigma}{d\Omega dE}P_l(\cos\theta)\,d\Omega \tag{10}$$

The neutron source spectrum, which is important for the calculation of thermal neutron spectrum, has also been calculated for light and heavy water. This is

$$S(E)=\int_{E_c}^{\infty}\sigma_0(E'\to E)\frac{dE'}{E'},\qquad E\le E_c \tag{11}$$

where E_c is the cut-off energy.

In reactor calculations, it is particularly important to predict the correct $\sigma_t(E)$ and $\bar{\mu}(E)$. When sharp peaks (including a narrow accoustical band) exist in the spectral density function, as is usually the case, the scattering kernel also exhibits the corresponding peaks, and these remain finite even at fairly high energy. Thus, the integration in Eq. (7) and Eq. (9) needs a great care.

The scattering law satisfy the well-known conditions for the detailed balance and the moment theorem. For monatomic system these are:

$$S(-\vec{\kappa},-\omega)=e^{-\frac{\hbar\omega}{T}}S(\vec{\kappa},\omega) \text{ for both } S_s(\vec{\kappa},\omega) \text{ and } S_d(\vec{\kappa},\omega) \tag{12}$$

$$\int_{-\infty}^{\infty}S_s(\vec{\kappa},\omega)\,d\omega=1 \tag{13}$$

$$\int_{-\infty}^{\infty}S_d(\vec{\kappa},\omega)\,d\omega=\sum_{i\neq j}\langle e^{-i\vec{\kappa}\,(\vec{r}_i-\vec{r}_j)}\rangle_T \tag{14}$$

$$\int_{-\infty}^{\infty}S_s(\vec{\kappa},\omega)\,\hbar\omega\,d\omega=R_0 \tag{15}$$

$$\int_{-\infty}^{\infty}S_d(\vec{\kappa},\omega)\,\hbar\omega\,d\omega=0 \tag{16}$$

Here $R_0=\hbar^2\kappa^2/2M$ is the free atom recoil energy. Eqs. (13) - (17) state that, at high energy, the distinct term of the scattering vanishes and the total scattering cross section as well as $\bar{\mu}$ (E) tend to those for free atom scattering. PLACZEK[3] derived the expressions for the higher moments when atoms move in a potential field. High energy cross section was expressed in terms of these moments as

$$\sigma_t(E_0)=\sigma_f\left(1+\frac{1}{3}\frac{m}{M}\frac{\langle K\rangle_T}{E_0}-\frac{1}{32}\hbar^2\frac{m}{M}\frac{\langle C\rangle_T}{E_0^3}+\cdots\cdots\right), \tag{17}$$

where K is the kinetic energy of atom, μ is the reduced mass and $C=\frac{\hbar^2}{3M}(\vec{\nabla}V)^2$. It is seen through the derivation of the above formula that the total cross section at high energy can take arbitrary value if the moment theorem is violated. The total scattering cross section at very low energy is simply proportional to $1/v$. In case of free gas, we can write

$$v\sigma_s(v)=\int|\vec{v}-\vec{V}|\,\sigma_s(v_r)P(\vec{V})\,d\vec{V} \tag{18}$$

where v_r is the relative velocity and $P(V)$ is the distribution function of velocity of target atom. The right hand side of the above equation becomes constant if $v \ll |\vec{V}|$

Spectral Density Function

The approximations usually employed in the calculation of scattering law are:

(a) the use of incoherent approximation except for the zero-phonon coherent elastic scattering,

(b) the Gaussian approximation for time correlation function, i. e.,

$$\chi_s(\kappa, t) = e^{-\kappa^2 w(t)} \tag{19}$$

where $w(t)$ is the width function given by (v is the velocity of atom)

$$w(t) = -i\frac{\hbar}{2M}t + \frac{1}{3}\int_0^t (t-t')\langle \vec{v}(o)\cdot\vec{v}(t')\rangle_T dt' \tag{20}$$

The real and imaginary part of the velocity correlation function are mutually related by fluctuation-dissipation theorem. This allows us to write, by defining the spectral density function as,

$$\rho(\omega) = \frac{4M}{3\pi\hbar}\frac{\hbar\omega}{\tanh\frac{\hbar\omega}{2T}}\int_0^\infty Re\langle \vec{v}(o)\cdot\vec{v}(t)\rangle_T \cos(\omega t)\,dt \tag{21}$$

that

$$w(t) = \frac{\hbar}{2M}(\gamma(o) - \gamma(t)) \tag{22}$$

where

$$\gamma(t) = \int_0^\infty \frac{\rho(\omega)}{\omega}\left[(n_\omega + 1)e^{i\omega t} + n_\omega e^{-i\omega t}\right] d\omega$$

$$n_\omega = \frac{1}{2}\left(\coth\frac{\hbar\omega}{2T} - 1\right)$$

$\rho(\omega)$ is shown to satisfy the normalization condition.

The approximation (a) is almost always a good approximation to calculate the integral scattering quantities of Eqs. (7)-(10). It is also expected to give the scattering law with reasonable accuracy when the structures due to coherent inelastic scattering are smeared. The discrepancy may arise in the case of the scattering from solid at low incident energy. CASSELS[4] has calculated the one-phonon total cross section of iron by the method due to WEINSTOCK[5] which is based on the Debye dispersion relation with single sound velocity. Cassels' calculation shows that the incoherent approximation gives substantially a lower cross section than the coherent calculation for neutron energies below 5 meV, and the effect is appreciable even for neutron energy about 20 meV when temperature is high. No effort has ever been directed to the calculation of the total cross section by using the more realistic dispersion relations than Debye type, including in particular the effect of polarization vectors.

The Gaussian approximation (b) is rigorous for harmonic solids. The classical time correlation function is, according to SCHOFIELD,[1]

$$\chi_s(\kappa, t) = \exp\left[-\frac{1}{2}\kappa^2\langle\eta^2\rangle_T + \frac{1}{4!}\kappa^4(\langle\eta^4\rangle_T - \langle\eta^2\rangle_T^2) + O(\kappa^6)\right] \tag{23}$$

where

$$\kappa\eta = \vec{\kappa}(\vec{\gamma}(t) - \vec{\gamma}(o))$$

The "computer experiment" by RAHMAN[6] on liquid argon at 94.4°K shows that the maximum separation of $\langle r^4\rangle$ from its Gaussian value $\frac{5}{9}\langle r^2\rangle^2$ is about 13%, occurring at $t \sim 3\times10^{-12}$ sec. It falls off to zero at shorter and longer time. Therefore, the Gaussian approximation seems to be valid for most of the reactor moderating materials at normal temperature.

Within the above approximations (a) and (b), the evaluation of the spectral density function is of the central importance in the calculation of neutron scattering. For harmonic crystal, $\rho_\nu(\omega)$ for the ν-th basis atom can be written approximately as

$$\rho_\nu(\omega) = \frac{1}{3N}\sum_s |C_s^\nu|^2\,\delta(\omega - \omega_s)$$

if atoms vibrate isotropically, and

$$\rho_\nu(\omega, \Omega_\kappa) = \frac{1}{N}\sum \frac{|\vec{\kappa}\cdot \vec{C}_{\nu s}|^2}{\kappa^2}\delta(\omega-\omega_s) \tag{25}$$

if the vibrations are anisotropic. Here Ω_κ is the solid angle subtended by $\vec{\kappa}$. The cross section must be averaged over the orientation of microcrystals. The vibrational amplitude of heavier atom in crystal is in general large in low frequency modes and small in high frequency modes. The opposite is true for the lighter atom. Thus, $\rho_\nu(\omega)$ of the heavier aton is softer than that of the lighter atom. The sum of $\rho_\nu(\omega)$ over ν divided by the number of basis atoms is just the frequency distribution as the density of normal modes.

The calculation of Eqs. (24) and (25) requires the complete solution of lattice dynamics. As will be discussed in section 3.4, the calculated frequency distributions of beryllium by YOUNG and KOPPEL[7] on one hand and by RAUBENHEIMER and GILAT[8] on the other differ considerably from each other. Both were based on the Born-von Karman model fitted to the measured dispersion curves of SCHMUNK *et al.*[9] This is rather surprising since the fitting of dispersion curves seems to be more or less reasonably good in both theories. The lattice dynamics of beryllium oxide is still more complicated and no firm theory as yet exists. An increasing interest is paid on the dynamics of liquid. Theoretical calculations have been reported for several simple liquid. But it is practical at the present stage to determine the low frequency part of the generalized frequency distribution in phenomenological way and the high frequency part by the theory of molecular vibrations and hindered rotations.

Experimentally, the spectral density function $\rho(\omega)$ is determined most easily by the extrapolation and iteration procedure first proposed by EGELSTAFF[1]:

$$\rho(\beta) = 2\beta \sinh\left(\frac{\beta}{2}\right)\left(\frac{S_s(\alpha,\beta)}{\alpha}\right)_{\alpha\to 0}. \tag{26}$$

For diatomic substance, $\rho(\beta)$ obtained in this way is

$$\rho(\beta) = \rho_1(\beta) + \frac{\langle a_2^2\rangle}{\langle a_1^2\rangle}\frac{M_1}{M_2}\rho_2(\beta),$$

where the index 1 refers, for example, to the main scatterer atom. The normalization of $\rho(\beta)$ is therefore,

$$\int_0^\infty \rho(\beta)\,d\beta = 1 + \frac{\langle a_2^2\rangle}{\langle a_1^2\rangle}\frac{M_1}{M_2}.$$

As the time correlation function of diatomic substance can not be expressed by a single Gaussian form, $\rho(\beta)$ loses the meaning as the spectral density function. The simplest way of analysis is to assume $\rho_1(\beta) = \rho_2(\beta)$ and to iterate until a reasonable agreement is obtained between the calculated and the measured scattering law, although a careful study of the time Fourier transform of the scattering law will give $\rho_1(\beta)$ and $\rho_2(\beta)$ separately.

In practice, the procedure of extrapolation suffers from the multiple scattering from sample and the coherent scattering at small momentum transfer. The effect of multiple scattering is sometimes significant even at the region of large momentum transfer. It is now generally recognized that the correction for this effect is very important for most of the existing experimental data. Theoretical correction (as MUSE code by HONECK[10]) is also not free from ambiguity in the point that the calculated correction factor depends on the assumed frequency distribution. Iteration can be performed but with exhaustive work. BRUGGER[11] and SCHMUNK[12] have respectively used the first moment theorem, Eq. (15), as a measure of the experimental check of the effect of multiple scattering on the measured scattering law of aluminum and beryllium. This method is well defined since the first moment is not affected by the presence of coherent scattering (elastic as well as inelastic) and thus will give a good support to the theoretical calculation of the correction factor. Unfortunately, many of the measurements that have been done so far for other types of materials do no cover the sufficiently wide range of β as to allow the direct calculation of the first moment.

The effect of coherent scattering on the scattering law becomes prominent at intermediate and small momentum transfer. This makes one to suspect if he has extrapolated the scattering law data correctly through $\alpha=0$. The calculation has been performed of the one-phonon coherent scattering from polycrystals of aluminum[13] and graphite. Fig. 1 shows the comparison of the calculated scattering law for aluminum with the

measured one for $|\hbar\omega|/T=0.5$ and $T=23°C$. As seen from the figure, the coherent effect is significant up to many reciprocal lattice zones away from the center. This is because that $|\hbar\omega|$ is small, the corresponding $|\vec{q}|$ is also small and therefore the contributions from different zones are well separated. The coherent scattering fluctuates around the self term of the scattering except for very small κ. Thus, the incoherent approximation will be fairly accurate if the coherent effect is smeared. The coherent calculation on graphite will be described in section 3. 3. 2.

Method of Computation

In the present evaluation, the Fortran IV programs UNCLE, ES, NELKER, FREE, GASKET-FLANGE and UNCLE-TOM have been used. The last code calculates the zero-phonon elastic scattering of crystals of f. c. c., b. c. c and hexagonal structures. ES is based on the method of EGELSTAFF and SCHOFIELD,[14] and can treat diffusive motion together with bound motion and optical levels. As an integral check of the kernel calculation, the diffusion parameter code DIP was also used. More details of these codes will be described in following sections.

To facilitate the presentation of later sections, some basic formulae of scattering kernel calculation are given below. UNCLE and ES calculate the scattering cross section by the method of phonon expansion when κ is small and by the short time expansion when κ is large.[1), 15)] Namely,

$$S_s(\kappa,\omega)=e^{-2W}\sum_{N=0}^{\infty}\frac{(2W)^n}{n!}G_n(\omega), \quad \text{for } 2W\leq 6 \tag{27}$$

$$=\frac{\hbar}{\sqrt{4\pi R_0 T_{eff}}}e^{-\frac{(\hbar\omega-R_0)^2}{4R_0T_{eff}}}\left(1+O\left(\frac{1}{\sqrt{2W}}\right)\right), \quad \text{for } 2W\geq 6. \tag{28}$$

Here $\hbar\omega=E_0-E$, R_0 is the free atom recoil energy, $2W$ is the Debye-Waller factor and T_{eff} is the effective temperature.

$$2W=\frac{\hbar\kappa^2}{2M}\int_0^{\infty}\frac{\rho(\omega)}{\omega}\coth\frac{\hbar\omega}{2T}d\omega, \tag{29}$$

$$T_{eff}=\frac{1}{2}\int_0^{\infty}\rho(\omega)\hbar\omega\coth\frac{\hbar\omega}{2T}d\omega, \tag{30}$$

$G_n(\omega)$ is the term for the process involving n real phonons, defined by and satisfying,

$$G_n(\omega)=\frac{1}{2\pi}\int_{-\infty}^{\infty}e^{-i\omega t}\left(\frac{\gamma(t)}{\gamma(0)}\right)^n dt=\int_{-\infty}^{\infty}G_1(\omega-\omega')\,G_{n-1}(\omega')\,d\omega', \quad \int_{-\infty}^{\infty}G_n(\omega)d\omega=1 \tag{37}$$

When n is sufficiently large, it follows from the central limiting theorem of statistics that $G_n(\omega)$ tends to the normal distribution.

$$G_n(\omega)=\frac{1}{\sqrt{2\pi n\kappa_2}}e^{-\frac{(\omega-n\kappa_1)^2}{2n\kappa_2}}\left(1+O\left(\frac{1}{\sqrt{n}}\right)\right) \tag{38}$$

where

$$\kappa_1=\langle\omega\rangle=\int_{-\infty}^{\infty}\omega G_1(\omega)d\omega, \tag{39}$$

$$\kappa_2=\langle(\omega-\langle\omega\rangle)^2\rangle=\int_{-\infty}^{\infty}(\omega-\langle\omega\rangle)^2\,G_1(\omega)d\omega$$

ES code can handle the diffusive motion of atoms. Splitting the spectral density function into the diffusive part and the bound part, the scattering law is calculated as

$$S(\kappa,\omega)=\int_{-\infty}^{\infty}S_{diff}(\kappa,\omega-\omega')\,S_b(\kappa,\omega')d\omega' \tag{40}$$

The diffusive part of the spectral density function is, following after EGELSTAFF and SCHOFIELD,

$$\rho_{diff}(\beta)=\frac{2d}{\pi}\frac{\sinh\beta/2}{\beta/2}\sqrt{c^2+\frac{1}{4}}\beta K_1\left(\sqrt{c^2+\frac{1}{4}}\beta\right), \tag{41}$$

$$\int_{-\infty}^{\infty}\rho_{diff}(\beta)=\frac{d}{c}, \tag{41}$$

where $K_1(x)$ is the modified Bessel function of the second kind, d is related to the diffusion constant by $D=$

$\frac{\hbar}{M}d$, and c is the relaxation time (divided by $\hbar/T$) for atom to start to diffuse. For water at room temperature, $c\sim10^{2}$ and $d\sim10^{-2}$. So $\rho_{diff}(\beta)$ is sharply localized near $\beta=0$. While the diffusive motion is only a very small part of the total freedom of atomic motion, the convolution integral of Eq. (40) has to be done very carefully. In the actual calculation the diffusive motion has been neglected and replaced by the free translation of a molecule as a whole. GASKET and FLANGE codes were used to this calculation.

Finally, UNCLE code has been used to calculate the interference scattering from atoms in heavy water molecule in liquid with minor modification of the code. The device is as follows. As in Butler's calculation,[16] by approximating the average of the products over the orientation of the molecule by the product of averages, the time correlation function for a pair of the ν -th and ν' -th atoms in a molecule may be written as,

$$\chi_{\nu\nu'}(\kappa,t)=\frac{\sin\kappa R_{\nu\nu'}}{\kappa R_{\nu\nu'}}\,e^{-\frac{\hbar\kappa^2}{4}\left(\frac{\gamma_{\nu\nu}(0)}{M_\nu}+\frac{\gamma_{\nu'\nu'}(0)}{M_{\nu'}}\right)}e^{\frac{\hbar\kappa^2}{2M_{\nu\nu'}}\gamma_{\nu\nu'}(t)} \tag{42}$$

where $R_{\nu\nu'}=|\vec{R}_\nu-\vec{R}_{\nu'}|$, $M_{\nu\nu'}=\sqrt{M_\nu M_{\nu'}}$, and

$$\gamma_{\nu\nu'}(t)=\int_0^\infty\frac{\rho_{\nu\nu'}(\omega)}{\omega}\left[(n_\omega+1)\,e^{i\omega t}+n_\omega e^{-i\omega t}\right], \tag{43}$$

$$\rho_{\nu\nu'}(\omega)=\frac{M_{\nu\nu'}}{3m}\sum_\lambda(C_{\nu'}^{(\lambda)*}\cdot C_\nu^{(\lambda)})\,\delta(\omega-\omega_\lambda). \tag{44}$$

The polarization vector $\vec{C}_\nu^{(\lambda)}$ is normalized as $\sum_\nu\frac{M_\nu}{m}(\vec{C}_\nu^{(\lambda)*}\cdot C_\nu^{(\mu)})=\delta_{\lambda\mu}$. $\rho_{\nu\nu'}(\omega)$ satisfies the ortho-normality condition that

$$\int_0^\infty\rho_{\nu\nu'}(\omega)\,d\omega=\delta_{\nu\nu'} \tag{45}$$

This condition ensures the first moment theorem. In the above equations, the molecular rotations have been replaced by torsional vibrations. The calculation of scattering law is similar to the procedure described in previous paragraphs. However, Eq. (45) states that the sign of $\rho_{\nu\nu'}(\omega)$ alternates for a distinct pair of atoms. This makes the central limiting theorem inapplicable to the calculation of successive phonon terms. Owing to the suggestion by H. Takahashi, this difficulty can be avoided if we divide $\rho_{\nu\nu'}(\omega)$ into the positive definite part and the negative definite part, and convolute the resulting two scattering law into a single n-phonon term. The central limiting theorem is now applicable to each part of the scattering law corresponding to the above division. Only a minor change of UNCLE code was necessary to this calculation. An interesting, but not practical, point is that the above method can be applied to calculate the coherent scattering from crystal.

References

1) see for example, Proceedings of IAEA Conference on Slow Neutron Scattering.
2) Nishigori *et al.* : present report.
3) Placzek G. : *Phys. Rev.* 86, 377 (1952).
4) Cassels J.M. : *Prog. Theor. Phys.* 1, 185 (1950).
5) Weinstock R. : *Phys. Rev.* 65, 1 (1944).
6) Raiman A. : *Phys. Rev.* 136, A 405 (1964).
7) Young J.A. and Koppel J.U. : *Nucl. Sci. Eng.*, 19, 367 (1964).
8) Raubenheimer L.J. and Gilat G. : *Phys. Rev.* 157, 586 (1967).
9) Schmunk R.E. Brugger R.M. Randolph P.D. and Strong K.A. : *Phys. Rev.* 128, 562 (1962).
10) Honeck H. : GA-5968 (1964).
11) Brugger R.M. : IDO-17063 (1965).
12) Schmunk R.E. : *Phys. Rev.* 136, A 1303 (1963).
13) Iijima S. : *J. Nucl. Sci. Technol. (Tokyo)*, 3, 164 (1966).
14) Egelstaff P.A. and Schofield P. : *Nucl. Sci. Eng.*, 12, 260 (1962).
15) Sjölander A. : *Ark. Fys.* 14, 315 (1958).
16) Butler D. : *Proc. Phys. Soc.* 81, 276 (1963).

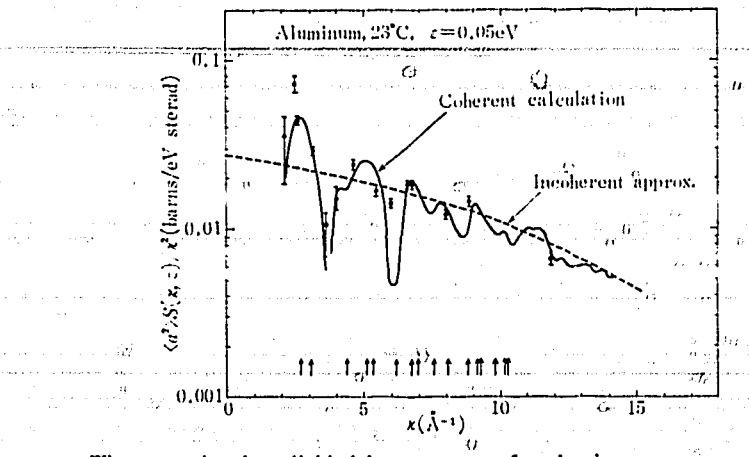

Fig. 1 The scattering law divided by κ^2 versus κ for aluminum at room temperature; Comparison of the coherent calculation with measurement by Brugger *et al.* for $|\varepsilon|/T=0.5$. The arrows at the bottom of the figure indicate the position of reciprocal lattice points. The solid line is the calculation based on the dispersion curves and the frequency spectrum obtained by Walker. Multi-phonon terms were treated in the incoherent approximation. The dotted line is the calulation in the incoherent approximation.

2.2 Codes Used in Evaluation

The codes which have been used for the evaluation of thermal neutron cross sections are listed below.

NELKER[1]: A program for bound hydrogen and deuterium based on Nelkin's formulation. This program computes (1) the scattering law, (2) the scattering kernel and its Legendre moments up to order 3, (3) the total scattering cross section and the transport cross section and produce punched card outputs of full kernels.

ES[2]: A program for general purpose based on Egelstaff-Schofield's formulation. By the use of theoretical or phenomenological frequency distributions or spectral densities for bound motions (including lattice vibrations), molecular vibrations and rotations and parameters for diffusive motion, scattering cross sections for crystals and molecules (solids and liquids) can be computed with this program. Anisotropic crystals, however, can not be handled with the ES code. A frequency distribution with continuous and discrete parts can be used as input data. The program computes (1) the scattering law, (2) the scattering kernel and its Legendre moments up to order 3, (3) the total scattering cross section, its Legendre moments and the transport cross section, (4) the source spectrum and produces punched card outputs of full kernel.

UNCLE[3]: A program for anisotropic and isotropic polycrystalline materials. A frequency distribution with discrete parts can not be used as input data. The discrete levels have to be approximated, for example, by triangular distributions when they are to be used as input data for UNCLE. The program computes in the incoherent approximation (1) the scattering law, (2) the scattering kernel and its Legendre moments up to order 3, (3) the total scattering cross section, its Legendre moments and the transport cross section and produces punched card outputs of full kernels.

UNCLE-TOM[4]: A program to compute coherent and incoherent elastic scattering cross sections for polycrystalline materials. Materials which can be handled with this program are those belonging to hexagonal, face centered cubic and body centered cubic lattices. The calculation for the anisotropic crystal is also possible. Main outputs from the program are incoherent and coherent total elastic scattering cross sections, the transport cross section and Legendre moments.

GASKET[5]: A unified program to compute scattering laws for any moderators (gases, molecules, solids and liquids) in the incoherent approximation. This program evaluates the intermediate scattering cross section and does Fourier inversion to obtain $S(\alpha, \beta)$. Provision has been made in the program for the following dynamical modes and different combinations of modes:

(1) Free translation,
(2) Diffusive motion,
(3) Harmonic isotropic vibrations with continuous frequency distribution,
(4) Harmonic isotropic vibrations with discrete frequency distribution.

The coding, however, has been completed only for combinations of modes (1), (3) and (4).

The punched card output of $S(\alpha,\beta)$ can be obtained in ENDF FORMAT, which can be used as input for FLANGE.

FLANGE[6] : A program which accepts as input the scattering law (calculated with GASKET, for example) and computes (1) the double differential scattering cross section, (2) the angular distribution, (3) the scattering kernel and its Legendre moments up to order 3, (4) the total scattering cross section and its Legendre moments and (5) the second energy transfer moment.

This program punches scattering kernels in ENDF FORMAT and also prepares an input tape for MUSE, which does multiple scattering corrections.

Other codes : Some other codes were used for the evaluation. These codes have been programed for special purposes. The explanations of codes such as MUSE, DIP, UNCLE-DISTINCT, etc. will be given in the following sections.

References

1) Shimada S. : "NELKER: A Code of Scattering Kernel Calculation for Bound Hydrogen" (written in Japanese), JAERI 1085 (1965).
2) Matsuoka K. and Arai K. : "Manual of Egelstaff-Schofield Model Code" (written in Japanese), JAERI 1094 (1965).
3) Iijima S. and Tokizawa M. : "UNCLE: An IBM-7090 Program for Calculating the Scattering Kernels for Anisotropic Crystal" (written in Japanese), JAERI 1087 (1965). UNCLE is a version of the SUMMIT code originally developed by J. Bell at Gulf General Atomics. The revision was made by *Japanese Nuclear Data Committee* with the permission of D. E. Parks at GGA and USAEC.
4) Iijima S. Tokizawa M., Nishijima H. and Yasogawa M. : "UNCLE-TOM: A Code for Calculating the Elastic Scattering Cross Sections for Poly-Crystals" (written in Japanese), unpublished.
5) Koppel J. U. Triplett J. R. and Naliboff Y.D. : "GASKET: A Unified Code for Thermal Neutron Scattering," GA-7417(Rev.)(1967), also, Argonne Code Center Reference Material Abstract 263 (1966). The source deck of GASKET was supplied by Argonne Code Center to Japanese Nuclear Data Committee.
6) Honeck H.C. and Naliboff Y.D. : Integral Neutron Thermalization, Appendix E, GA-6824 (1965), also, Argonne Code Center Reference Material Abstract 247 (1966). The source deck of FLANGE was supplied by Argonne Code Center to Japanese Nuclear Data Committee.

2.3 Multiple Scattering Correction

Multiple scattering effect may be the most ill-natured one among errors which cause inacuracy to the cross section determined by experiment. The reason for this situation is firstly due to the fact that to avoid this effect is difficult in present experimental procedures since we are obliged to use relatively thick sample by the limited intensity of source neutron. Therefore necessity of the correction seems obvious. Secondly to perform this multiple scattering correction needs essentially the knowledge of cross section which we are going to measure. Therefore we should assume a theoretical cross section to perform this correction.

The reliability of the correction depends partly on the exactness of this assumed cross section. If one can extract the generalized phonon frequency distribution from experimental data, though this data contain

multiple scattering, the kernel which is constracted by this frequency distribution may be used as the assumed cross section. Similarly one can extract the generalized phonon frequency distribution from the corrected data, and constract the kernel from this distribution to use for the correction. By the interation procedure we can obtain a kernel which is free from multiple scattering and also independent of the theoretical model employed. A number of methods for this correction based on different approximations have been developed. In the present report we employed the method developed by HONECK[1]. This method employed in the computer code MUSE treats the scattering kernel rather exactly.

The assumptions in the procedure are:

(1) The geometry of the sample is slab with infinite extent.

(2) The scattering kernel $\sigma_s(E_0 \to E, \theta)$ is assumed to be represented by P_3 terms. Legendre moments up to order 3.

(3) The sample is thin so that the flux distribution across the sample can be expressed by a few space meshes.

(4) A theoretical scattering kernel is used.

The integral transport equation is solved by the direct and numerical procedure. Experimental arrangements are shown in Fig. 1. A neutron enters the sample on the x-z plane. Before a neutron escapes the sample it may make single or multiple collisions in the sample. Neutron detectors are assumed to be placed on the x-z plane, therefore, only the neutron which can escape the slab can reach the detectors.

The basic equations for the neutron transport are,

$$\phi(z, E, \vec{\Omega}) = \frac{1}{\mu} \int_0^z dz' H(z', E, \vec{\Omega})\, e^{-\Sigma(E)\left(\frac{z-z'}{\mu}\right)}, \quad \text{for } \mu>0 \text{ and } z>z', \tag{1}$$

$$= -\frac{1}{\mu} \int_z^a dz' H(z', E, \vec{\Omega})\, e^{-\Sigma(E)\left(\frac{z-z'}{\mu}\right)}, \quad \text{for } \mu<0 \text{ and } z<z', \tag{2}$$

$$H(z', E, \vec{\Omega}) = \int d\vec{\Omega}' \int dE \Sigma_s(E' \to E, \mu_0)\, \phi(z', E, \vec{\Omega}'), \quad \mu_0 = \vec{\Omega} \cdot \vec{\Omega}', \tag{3}$$

where $\mu = \cos\theta$, and θ is the angle between the neutron vector and the z axis. $\phi(z, E, \vec{\Omega})$ is the neutron flux. The advantage of the use of Eqs. (1) and (2) is that we can obtain the neutron flux according to its order of collisions, that is one iteration corresponds to one scattering order. Thus, inserting the flux of uncollided neutrons into Eq. (2), we can obtain the first collision source. Inserting this source into Eq. (1), we can obtain the first collision flux. Repeating the same procedure we can obtain the higher order collided neutron flux.

The uncollided neutron flux in the sample is,

$$\phi_0(z, E, \vec{\Omega}) = e^{-\Sigma(E)z/\mu}\, \delta(E - E_1)\, \delta(\vec{\Omega} - \vec{\Omega}_1) \tag{3}$$

where E_1 and $\vec{\Omega}_1$ are the incident energy and solid angle of neutron velocity. As the first collision neutron flux, one can write, inserting Eq. (3) into Eqs. (1) and (2),

$$\phi^1(z, E, \vec{\Omega}_1) = \Sigma_s(E_1 \to E_2, \mu_0) \frac{1}{\mu_2} \int_0^z dz'\, e^{-\Sigma(E_2)\frac{z-z'}{\mu} - \frac{\Sigma(E_1)z'}{\mu_1}}$$

$$= \frac{z}{\mu_2} \cdot \frac{e^{-x_1} - e^{-x_2}}{x_2 - x_1} \Sigma_s(E_1 \to E_2)\, \mu_0 \tag{4}$$

for $\mu > 0$ and

$$x_1 = \frac{z}{\mu_1} \Sigma(E_1), \quad x_2 = \frac{z}{\mu_2} \Sigma(E_2).$$

For the calculation of higher order collided flux, angular dependence of flux and kernel is expressed as the expansion in terms of the spherical harmonics, and energy and spatial variables are put into discrete meshes so that the integrals are replaced by the summation.

By the use of the flux of higher order collisions calculated by the MUSE code, the multiple scattering correction factor becomes,

$$C = \frac{\sigma_s(E_1 \to E_2, \mu_0)}{\frac{1}{N_0 a} \mu_2 \sum_{i=1}^{4} \phi^i(a, E_2, \vec{\Omega}_2)} \tag{5}$$

where $\phi^i(z, E, \vec{\Omega})$ is the i-th collided neutron flux. In the MUSE code up to the fourth collisions are considered.

For example, the results of a vanadium sample are shown in Fig. 2. The thickness of the vanadium sample is 0.2 cm (transmission is about 0.9) and the neutron is assumed to enter the sample perpendicularly. The kernel is calculated using the phonon frequency distribution evaluated by GLÄSER[2]. The multiple scattering correction is found to be 20 to 30%, and shows a complicated pattern.

The structure of the correction factor is due to the structure of $\sigma_s(E_1 \to E_2, \mu_2)$ (see Fig. 3). Since $\sigma_s(E_1 \to E_2, \mu_2)$ is calculated theoretically, this pattern may depend largely upon the theoretical model employed. In the actual measurement, however, the resolution of energy analysis may not be so sharp to reproduce the structure of flux in Fig. 3. This situation makes the single collided flux rather independent of a model employed. Multiple scattered flux is less sensitive to the theoretical model. Therefore, the factor C should overestimate the multiple scattering effect. To avoid this situation SLAGGIE[3] proposed a new method which is rather independent of the model. The correction factor of this method which is called the subtraction method is,

$$C_s = \frac{x_2 - x_1}{e^{-x_1} - e^{-x_2}} \left\{ 1 - \frac{\sum_{i=2}^{4} \phi^i(a, E_2, \vec{\Omega}_2)}{\sum_{i=1}^{4} \phi^i(a, E_2, \vec{\Omega}_2)} \right\} \tag{6}$$

In the following sections we have corrected the multiple scattering effect on the scattering law using C and have not used the subtraction method. Further analysis seems to be necessary using the subtraction method.

References

1) HONECK H.C. : GA-5968 (1964).

2) GLÄSER W., *et al.*: "Inelastic Scattering of Neutrons in Solids and Liquids" Vol. I, P. 99, IAEA, Vienna, (1965).

3) SLAGGIE E.L. : *Nucl. Sci. Eng.*, 30, 199 (1967).

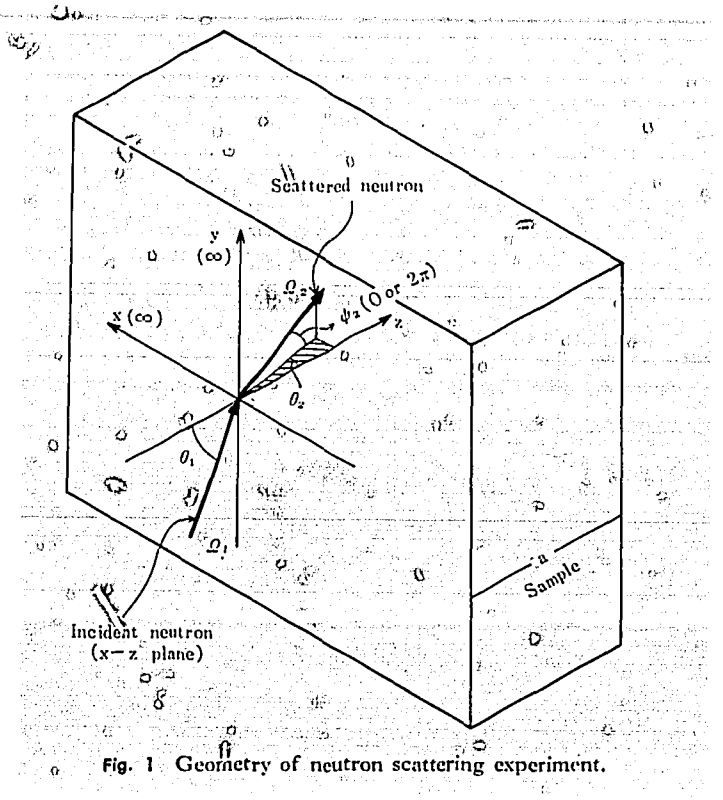

Fig. 1 Geometry of neutron scattering experiment.

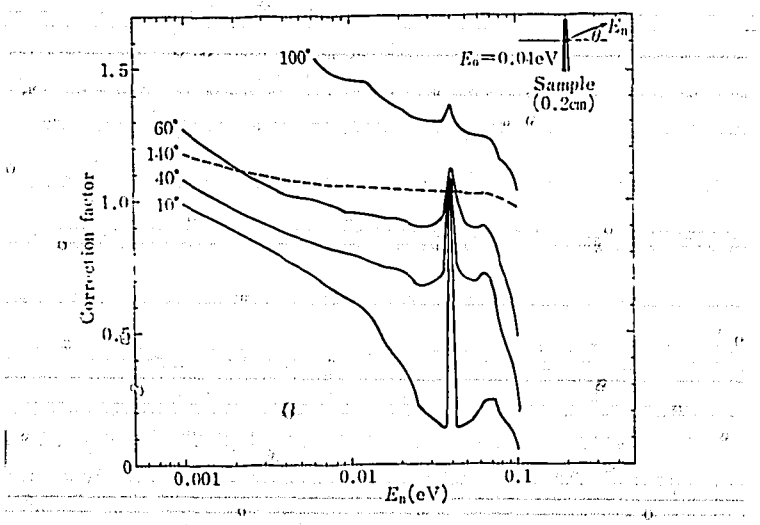

Fig. 2 Multiple scattering correction factor on vanadium sample.

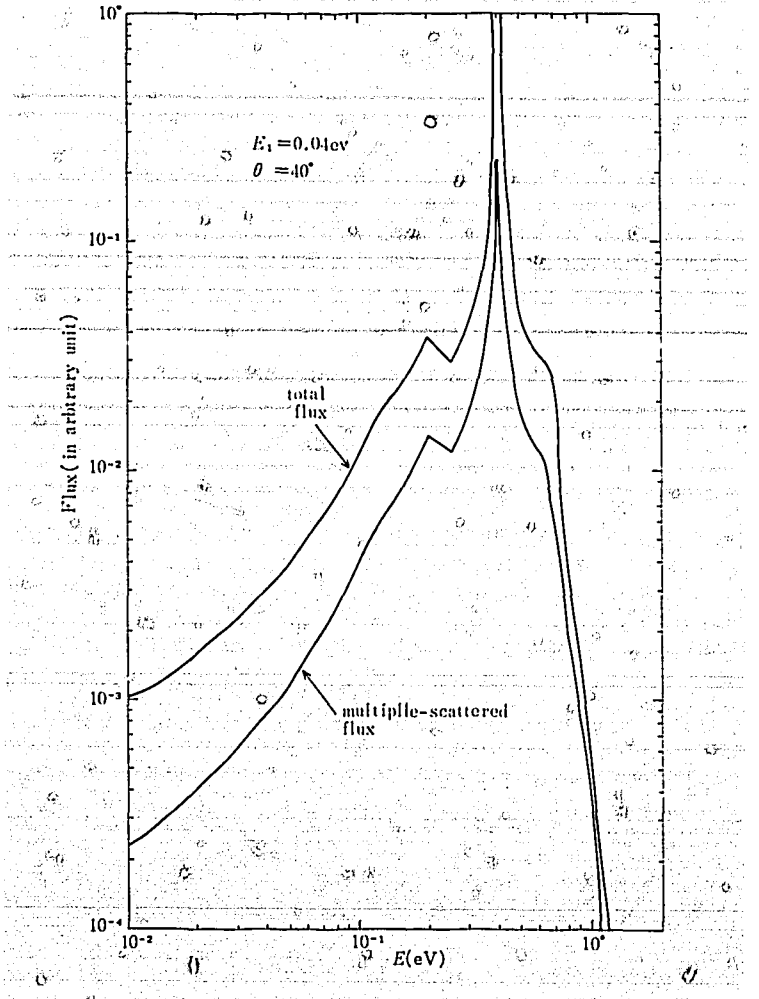

Fig. 3 Neutron flux from vanadium sample.

2.4 Diffusion Parameters (DIP Code)

The method used to calculate the diffusion parameters of various moderators is based essentially on CALAME's[1] formalism. The solution $\phi(B,E,\mu,t)$ of the spatially Fourier transformed, homogeneous Boltzmann equation for a non-multiplying medium in plane geometry, viz.,

$$\left[\frac{1}{v}\frac{\partial}{\partial t} - tB\mu+\Sigma_t(E)\right]\phi(B,E,\mu,t)$$
$$=\int_{-1}^{1} d\mu' \int_0^\infty dE'\,\Sigma_s(E',\mu'\to E,\mu)\;\phi(B,E',\mu',t) \tag{1}$$

is assumed to be of the form

$$\phi(B,E.\mu,t)=\phi(B,E,\mu)\exp(-\lambda t), \tag{2}$$

where B is the Fourier Transform variable, E is the neutron energy, μ is the angular variable, and λ the time decay constant.

The insertion of Eq. (2) into Eq. (1) yields

$$\left[-\frac{\lambda}{v} - iB\mu+\Sigma_t(E)\right]\phi(B,E,\mu)$$
$$=\int_{-1}^{1} d\mu' \int_0^\infty dE'\Sigma_s(E',\mu'\to E,\mu)\;\phi(B,E',\mu'). \tag{3}$$

The angular dependence of $\phi(B,E,\mu)$ and $\Sigma_s(E',\mu'\to E,\mu)$ is expanded in Legendre-polynomials

$$\phi(B,E,\mu)=\sum_{m=0}^{\infty}\frac{2m+1}{2}\phi_m(B,E)\,P_m(\mu) \tag{4}$$

$$\Sigma_s(E',\mu'\to E,\mu)=\sum_{l=0}^{\infty}\frac{2l+1}{2}\Sigma_{sl}(E'\to E)P_l(\mu_0), \tag{5}$$

μ_0 being the cosine of the angle between a neutron's initial and final directions.

The insertion of Eqs. (4) and (5) into Eq. (3) and use of the orthogonality of the Legendre polynomials yield

$$\left[-\frac{\lambda}{v}+\Sigma_t(E)\right]\phi_m(B,E)-iB\left[\frac{m}{2m+1}\phi_{m-1}(B,E)+\frac{m+1}{2m+1}\phi_{m+1}(B,E)\right]$$
$$=\int_0^\infty\Sigma_{sm}(E'\to E)\,\phi_m(B,E')dE'. \tag{6}$$

The m-th spherical harmonics moment, $\phi_m(B,E)$, and the decay constant, λ, are expanded in power series in B

$$\phi_m(B,E)=(iB)^m\sum_{n=0}^{\infty}\phi_{2n,m}(E)\,(iB)^{2n} \tag{7}$$

$$\lambda=\alpha_0-\sum_{j=1}^{\infty}\alpha_{2j}(iB)^{2j}=\alpha_0+D_0B^2-CB^4+FB^6\cdots\cdots \tag{8}$$

From Eqs. (6) through (8), the following coupled set of equations is obtained for the expansion coefficients, $\phi_{2n,m}(E)$ and α_{2j},

$$\left[\Sigma_t(E)-\frac{\alpha_0}{v}\right]\phi_{0,m}(E)-\frac{m}{2m+1}\phi_{0,m-1}(E)$$
$$=\int_0^\infty\Sigma_{sm}(E'\to E)\,\phi_{0,m}(E')dE' \tag{9}$$

$$\left[\Sigma_t(E)-\frac{\alpha_0}{v}\right]\phi_{2n,m}(E)+\sum_{j=1}^{n}\frac{\alpha_{2j}}{v}\phi_{2(n-j),m}(E)$$
$$-\frac{m}{2m+1}\phi_{2n,m-1}(E)-\frac{m+1}{2m+1}\phi_{2n-2,m+1}(E)$$
$$=\int_0^\infty\Sigma_{sm}(E'\to E)\;\phi_{2n,m}(E')dE'\quad(n\geq 1). \tag{10}$$

The solution of above equations is obtained successively as follows:

a) $n=0,\ m=0$

By integrating the both sides of Eq. (9) over energy and using relation

$$\Sigma_s(E)=\Sigma_{s0}(E)=\int_0^\infty \Sigma_{s0}(E\to E')dE',$$

one obtains

$$\int_0^\infty \left[\Sigma_a(E)-\frac{\alpha_0}{v}\right]\phi_{0,0}(E)dE=0. \tag{11}$$

In case the absorption is inversely proportional to the velocity, Eq. (9) has an eigenvalue

$$\alpha_0=\Sigma_0 v_0, \tag{12}$$

where v_0 is a standard velocity and Σ_0 is the absorption cross section corresponding to v_0.

Eq. (9) with this eigenvalue is written as

$$\Sigma_{s0}(E)\phi_{0,0}(E)=\int_0^\infty \Sigma_{s0}(E'\to E)\phi_{0,0}(E')dE'. \tag{13}$$

It is well known that Eq. (13) has an eigenvector

$$\phi_{0,0}(E)=M(E) \tag{14}$$

with M(E) the Maxwellian flux spectrum.

b) $n=0,\ m>0$

The equation,

$$\Sigma_{s0}(E)\,\phi_{0,m}(E)-\int_0^\infty \Sigma_{sm}(E'\to E)\,\phi_{0,m}(E')dE'=\frac{m}{2m+1}\,\phi_{0,m-1}(E), \tag{15}$$

is solved for $\phi_{0,m}(E)$. The solution is effected by writing the equation at discrete energy points E_i, and replacing the integral by a numerical quadrature formula, to obtain

$$\Sigma_{s0}(E_i)\phi_{0,m}(E_i)-\sum_{j=1}^{N}\Sigma_{sm}(E_j\to E_i)\phi_{0,m}(E_j)\Delta E_j=\frac{m}{2m+1}\,\phi_{0,m-1}(E_j). \tag{16}$$

This equation is written in matrix form

$$A_m\,\phi_{0,m}=\frac{m}{2m+1}\,\phi_{0,m-1}, \tag{17}$$

where A_m is a matrix defined as

$$A_m(i,j)=\Sigma_{s0}(Ei)\,\delta_{ij}-\Sigma_{sm}(E_j\to E_i)\,\Delta E_j. \tag{18}$$

Eq. (17) is solved numerically by a matrix inversion routine.

c) $n=1,\ m=0$

Eq. (10) has a form in this case

$$\Sigma_{s0}(E)\ \ \phi_{2,0}(E)+\frac{\alpha_2}{v}\,\phi_{0,0}(E)-\phi_{0,1}(E)=\int_0^\infty \Sigma_{s0}(E'\to E)\phi_{2,0}(E')dE' \tag{19}$$

$D_0(=\alpha_2)$ is determined by numerically integrating Eq. (19) over energy

$$D_0=\alpha_2=\int_0^\infty \phi_{0,1}(E)dE\Big/\int_0^\infty \frac{1}{v}\phi_{0,0}(E)dE. \tag{20}$$

The equation which determines $\phi_{2,0}(E)$ is, in matrix form,

$$A_0\,\phi_{2,0}=\phi_{0,1}-\frac{\alpha_2}{v}\phi_{0,0}. \tag{21}$$

This is not solvable by the straightforward matrix inversion method, because A_0 is not a normal matrix. SHIBA[2] showed that the rank of A_0 is N-1 (N being the dimension of A_0) and one additional condition is necessary to solve Eq. (21). The additional condition is obtained from the fact that $\phi_{2,0}(E)$ does not contribute to the net neutron density[3], viz.,

$$\int_0^\infty \frac{1}{v}\,\phi_{2,0}(E)\,dE=0 \tag{22}$$

d) Higher components

The same procedure is repeated to obtain $C(=\alpha_4)$ and $F(=\alpha_6)$. It should be noted that the Legendre components of the scattering kernel with l up to 2 are necessary for the calculation of diffusion parameters D_0,

C and F.

An example of the eigenfunction calculation is shown in Fig 1. In Table 1 are shown some results of diffusion parameter calculations for H_2O at 20°C. Experimental results are included in the table for the sake of comparison. From Table 1 one can see that the maximum energy of 0.625 eV is sufficient but 50 energy points are required for the calculation of diffusion parameters. Scattering kernels were computed by using GAKER and NELKER codes, both of which are based on the Nelkin's model. Table 1 shows that the slight *difference in methods to calculate scattering kernels leads to a rather large difference in calculated diffusion parameters.* The effects of the scattering model on diffusion parameters will be discussed in more details in Chapter 3.

The thermal diffusion length L in Table 1 was calculated from the following equation

$$L^2=\frac{D_0}{2\alpha_0}\left[1+\sqrt{1+\frac{4\alpha_0 C}{D_0^2}}\right], \tag{23}$$

which is known to be correct to order B^4.

Table 1. Results of diffusion parameters of H_2O at 20°C

NO.	Maximum energy (eV)	NO. of groups	NO. of angle Pts.	Max. l	Code used	D ($cm^2 \cdot sec^{-1}$)	C ($cm^4 \cdot sec^{-1}$)	F ($cm^6 \cdot sec^{-1}$)	L^2
1	0.900	30	11	1	GAKER	38016.5	3114.2	161.6	7.9936
2	0.900	30	24	1	〃	38017.0	3120.0	163.2	7.9938
3	0.625	25	24	1	〃	〃	〃	〃	〃
4	0.625	50	24	1	〃	37515.6	3089.2	155.7	7.8897
5	0.707	30	24	1	〃	37501.6	3072.6	153.7	7.8864
6	0.900	30	11	1	NELKER	37482.1	2890.6	123.2	7.8777
7	GHATAK, HONECK ('65)				(Nelkin)	37045	3361	169	
8	CLENDENIN ('64)				(〃)	37570	3380	210	
9	KALLFELZ ('65)				(Goldman-Nelkin)	37400	3350	144	
10	CLENDENIN ('64)				(Radkowski)	38230	2730	250	
11	KALLFELZ ('65)				(Haywood $P(B)$)	33900	3080	218	
12	GLASER ('67)				(〃)	34520	4220	363	
13	SPRINGER ('64)				(from $\Sigma_s(E)$ and $\mu(E)$)	35300			
14	Experiment of ARAI & KUCHILE					35630±80	3420±170	214±139	
15	STARR, KOPPEL ('61)								7.62±0.016
16	de JUREN, REIER ('61)								7.701±0.012

References

1) CALAME G.P. : *Nucl. Sci. Eng.* 19, 189-185 (1964).

2) SHIBA K. : *J. Nucl. Sci Technol.* (*Tokyo*) 5, 201-209 (1968).

3) FURUHASHI A. : private communication.

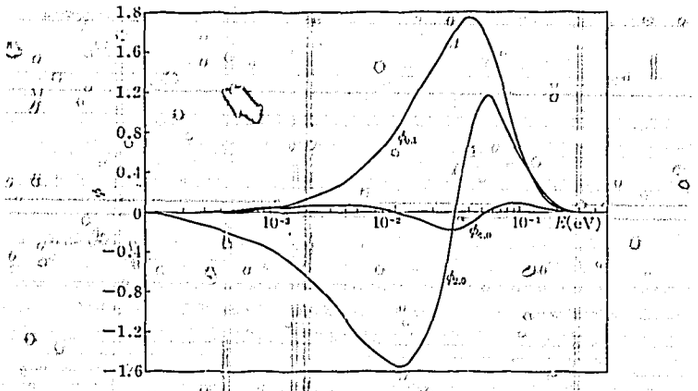

Fig. 1 An example of the calculation of eigenfunctions. (calculated with Nelkin kernel for H_2O)

3. Evaluation

3.1 Light water

3.1.1 Light Water

For liquid H_2O a lot of frequency distributions $\rho(\beta)$ have been derived experimentally from neutron scattering laws because scattering by hydrogen is mainly incoherent. Here, frequency distributions of hydrogen in water are argued to fit measured total and differential scattering cross sections. If it is assumed that the rotation of H_2O molecule around its three principal axes of inertia are hindered and can be approximated by a harmonic torsional oscillation and two bond-stretching vibrations of the H_2O molecule are degenerate into one vibrational mode, the frequency distribution of freely recoiling H_2O molecule is expressed as:

$$\rho(\beta)=\frac{1}{18}\delta(\beta)+\frac{1}{2.25}\delta(\beta-\beta_r)+\frac{1}{6}\delta(\beta-\beta_{v1})+\frac{1}{3}\delta(\beta-\beta_{v2}) \qquad (1)$$

where β_r, β_{v1}, β_{v2} are the energies of hindered rotation, bending and stretching vibrations.

However water has a broad band of torsional oscillation because of inharmonic potentials and of the collective modes of clustering molecules. As suggested in the literatures, the shape of the rotational band in the frequency spectrum will partly improve the agreements of the calculated total and differential scattering cross sections with experimental data.

Recently the availability of accurate differential and integral cross section measurements for water[1)-4)] has encouraged the development of more detailed models. Here, two of these, the model modified by KOPPEL[5)] from HAYWOOD's experimental frequency spectrum and the model derived by HAYWOOD[6)] from his experimental data on scattering law are introduced for comparison with ours. Both frequency spectra are shown in Fig. 1. In Koppel model, the frequency distribution near $\beta=8$ is approximated by a discrete line of the same frequency with a weight of 1/6 in accordance with Eq. (1). At low frequency end, an ω^2 behavior is introduced and the remaining part, which is adjusted to 1/18 of the total area, is treated in the short collision time approximation. The area corresponding to the torsional mode is obtained by cutting off the distributed part of the Haywood's experimental spectrum at 0.165 eV, the energy corresponding to the bottom of the valley between the torsional and first vibrational peaks. The suppressed part is then replaced by an additional discrete line at 0.205 eV with the weight of 1/6 required by Eq. (1).

Although integral and single differential quantities can be well reproduced by these models, small discrepancies in total scattering cross sections are still seen, for example, at energies around 0.045 eV or below 0.001 eV, as shown in Fig. 2, and the calculated average cosine of scattering angle is large compared with the measured value for energies below 0.02 eV. In our models, same as in Koppel model, the assumption of free mass-18 translation was adopted for the evaluations of scattering cross sections so the discrepancy in low energy region is not surprising.

The agreement in this energy region is easily obtained by introducing diffusive mode of water and quasi-crystalline frequency spectrum. The discrepancy in the energy range of 0.02 to 0.2 eV is seen in the previous models and this is partly diminished by broadening the rotational band (model-1), although the discrepancy shifts to other energy region. In order to isolate the rotational band from the higher vibrational band, in one of the models (model-2) the high frequency part of the torsional oscillation band is cut off sharply. This brings the calculated results to a good agreement with the experimental data in total cross section, but the average cosine value of scattering angle shift upward at low energy part, as shown in Fig. 3. The difference in average

cosine values at fairly low energy depends on the assumption of free translation. A few typical results of $S(\alpha, \beta)$ values are also shown in Fig. 4. At low energy transfers, Haywood model which takes into consideration the quasi-crystalline structure of water phenomenologically, fits quite well to experimental data. At low β the good agreement between Koppel model and the model-2 is observed. As β increases, Koppel model comes close to Haywood model. Also at high β, a fair agreement between the model-2 and the experimental values is noticed.

For reference, scattering kernels for the zero-th and the first Legendre moments are shown in Figs. 5 and 6, respectively. The calculated values of diffusion parameters using Koppel model and model-2 are compared in Table 2 with the values derived from pulsed neutron measurements as a integral check of these scattering kernels. Also the spectrum of thermal neutron source from hydrogen in water is shown in Fig. 7.

In summarizing the preceding results, we might say that although the present status of the model is satisfactory for calculating each experimental quantity, there is no model at present which fits all the integral and differential data equally well.

Table 1. Total cross section and average cosine of H_2O

E (eV)	σ_{tot} for Koppel model	σ_{tot} for Model-2	$\bar{\mu}$ for Koppel model	$\bar{\mu}$ for Model-2
0.00025	439.8	452.0	—	—
0.00101	248.1	252.0	0.0035	0.0038
0.00228	196.3	198.3	0.0289	0.0328
0.00405	170.9	171.0	0.0495	0.0545
0.00632	155.6	154.1	0.0655	0.0728
0.00911	143.6	140.8	0.0806	0.0904
0.01240	134.8	130.9	0.0995	0.112
0.01619	126.5	120.7	0.118	0.134
0.02049	118.7	113.3	0.136	0.154
0.02530	111.5	105.6	0.155	0.174
0.03061	105.1	99.0	0.175	0.195
0.03643	99.0	92.9	0.193	0.214
0.04276	93.6	87.7	0.211	0.232
0.04959	88.8	83.4	0.229	0.248
0.05692	84.8	79.9	0.245	0.262
0.06517	81.0	76.9	0.260	0.275
0.07485	77.6	74.3	0.274	0.286
0.08612	74.4	72.0	0.287	0.298
0.09919	71.7	70.0	0.302	0.311
0.11398	69.3	68.2	0.317	0.325
0.13123	66.6	66.0	0.329	0.336
0.1525	63.7	63.2	0.342	0.351
0.1790	61.5	61.3	0.358	0.364
0.2124	59.1	59.0	0.377	0.381
0.2546	57.0	56.7	0.398	0.401
0.3081	54.8	54.3	0.417	0.420
0.3760	52.5	52.1	0.434	0.443
0.4618	50.2	49.4	0.447	0.463
0.5702	48.1	47.1	0.458	0.475
0.7067	46.6	44.3	0.473	0.498

Table 2. Diffusion parameters in H_2O at 20°C

D_0 (cm^2/s)	C (cm^4/s)	F (cm^6/s)	Refs
35,630±80	3,420±170	214±139	Experimental[9]
37,516	3,089	156	Nelkin kernel
34,825	3,232	351	Koppel model
37,125	3,047	240	Model-2

References

1) Haywood B. C., Thorson I. M. : "The Scattering Law for Light and Heavy Water at 20°C and 150°C," BNL-719, p. 26, 1962, Haywood, B.C. : "Comparison of the Scattering Law for Water at 22°C and 150°C," AERE—R4484, 1964.

2) Kottwitz D. A., Leonard B. R. : "Proceedings of Symposium on Inelastic Scattering of Neutrons in Solids and Liquids, Chalk River," Vol. 1, p. 359, IAEA, 1963.

3) Kirouac G. J., Moore W. E. and Seemann K. W. : "Double Differential Scattering Cross Sections and Scattering Law for H_2O at 302°K," KAPL-M-6536, 1966.

4) Harling O. K. : "Compilation of Doubly Differential Cross Sections and the Scattering Law for H_2O and D_2O at 299°K and for H_2O at 268°K," BNWL-436 (UC-34), 1967.

5) Koppel J. U. : "Reactor Physics in the Resonance and Thermal Regions," MIT Press, p. 27, 1967.

6) Haywood B.C. : *J. Nucl. Energy*, 21, 249 (1967).

7) Beyster J.R. : *Nucl. Sci. Eng.* 31, 254 (1968).

8) Arai E. and Kuchle N. : *Nukleonik*, 7, 416 (1965).

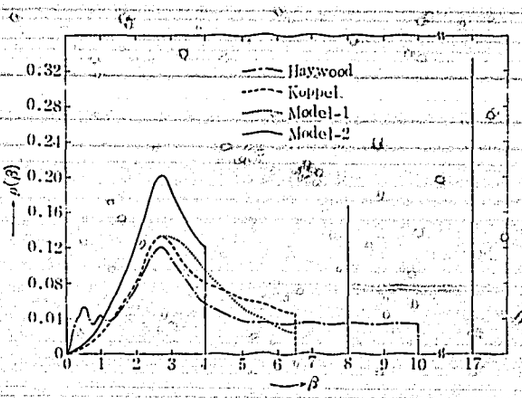

Fig. 1 Frequency distributions for room temperature H_2O.

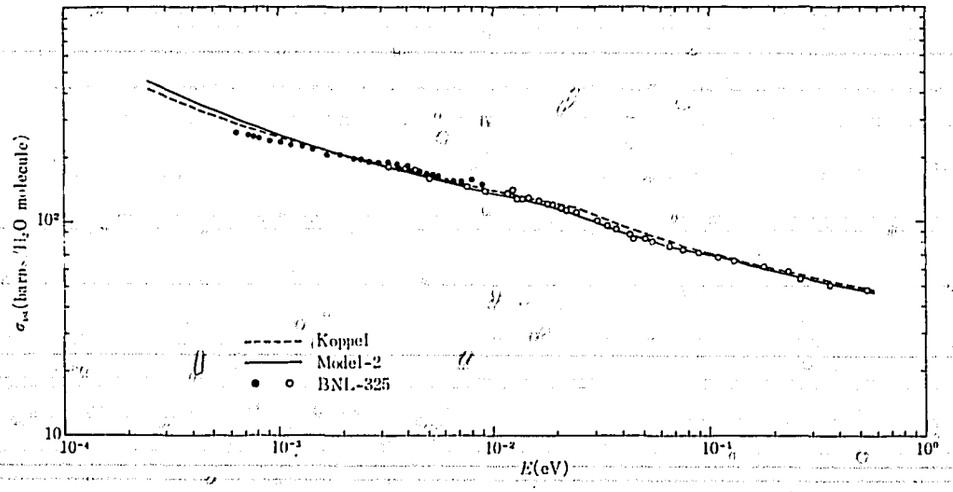

Fig. 2 Total cross section of H_2O.

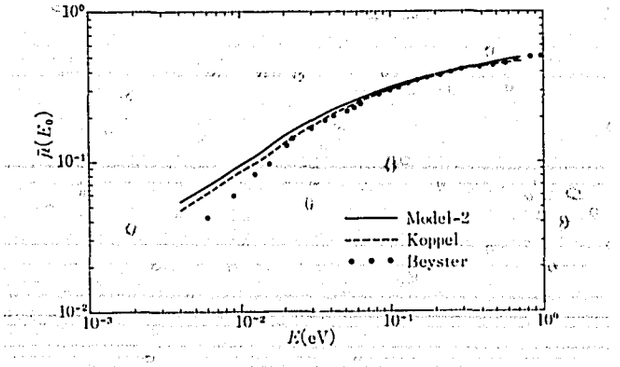

Fig. 3 Average cosine of scattering angle for H in H_2O. (oxygen included)

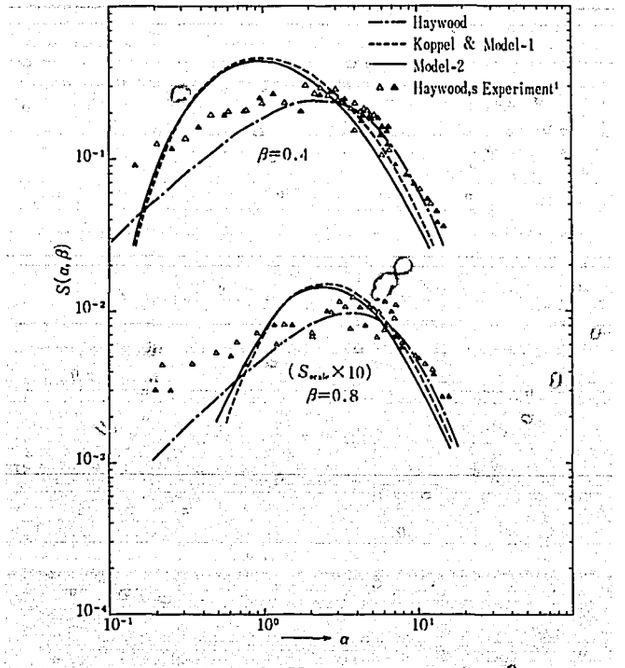

Fig. 4 a $S(\alpha, \beta)$ for H_2O at room temperature.

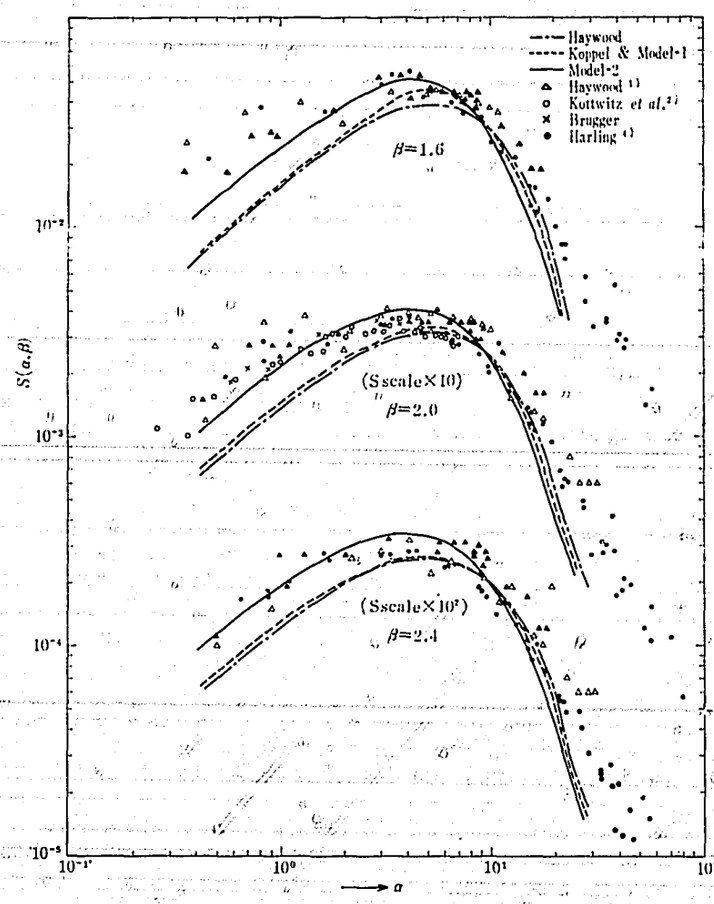

Fig. 4 b S(α, β) for H_2O at room temperature.

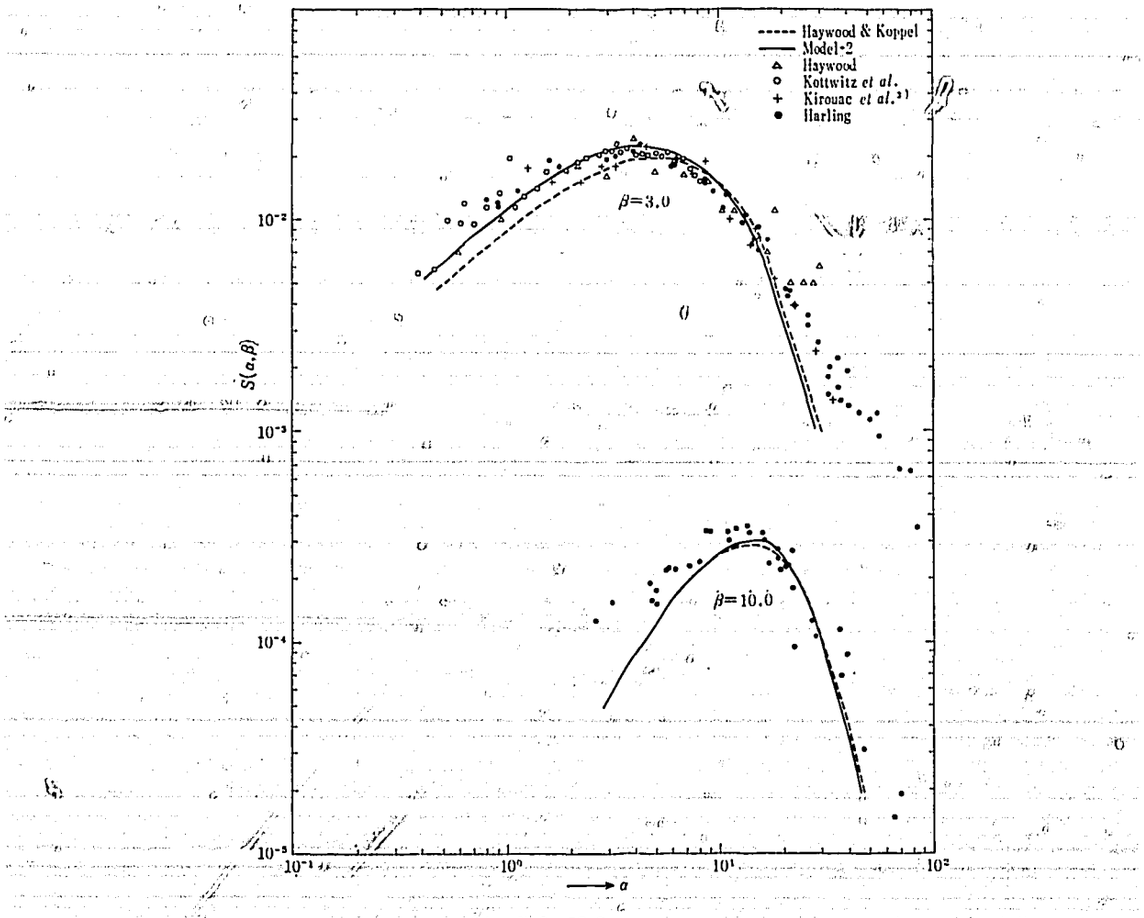

Fig. 4 c S(α, β) for H_2O at room temperature.

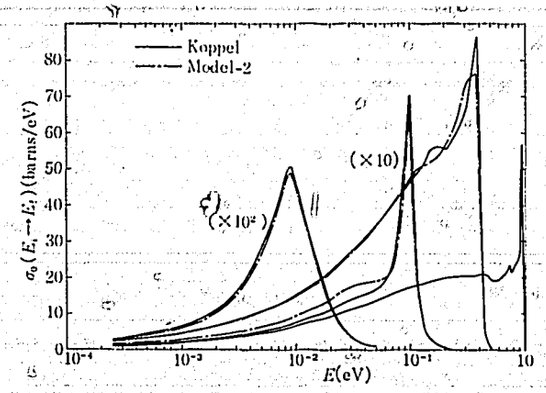

Fig. 5 $\sigma_0(E_1 \rightarrow E_l)$ for H in H_2O.
(Legendre moment : $L=0$)

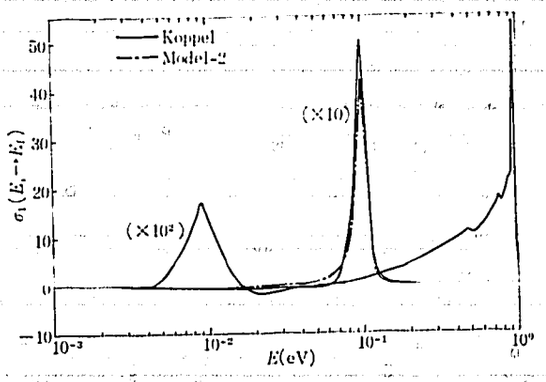

Fig. 6 $\sigma_1(E_1 \to E_1)$ for H in H_2O.
(Legendre moment : $L=1$)

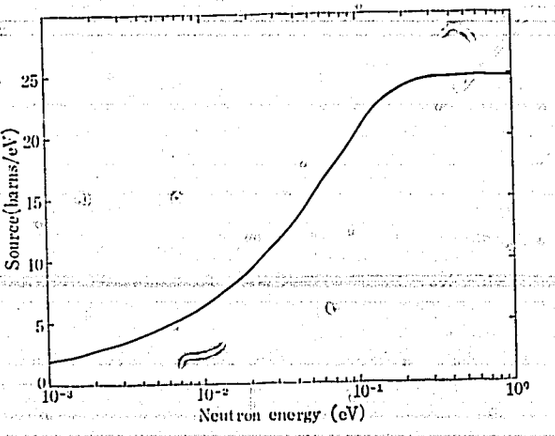

Fig. 7 Spectrum of thermal neutron source from hydrogen in H_2O (E_c=0.7067 eV)

3. 1. 2 Light Water (Supplement)

Thermal Neutron Scattering by Water Vapour

(1) Introduction

As the most typical model for water scattering kernel such as the Nelkin model[1] assumes the free translational motion of a molecule as a whole, the model for liquid water could be applied to water vapour when the rotational motion is treated appropriately. In the present note we calculate the scattering law and total scattering cross section for water vapour using simple models and compare them with the experimental results, especially paying some attentions to the temperature dependence of the total scattering cross sections. Theoretical models employed here are the free gas model, Krieger-Nelkin model which can be deduced from Nelkin model by treating the free rotation classically and the spherical top model in which the free rotation is treated quantum mechanically. The assumption of symmetrical top molecule is inadequate for the case of water vapour, but this model gives the reasonable theoretical prediction of scattering law.

The experiments performed on the water vapour are few and there are large and unexplained differences between two total cross section data[2),3)]. The scattering law for water vapour which was measured by GLÄSER[4] are the only experimental values available. It is desirable that more experiments are performed on water vapour.

(2) Calculation

Models employed here are the free gas model, Krieger-Nelkin model and the spherical top model. In the last two models we have neglected the excitation of vibrational motion.

Free gas model

This is the simplest model which neglects the internal vibration and the rotational motion, and assumes the scattering by water vapour as the scattering by a single proton.

The scattering law is,

$$S(\alpha,\beta)=\sqrt{\frac{1}{4\pi\alpha}}\cdot e^{-\frac{\alpha^2+\beta^2}{4\alpha}} \tag{1}$$

The total scattering cross section is,

$$\sigma(E)=\sigma_f\left\{\left(1+\frac{1}{2E}\right)\mathrm{erf}\left(\sqrt{\frac{E}{T}}\right)+\frac{1}{\sqrt{\pi}}\sqrt{\frac{T}{E}}\,e^{-E/T}\right\} \tag{2}$$

Krieger-Nelkin model[5]

This model treats the rotational motion classically, which corresponds to the increase of the effective mass for translational motion.

The scattering law is,

$$S(\alpha,\beta)=\sqrt{\frac{1}{4\pi\bar{\alpha}}}\,e^{\frac{-\bar{\alpha}^2+\beta^2}{4\bar{\alpha}}}\,e^{-2\bar{A}\gamma T\alpha} \tag{3}$$

where $\bar{\alpha}=\frac{M_H}{M}\alpha$, $\quad \bar{A}=\frac{\bar{M}}{m}=2.055$

The total scattering cross section is,

$$\sigma(E)=\frac{2\sigma_f\bar{\omega}}{E}\left\{\mathrm{erf}\left(\sqrt{C}\right)-\sqrt{1-p}\,e^{-C_p}\,\mathrm{erf}\left(\sqrt{C(1-p)}\right)\right\} \tag{4}$$

where

$$\bar{\omega}=\frac{1}{2m\gamma},\qquad C=\frac{\bar{M}E}{mT},\qquad p=\frac{1}{1+\frac{\alpha'^2}{4\beta'}}$$

$$\alpha'=\frac{m+\bar{M}}{mT}$$

$$\beta'=\frac{2\bar{M}\gamma}{T}$$

$$\gamma=\sum_\lambda\frac{1}{6\omega_\lambda}(\vec{C}^{(\lambda)})^2=0.753\ eV^{-1}$$

Spherical top model[6]

This model treats the rotational motion of spherical top quantum mechanically. We assume the average of the three components of moment of inertia of a water molecule as the one for a spherical top molecule.

The scattering law is,

$$S(\alpha,\beta)=\sqrt{\frac{1}{4\pi\alpha}}\,e^{-\frac{\alpha^2+\beta^2}{4\alpha}}\,e^{-2MT\gamma\alpha}$$

$$+\sum_j B_T(j)\sum_J\frac{2J+1}{2j+1}\,e^{-\frac{U_{jJ}}{4\alpha}}\sum_{n=|j-J|}^{|j+J|}j^2{}_n(\sqrt{2MT\alpha}\,b)$$

where

$$B_T(j)=\frac{(2j+1)\exp\left(-\frac{j(j+1)}{2IT_c}\right)}{\sum_j(2j+1)^2\exp\left(-\frac{j(j+1)}{2IT}\right)},$$

$$U_{jJ}=\left(\frac{S_{jJ}}{T^2}-2\beta\frac{S_{jJ}}{T}-2\alpha\frac{S_{jJ}}{T}\right),$$

$$S_{jJ}=\frac{j(j+1)}{2I}-\frac{J(J+1)}{2I},$$

b : distance from a center of mass to a scattering atom,

I : moment of inertia,

$j_n(x)$: spherical Bessel function.

The total scattering cross section for this model has not been calculated.

(3) Results and Comparison

In Fig. 1 the total cross sections at 100°C are compared with theories. According to HEINLOTH, the total cross sections of two different phase of water differs about 30 barns, which is close to the difference between the calculated values by the liquid model and the free gas model. This difference can not be explained by the Krieger-Nelkin model In Fig. 2 the temperature dependence of the total cross section is shown. The energy gradient of Hofmeyer's experimental results can be predicted by the Krieger-Nelkin model but the experimental data are always larger than the theoretical value by 5 to 10 barns.

The scattering laws calculated with three models are compared with experiment in Fig. 3. As far as the scattering law data are concerned, the spherical top model can predict most precisely the experiment. This shows that, at least for this molecule the treatment of rotation is essential. Asymmetrical treatment of rotation may give further improvement.

As water vapour is one of the important and simple molecules, more experimental informations are desirable to check the theory or theoretical assumptions. At present, we can conclude that the precise treatment of rotational motion is neccessary for the analysis of the thermal neutron scattering from water vapour.

References

1) NELKIN M.S. : *Phys. Rev.* 119, 741 (1960).
2) HEINLOTH K. : *Z. Physik,* 163, 218 (1961).
3) HOFMEYER C.H. : Unpublished (1963), see SPRINGER, T. : *Nukeonik,* 6, 87, (1964).
4) GLÄSER W. : "Inelastic Scattering of Neutrons in Solids and Liquids," Vol. I, p. 307, IAEA, Vienna, (1963).
5) KRIEGER T.J., NELKIN M.S. : *Phys. Rev.,* 106, 290 (1957).
6) GRIFFING G.W. : "Inelastic Scattering of Neutrons in Solids and Liquids," Vol. I, p. 435, IAEA, Vienna (1963).

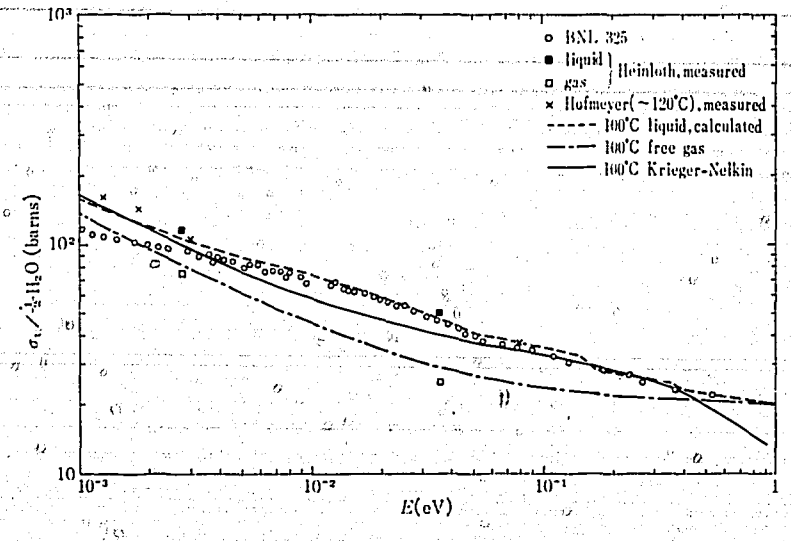

Fig. 1 Total scattering cross section of water at 100°C.

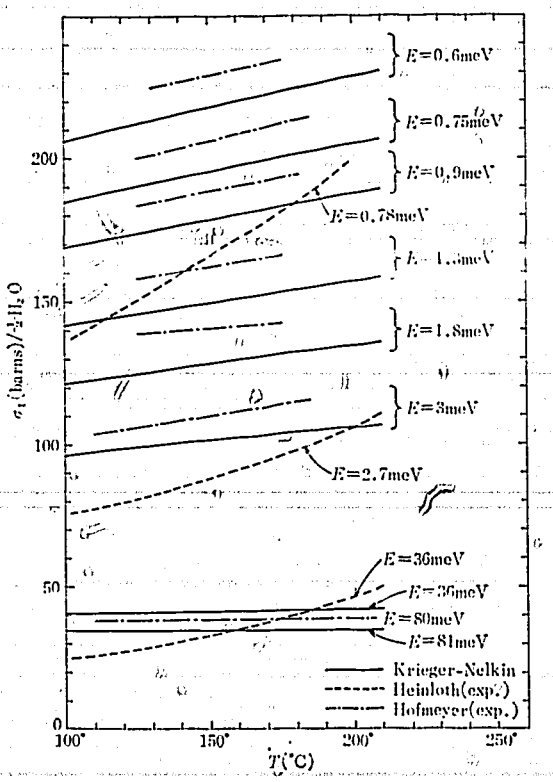

Fig. 2 Temperature dependency of total cross section of water vapour.

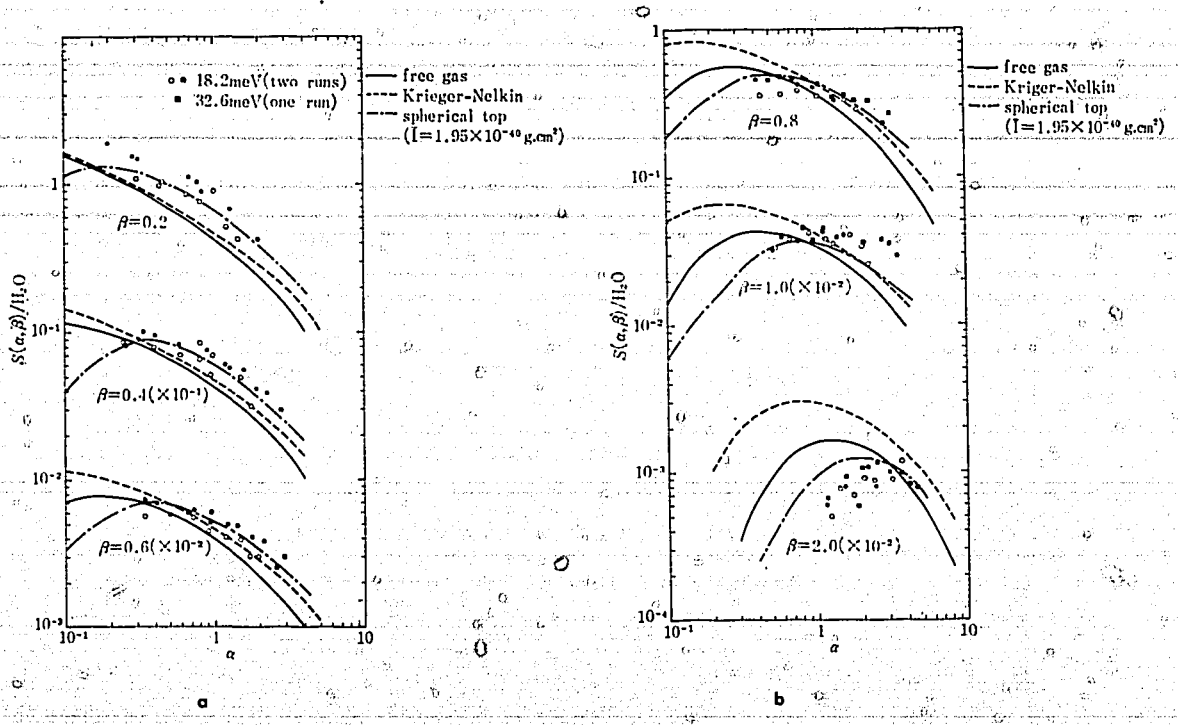

Fig. 3 Scattering law for water vapour at 241°C and 25 atm.

3. 2 Heavy Water

3. 2. 1 Heavy Water

(1) Introduction

We present here the spectral density function for heavy water which can predict successfully, to some extent, the experimental results on thermal neutron scattering properties. Although the formulation is essentially based on the coherent scattering which will be discussed in the next chapter, the calculation is limited within the frame of the incoherent scattering approximation. In near future, coherent scattering calculation is planned.

Physical interpretation of the present model will be given in the next chapter, so that here we only give the results and comparison with experiment. Calculation was performed with the UNCLE, GASKET and FLANGE codes.

(2) Spectral Density Function

Spectral density functions for deuteron and oxygen atoms are given in Table 1 and also shown in Fig. 1.

(3) Scattering Law

Scattering law of heavy water in the incoherent scattering approximation is,

$$S(\alpha,\beta)=\frac{1}{2(A_D^2+C_D^2)}\cdot\sum_{\nu=D,O}(A_\nu^2+C_\nu^2)S_{\nu\nu}(\alpha,\beta) \qquad (1)$$

where A_ν and C_ν are the amplitudes of coherent and incoherent scatterings respectively. $S_{\nu\nu}(\alpha,\beta)$ is self term of scattering law for deuteron and oxygen.

Comparison with experimental results is performed in the next chapter (see Fig. 4 on p. 41). Contribution of each term of Eq. (1) will be seen in Fig. 3 on p. 40. Although the present spectral density function can also fit the scattering law at high temperature (423°K), the following kernel estimation was performed for only room temperature.

(4) Scattering Kernel

Scattering kernels for deuteron and oxygen are listed in Appendix. Typical kernels as the function of final energy are shown in Figs. 2 and 3.

(5) Total Scattering Cross Section and $\bar{\mu}$ (E)

Total scattering cross section $\sigma_0(E)$ and the first Legendre moment $\sigma_1(E)$ are listed in Table 2. Total cross section is compared with experiments compiled in BNL-325 in Fig. 4. Agreement is excellent except at low neutron energy, where experimental result is low because of coherent scattering effect.

In Fig. 5, $\bar{\mu}(E)$ is compared with experiments.[1), 2)] The reason of fluctuation of calculated $\bar{\mu}(E)$ at higher energy is due to $\sigma_1(E)$, whose oscillatory values depend on the mesh of energies as shown in Fig. 6. This indicates the necessity of employing the fine energy mesh up to high energy region to calculate the reliable scattering kernels.

(6) Conclusion

Further check for the kernel was performed using the DIP code. Diffusion parameters using up to $l=1$ kernels are compared with experiment (Table 3). Agreement between theory and experiment for diffusion constant is fairly good. The calculated diffusion cooling constant C falls between the largest and the lowest experimental data. Therefore, the present model can be used for the calculation for neutron thermalization properties of heavy water.

References

1) Beyster J.R. *et al.*, : "Pulsed Neutron Research", Vol. 1, p. 407, 1965, IAEA, Vienna.
2) Springer T., *et al.*, Proc. 3rd. UN Int. Conf. PUAE 1964, P/763.
3) Kallfelz J. : Arbeitsbericht Nr. 17/65, 1965, Karlsruhe.
4) Kussmaul G., Meister, H. : J. *Nucl. Engergy A/B*, 17, 411 (1963).
5) Malaviya B.K., Profio, A.E. : *Trans. ANS.*, 6, 58 (1963).
6) Parks P.B., *et al.* : *Nucl. Sci. Eng.*, 33, 209 (1968).

Table 1. Spectral density for D_2O

		ε (eV)	$\rho_{DD}(E)$	$\rho_{OO}(E)$
ρ^{ac} (E)		0.004	3.855	30.84
		0.008	4.426	35.41
		0.012	3.534	28.27
		0.016	3.462	27.70
		0.020	3.248	25.98
		0.024	2.868	22.94
		0.028	2.320	18.56
		0.032	1.258	10.28
		0.036	0.0	0.0
	Discrete levels	0.048	0.4560	0.08801
		0.146	0.1483	0.03779
		0.3385	0.2957	0.07419

Table 2a. $\sigma_0(E)$ and $\sigma_1(E)$ for a deuteron atom in D_2O

Energy (eV)	$\sigma_0(E)$ Inelastic (barns)	$\sigma_0(E)$ Elastic (barns)	$\sigma_1(E)$ Inelastic (barns)	$\sigma_1(E)$ Elastic (barns)
0.00025	7.35424	7.61268	−0.47783	0.06136
0.00101	4.07890	7.07109	−0.51006	0.23591
0.00228	3.32483	6.27711	−0.57322	0.47147
0.00405	3.16337	5.36353	−0.62579	0.71042
0.00632	3.41166	4.44778	−0.66666	0.90572
0.00911	3.65728	3.60964	−0.66711	1.03208
0.0124	3.87995	2.90158	−0.62020	1.08442
0.01619	4.08775	2.33212	−0.49586	1.07547
0.02049	4.10182	1.88712	−0.38066	1.02436
0.0253	4.10377	1.54478	−0.22056	0.94964
0.03061	4.00668	1.28234	−0.10249	0.86582
0.03643	3.93824	1.07918	0.03925	0.78203
0.04276	3.82206	0.91990	0.11290	0.70334
0.04959	3.85635	0.79333	0.20793	0.63209
0.05692	3.89565	0.69119	0.25966	0.56876
0.06517	3.95897	0.60370	0.35486	0.51029
0.07485	3.92689	0.52563	0.41185	0.45481
0.08612	3.89598	0.45684	0.48971	0.40335
0.09919	3.86129	0.39665	0.55340	0.35632
0.11398	3.84385	0.34518	0.61645	0.31464
0.13123	3.80278	0.29980	0.66934	0.27677
0.1525	3.71867	0.25799	0.69205	0.24093
0.179	3.75000	0.21980	0.81672	0.20741
0.2124	3.63327	0.18523	0.81567	0.17644
0.2546	3.64271	0.15453	0.91251	0.14841
0.3081	3.64530	0.12770	0.99618	0.12352
0.376	3.33586	0.10464	0.81679	0.10183
0.4618	3.33074	0.08520	0.86754	0.08334
0.5702	3.41785	0.06900	0.98934	0.06778
0.7067	3.35372	0.05567	0.97983	0.05488

Table 2b. $\sigma_0(E)$ and $\sigma_1(E)$ for a oxygen atom in D_2O

Energy (eV)	$\sigma_0(E)$ Inelastic (barns)	$\sigma_0(E)$ Elastic (barns)	$\sigma_1(E)$ Inelastic (barns)	$\sigma_1(E)$ Elastic (barns)
0.00025	4.14745	4.1267	−0.21392	0.03554
0.00101	2.38256	3.82150	−0.22393	0.13288
0.00228	2.06147	3.37637	−0.23928	0.26425
0.00405	2.01648	2.86811	−0.26423	0.39560
0.00632	2.20873	2.36345	−0.29403	0.50056
0.00911	2.40502	1.90647	−0.32834	0.56575
0.01240	2.63148	1.52462	−0.34849	0.58960
0.01619	2.84181	1.22066	−0.34400	0.058027
0.02049	2.98850	0.98522	−0.32589	0.54895
0.02530	3.10295	0.80529	−0.29740	0.50601
0.03061	3.19887	0.66798	−0.26375	0.45924
0.03643	3.26980	0.56197	−0.23991	0.41333
0.04276	3.32079	0.47897	−0.20176	0.37073
0.04959	3.36560	0.41304	−0.17416	0.33249
0.05692	3.40278	0.35986	−0.15071	0.29870
0.06517	3.43552	0.31431	−0.12496	0.26765
0.07485	3.47059	0.27366	−0.09427	0.23829
0.08612	3.49140	0.23785	−0.07271	0.21113
0.09919	3.51470	0.20651	−0.05172	0.18637
0.11398	3.54401	0.17971	−0.02819	0.16446
0.13123	3.55847	0.15609	−0.91271	0.14458
0.15250	3.56949	0.13432	0.00463	0.12580
0.17900	3.58685	0.11443	0.02925	0.10825
0.2124	3.58208	0.09644	0.03694	0.09205
0.2546	3.57486	0.08045	0.04008	0.07740
0.3081	3.56259	0.06648	0.03030	0.06440
0.3760	3.55780	0.05448	0.02632	0.05308
0.4618	3.56530	0.04356	0.01541	0.04343
0.5702	3.56980	0.03592	0.00763	0.03531
0.7067	3.41358	0.02898	0.00136	0.02859

Table 2c. $\sigma_0(E)$, $\sigma_1(E)$ and $\overline{\mu}(E)$ for D_2O

Energy (eV)	$\sigma_0(E)$ (barns)	$\sigma_1(E)$ (barns)	$\overline{\mu}(E)$
0.00025	38.208	−1.01132	−0.02462
0.00101	28.504	−0.63935	−0.02243
0.00228	24.642	−0.17853	−0.007245
0.00405	21.938	0.30063	0.013704
0.00632	20.291	0.68465	0.03374
0.00911	18.845	0.96725	0.05133
0.0124	17.719	1.16955	0.06600
0.01619	16.902	1.39549	0.08256
0.02049	15.9596	1.5105	0.09465
0.0253	15.205	1.6567	0.10895
0.03061	14.445	1.7221	0.11922
0.03643	13.866	1.8160	0.13097
0.04276	13.284	1.8015	0.13561
0.04949	13.078	1.8384	0.14057
0.05692	12.936	1.8048	0.13952
0.06517	12.875	1.8729	0.14547
0.07485	12.649	1.8773	0.14841
0.08612	12.435	1.9245	0.15476
0.09919	12.237	1.9541	0.15969
0.11398	12.102	1.9985	0.16513
0.13123	11.919	2.0241	0.16982
0.1525	11.657	1.9964	0.17126
0.179	11.641	2.1858	0.18776
0.2124	11.3155	2.1132	0.18675
0.2546	11.2497	2.2393	0.19905
0.3081	11.1751	2.3341	0.20887
0.376	10.4933	1.9166	0.18265
0.4618	10.4407	1.9606	0.18718
0.5702	10.5192	2.1572	0.20391
0.7067	10.2613	2.09937	0.20459

Table 3. Diffusion parameters for D_2O

		D_0 $\times 10^4$ (cm²/sec)	C $\times 10^4$ (cm⁴/sec)
Theory	Present	2.058	5.67
	Kallfelz[3]	2.024	4.72
Experiment	Kussmaul, Meister[4]	2.00±0.01	5.25 ±0.25
	Malaviya, Profio[5]	2.04±0.04	4.706±0.38
	Parks[6]	2.09±0.02	6.6 ±0.3

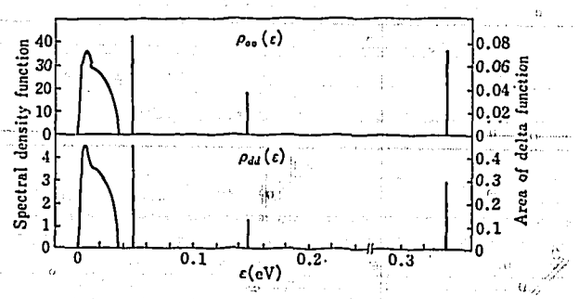

Fig. 1 Spectral density function for D_2O liquid at T=295°K.
(Note the change in scale of theordinate)

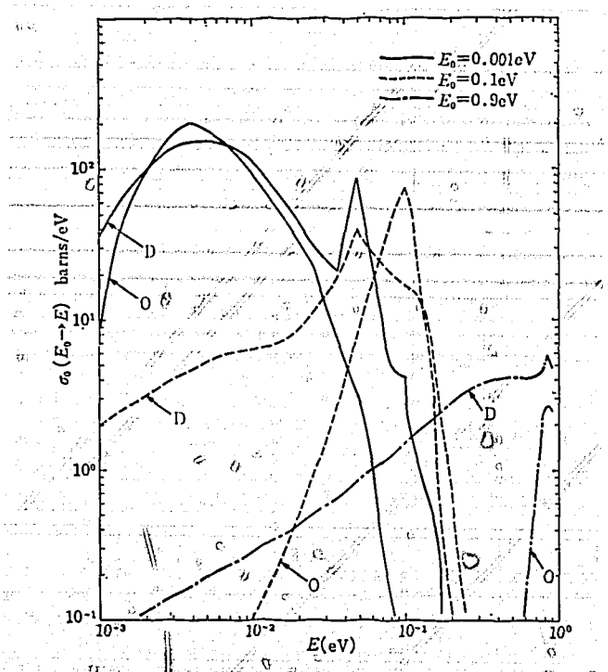

Fig. 2 $\sigma_0(E_0 \to E)$ for D_2O.
(Cross section due to 0 phonon process is not included)

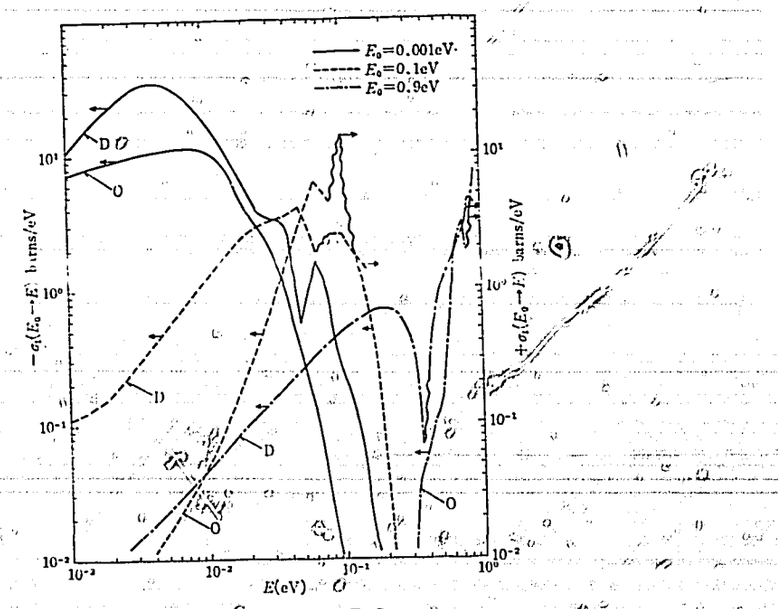

Fig. 3 $\sigma_1(E_0 \to E)$ for D_2O.
(Cross section due to 0 phonon process is not included. Note change of signs of kernel)

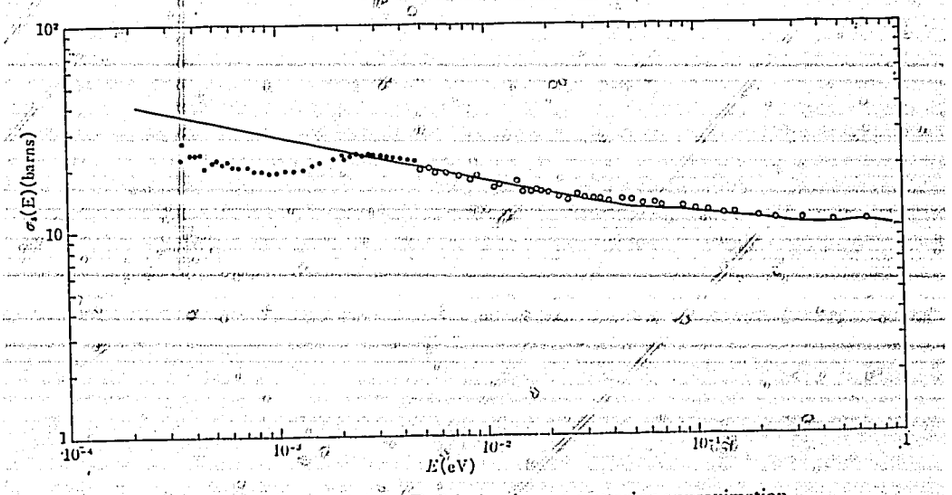

Fig. 4 Total cross section for D_2O in incoherent scattering approximation.
(Experimental from BNL 325)

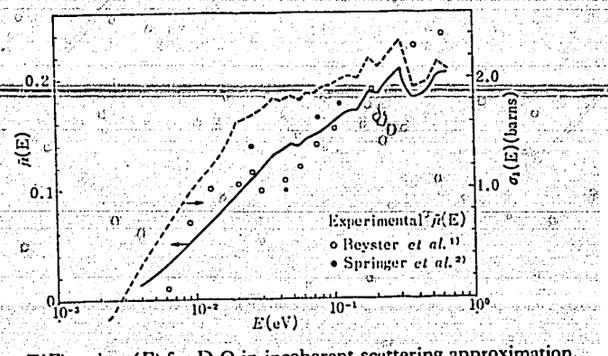

Fig. 5 $\bar{\mu}(E)$ and $\sigma_1(E)$ for D_2O in incoherent scattering approximation.

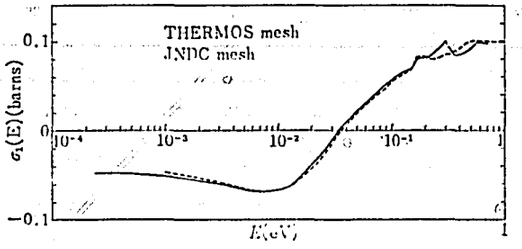

Fig. 6 Effect of energy mesh points on $\sigma_1(E)$ (inelastic)

3.2.2 Heavy Water (Supplement)

Coherent Scattering from Heavy Water

(1) Introduction

Neutron thermalization in heavy water, which is one of the two liquid moderators for a thermal neutron reactor, is more complicated than in another liquid moderator, i.e. light water. The reasons for this complicacy are:

(i) Deuteron is a coherent scatterer, in contrast with hydrogen which can be treated as an incoherent scatterer. This means that for the scattering from heavy water the contribution from atom pairs can not be neglected.

(ii) Free atom cross sections for deuteron and oxygen are comparable, while this is not the case for hydrogeneous moderator because the free atom cross section for hydrogen is usually much greater than those for the other atoms. This means that even if under the incoherent scattering approximation the scattering from oxygen can not be neglected.

Furthermore the scattering property of heavy water has the usual difficulty that may be encountered when one is treating with the thermal neutron scattering by liquid.

From scattering law data it is possible to determine the spectral density function when the scatterer is incoherent and only one type of nucleus contributes to the scattering. But since heavy water does not satisfy these conditions, the spectral density function which is deduced from scattering law data has ambiguity. Therefore, to determine the spectral density function for heavy water, a molecular dynamical treatment is required.

An incoherent scattering model for heavy water was presented by HONECK[1], which is equivalent to the Nelkin's model for light water[2]. MCMURRY[3] presented another incoherent scattering model, extending his MR model[4] for light water to heavy water. Coherent scattering calculation was performed by BUTLER[5] for the first time and the structure of the scattering law was explained successfully, which had not been predicted in the incoherent scattering approximation. This model was employed by KOPPEL and YOUNG[6] to calculate the integral parameters of scattering kernel for heavy water. They showed that in general the coherent scattering terms from the inter- and intra-molecular interference cancel largely each other in the case of total scattering cross section for example.

Recently PUCHER[7] presented the crystal model which described the translational motion as the mode with the Debye-Einstein frequency spectrum. He also successfully predicted the low energy structure of the total scattering cross section considering the pair distribution function in heavy water.

The different treatment of the coherent neutron scattering from heavy water was proposed by us[8]. The calculation is based on the Butler's model with experimentally determined acoustic spectral density for the translational motion of a molecule as a whole. In the present note we will describe the model in some detail and also comment on the effect of the multiple scattering.

(2) Definition of Generalized Spectral Density Function for Coherent Scatterer

We assume the isotropic harmonic vibrations for internal vibrations of a molecule as well as the translational motion of the molecule as a whole, and strongly hindered rotational motion expressed as the harmonic oscillation.

Scattering law for a pair of intra-molecular atoms ν and ν' of a molecular liquid is,

$$S_{\nu\nu'}(\vec{\kappa},\varepsilon)=e^{i\vec{\kappa}(\vec{R}_\nu-\vec{R}_{\nu'})}\frac{1}{2\pi}\int_{-\infty}^{\infty}dt\,e^{-i\varepsilon t}\,e^{-\frac{1}{2}(m_{\nu\nu}(0)+m_{\nu'\nu'}(0))\vec{\kappa}\vec{\kappa}}\,e^{m_{\nu\nu'}(t)\vec{\kappa}\vec{\kappa}} \tag{1}$$

where

$$\vec{\kappa}\vec{\kappa}m_{\nu\nu'}(t)\vec{\kappa}\vec{\kappa}=\frac{\hbar^2}{2m}\sum_{\lambda=1}^{3N}\frac{(\vec{\kappa}\vec{C}_{\nu'}{}^{(\lambda)*})(\vec{\kappa}\vec{C}_{\nu}{}^{(\lambda)*})}{\omega_\lambda}\left[(n_\lambda+1)e^{i\omega_\lambda t}+n_\lambda e^{-i\omega_\lambda t}\right] \tag{2}$$

$$n_\lambda=\frac{1}{2}\left\{\coth\left(\frac{\omega_\lambda}{2T}\right)-1\right\} \tag{3}$$

R_ν : equilibrium position vector for ν^{th} atom.

N : total number of atoms in a molecule.

Averaging over the orientation of a molecule in the sense of the Krieger-Nelkin approximation[9], one obtains

$$<e^{i\vec{\kappa}(\vec{R}_\nu-\vec{R}_{\nu'})}>_{\vec{\Omega}}=\frac{\sin(\kappa R_{\nu\nu'})}{\kappa R_{\nu\nu'}}, \tag{4}$$

$$<\vec{\kappa}\vec{\kappa}m_{\nu\nu'}(t)\vec{\kappa}\vec{\kappa}>_{\vec{\Omega}}=\frac{\hbar^2}{2m}\sum_{\lambda=1}^{3N}\frac{\kappa^2}{3}\frac{(\vec{C}_{\nu}{}^{(\lambda)*}\vec{C}_{\nu'}{}^{(\lambda)})}{\omega_\lambda}\left[(n_\lambda+1)e^{i\omega_\lambda t}+n_\lambda e^{-i\omega_\lambda t}\right] \tag{5}$$

where

$$R_{\nu\nu'}=|R_\nu-R_{\nu'}|$$

Then, on inserting Eqs. (4) and (5) into Eq. (1), we have

$$S_{\nu\nu'}(\vec{\kappa},\varepsilon)=\frac{\sin(\kappa R_{\nu\nu'})}{\kappa R_{\nu\nu'}}\overline{S}_{\nu\nu'}(\vec{\kappa},\varepsilon), \tag{6}$$

where

$$\overline{S}_{\nu\nu'}(\vec{\kappa},\varepsilon)=\frac{1}{2\pi}e^{\frac{-\hbar^2\kappa^2}{2M_{\nu\nu'}}\frac{1}{2}\left(\frac{M_{\nu\nu'}}{M_\nu}\right)\gamma_{\nu\nu}(0)+\frac{M_{\nu\nu'}}{M_{\nu'}}\gamma_{\nu'\nu'}(0)}\int dt\,e^{-i\varepsilon t}\,e^{\frac{\hbar^2\kappa^2}{2m}\gamma_{\nu\nu'}(t)} \tag{7}$$

$$\gamma_{\nu\nu'}(t)=\int_0^\infty\rho_{\nu\nu'}(\omega)\left[(n_\omega+1)\,e^{-i\omega t}+n_\omega\,e^{-i\omega t}\right]d\omega, \tag{8}$$

$$M_{\nu\nu'}=\sqrt{M_\nu M_{\nu'}}$$

Here we define the generalized spectral density function $\rho_{\nu\nu'}(\omega)$, as

$$\rho_{\nu\nu'}(\omega)=\rho_{\nu\nu'}^{ac}(\omega)+\frac{M_{\nu\nu'}}{3m}\sum_{\lambda=1}^{3N-3}(\vec{C}_{\nu'}{}^{(\lambda)*}\vec{C}_{\nu}{}^{(\lambda)})\delta(\omega-\omega_\lambda) \tag{9}$$

In the limit of free translation, $\rho_{\nu\nu'}^{ac}(\omega)$ should be

$$\rho_{\nu\nu'}^{ac}(\omega)=\frac{M_{\nu\nu'}}{M_{\text{mol}}}\delta(\omega), \tag{10}$$

where M_{mol} is the molecular mass.

The second term of the r.h.s. of Eq. (9) corresponds to three hindered rotations, approximated by triply degenerate torsional vibrations, and three optical vibrations, two of which are degenerate. From the orthonormality conditions and the completeness of the eigenvectors, it follows that

$$\int_0^\infty\rho_{\nu\nu'}(\omega)d\omega=\delta_{\nu\nu'} \tag{11}$$

This ensures applicability of Placzek's moment theorem, which can be written as

$$\int_{-\infty}^{\infty}S_{\nu\nu'}(\vec{\kappa},\omega)\,d\omega=<e^{i\vec{\kappa}(\vec{R}_\nu-\vec{R}_{\nu'})}>_T\fallingdotseq<\frac{\sin(\kappa R_{\nu\nu'})}{\kappa R_{\nu\nu'}}>_T, \tag{12}$$

$$\int_{-\infty}^{\infty} S_{\nu\nu'}(\vec{\kappa}, \omega)\hbar\omega d\omega = \frac{\hbar^2\kappa^2}{2M_\nu}\delta_{\nu\nu'}. \tag{13}$$

(3) Calculation of Scattering Law

The calculation of $\overline{S}_{\nu\nu'}(\vec{\kappa}, \omega)$ can be carried out by the phonon expansion procedure. But, the application of the Sjölander approximation needs some care in the present case. For the self term the validity of the approximation is assured by the central limiting theorem of statistics. For interference scattering, however, $\rho_{\nu\nu'}(\omega)$ can equally be negative or positive because of the orthogonality, as expressed by Eq. 11). The central limiting theorem is then no longer valid and, in fact, the Sjölander approximation occasionally gives a divergent result. The difficulty can be overcome as follows. We divide $\rho_{\nu\nu'}(\omega)$ into two parts, positive and negative definite parts. We apply the Sjölander approximation sepatately to each part of the scattering law corresponding to the above division. The final result is obtained by the convolution integral of these two scattering laws.* The short collision time approximation also leads to a divergent result. We can apply the short time expansion only to the scattering part corresponding to the positive definite spectral density, and the negative definite part has to be treated by the phonon expansion. The final expression for the calculation is as follows. In the following expressions we drop the subscripts ν and ν', if net necessary.

a) Phonon expansion

The usual phonon expansion method can be applied to the present case. The scattering law is, by using the notations closely after SUMMIT code,

$$\overline{S}_{\nu\nu'}(\vec{\kappa}, \omega) = \sum_n e^{-2W}\frac{1}{n!}(2W)^n\phi_n(\varepsilon), \tag{15}$$

where

$$2W = \frac{\hbar^2\kappa^2}{2M}\tilde{\gamma}(0), \tag{14}$$

$$\tilde{\gamma}(0) = \frac{1}{2}\left\{\frac{M}{M_\nu}\gamma_{\nu\nu}(0) + \frac{M}{M_{\nu'}}\gamma_{\nu'\nu'}(0)\right\}, \tag{16}$$

$$\phi_1(\varepsilon) = \frac{\rho(\omega)}{2\varepsilon\tilde{\gamma}(0)\sinh(\varepsilon/2T)}e^{\varepsilon/2T}, \tag{17}$$

$$\phi_n(\varepsilon) = \int\phi_1(\varepsilon-\varepsilon')\phi_n(\varepsilon')d\varepsilon', \tag{18}$$

b) Sjölander expansion

As it has been suggested, above, we divide the generalized spectral density as

$$\rho(\varepsilon) = \rho^{(1)}(\varepsilon) + \rho^{(2)}(\varepsilon), \tag{19}$$

where $\rho^{(1)}(\varepsilon) \geq 0$ and $\rho^{(2)}(\varepsilon) \leq 0$,

The scattering law in Sjölander approximation is,

$$\overline{S}(\vec{\kappa}, \varepsilon) = \sum_n e^{-2W}\left(\frac{\hbar^2\kappa^2}{2M}\right)^n\sum_{r=0}^{n} f_1 \cdot f_2 \cdot f_{34}, \tag{20}$$

where

$$f_1 = \frac{(\gamma^{(1)}(0))^r}{r!},$$

$$f_2 = \frac{(\gamma^{(2)}(0))^{n-r}}{(n-r)!},$$

$$f_{34} = \frac{1}{\sqrt{2\pi\kappa_2(n,r)}}e^{-\frac{(\varepsilon-\kappa_1(n,r))^2}{2\kappa_2(n,r)}},$$

$$\kappa_\nu(n,r) = r\kappa_\nu^{(1)} + (n-r)\kappa_\nu^{(2)},$$

$$\kappa_1^{(i)} = \frac{\alpha_1^{(i)}}{\alpha_\nu^{(i)}},$$

* This point was suggested by H. TAKAHASHI.

$$\kappa_2^{(i)} = \frac{\alpha_2^{(i)}}{\alpha_0^{(i)}} - \left(\frac{\alpha_1^{(i)}}{\alpha_0^{(i)}}\right)^2,$$

$$\alpha_0^{(i)} = \int_0^\infty \frac{\rho^{(i)}(\varepsilon)}{\varepsilon} \coth\left(\frac{\varepsilon}{2T}\right) d\varepsilon = \gamma^{(i)}(0),$$

$$\alpha_1^{(i)} = \int_0^\infty \rho^{(i)}(\varepsilon)\, d\varepsilon,$$

$$\alpha_2^{(i)} = \int_0^\infty \rho^{(i)}(\varepsilon)\, \varepsilon \cosh\left(\frac{\varepsilon}{2T}\right) d\varepsilon.$$

c) Short time expansion

Using the same notation, one can write $\overline{S}(\vec{\kappa}, \varepsilon)$ as,

$$\overline{S}(\vec{\kappa}, \varepsilon) = \sum_n e^{-2W} e^{\frac{\hbar^2\kappa^2}{2M}\gamma^{(1)}(0)} \frac{1}{n!}\left(\frac{\hbar^2\kappa^2}{2M}\right)^n (\gamma^{(2)}(0))^n \frac{1}{\sqrt{2\pi x_2^{(n)}}} e^{-\frac{(\varepsilon - x_1^{(n)})^2}{2x_2^{(n)}}}, \tag{21}$$

where

$$x_\nu^{(n)} = \frac{\hbar^2\kappa^2}{2M}\alpha_\nu^{(1)} + n\kappa_\nu^{(2)}.$$

(4) Generalized Spectral Densitral for Heavy Water

Inserting into Eq.(9) the eigenvectors and the eigen frequencies calculated by BUTLER, we obtain,

$$\rho_{DD}(\varepsilon) = \rho_{DD}^{ac}(\varepsilon) + 0.4560\delta(\varepsilon-\varepsilon_1) + 0.1483\delta(\varepsilon-\varepsilon_2) + 0.2957\delta(\varepsilon-\varepsilon_3), \tag{22}$$

$$\rho_{OO}(\varepsilon) = \rho_{OO}^{ac}(\varepsilon) + 0.08801\delta(\varepsilon-\varepsilon_1) + 0.03779\delta(\varepsilon-\varepsilon_2) + 0.07419\delta(\varepsilon-\varepsilon_3), \tag{23}$$

$$\rho_{D_1D_2}(\varepsilon) = \rho_{D_1D_2}^{ac}(\varepsilon) - 0.1039\delta(\varepsilon-\varepsilon_1) + 0.001003\delta(\varepsilon-\varepsilon_2) + 0.005042\delta(\varepsilon-\varepsilon_3), \tag{24}$$

$$\rho_{DO}(\varepsilon) = \rho_{OD}(\varepsilon) = \rho_{DO}^{ac}(\varepsilon) - 0.1245\delta(\varepsilon-\varepsilon_1) - 0.05203\delta(\varepsilon-\varepsilon_2) - 0.1063\delta(\varepsilon-\varepsilon_3), \tag{25}$$

where,

$$\varepsilon_1 = 0.048\text{eV}, \quad \varepsilon_2 = 0.146\text{eV} \text{ and } \varepsilon_3 = 0.3385\text{eV}$$

For the acoustic part of the frequency distribution $\rho_{\nu\nu}^{ac}(\varepsilon)$, we use the spectral density determined from the slow neutron experiment by LARSSON and DAHLBORG[10]. The shape of $\rho_{\nu\nu}^{ac}(\varepsilon)$ is assumed to be the same for every pair of atoms. The normalization is done with the use of Eq.(11) (see Figs. 1 and 2).

(5) Comparision with Experiment

As it will be seen from the discussion in section 3, the UNCLE code[11], which is a version of the SUMMIT code[12], is most readily utilized for the numerical calculation of the present problem with minor changes in the input quantities, input processing and formulas for the short collision time approximation. The version, UNCLE-DISTINCT, was prepared for use of IBM 7090 and 7044.

The total scattering law for the molecule is given by

$$S(\vec{\kappa}, \varepsilon) = \frac{1}{2(A_D^2 + C_D^2)} \sum_{\nu\nu'} (A^2_{\nu\nu'} + \delta_{\nu\nu'} C^2_{\nu\nu'}) S_{\nu\nu'}(\vec{\kappa}, \varepsilon), \tag{26}$$

where A_ν and C_ν are the amplitudes of coherent and incoherent scatterings, respectively.

In Figs. 3, the contributions of the interference scattering terms to the total scattering law are shown, and in Figs. 4 and 5, the calculated scattering laws are compared with the experimental data by HAYWOOD at $T=$ 295°K and 423°K[13]. Although $\rho_{\nu\nu'}(\varepsilon)$ may be temperature dependent, the spectral density function was assumed to be the same for both temperatures in the present calculations. The contribution from the distinct atom pair becomes less important as β becomes larger and the temperature becomes higher. The agreement between theory and experiment is good on the whole, especially in the range of large α. For small α, the measured scattering law is generally larger than calculated one. A part of this discrepancy may be attributed to the multiple scattering effect. This point will be discussed in the next section. In Fig. 6, Butler's result is compared for $\beta = 0.5$ with the present calculation. Since BUTLER assumed free translational motion of a molecule as a whole, his result failed to agree with measurement except for the large α region.

(6) Effect of Multiple Scattering

As it had been discussed by SLAGGIE[15], the multiple scattering correction for double differential scattering data is a very important factor. We made this correction for the experimental data by HAYWOOD, using the incoherent scattering kernel (see the previous section). SLAGGIE also discussed the model dependence of the multiple scattering correction. Further analysis using a more realistic model for heavy water, for example, a model including the coherent scattering, may be desirable.

The experimental geometry is assumed as shown in Fig. 7. The specimen is a disk of 6 cm diameter and held at 45° to the incident beam. The thicknesses of the samples are, 0.209 cm for E_0=0.109 eV and 0.242 cm for E_0=0.039 eV[14], where E_0 is the incident neutron energy. The calculation was performed only for room temperature case using the MUSE code.

In Figs. 8 and 9 the multiple scattering correction factors are shown for E_0=0.11 eV and E_0=0.04 eV. At small angles the multiple scattering correction factor becomes large and strongly dependent of the final energy, for small scattering angle. But for larger angles it tends to be flatter and approaches to unity.

From these results we corrected the multiple scattering for β=0.5 and β=1.0 (Figs. 10, 11, 12, 13 and 14). Agreement between theory and experiment was considerably improved especially in low α region. The multiple scattering correction seems one of the most important correction for experimental data, and produces some ambiguity when comparison is made between theory and experiment. Therefore it is desirable to establish a reliable method for the multiple scattering correction.

(7) Conclusion

The present model for heavy water can predict well the scattering laws at room and high (423°K) temperatures. The main part of the discrepancy between the present theory and experiment by HAYWOOD may be attributed to the multiple scattering effect.

One of the future problems is the calculation of the scattering kernel including the coherent scattering. By making a comparison with other recent experiments[16] we can develop a more realistic model for heavy water.

Acknowledgements

The author wishes to thank Dr. HAYWOOD for supplying detailed information concerning his experiment.

References

1) HONECK H.C. : *Trans. ANS.*, 5, 48 (1962)
2) NELKIN M.S. : *Phys. Rev.*, 119, 741 (1960)
3) MCMURRY H.L. : IN-1020 (1966)
4) MCMURRY H.L., RUSSEL G.J., BRUGGER R.M. : *Nucl. Sci. Eng.*, 25, 248 (1966)
5) BUTLER D. : *Proc. Phys. Soc.*, 81, 276 (1963)
6) KOPPEL J.U., YOUNG J.A. : *Nukleonik*, 7, 408 (1965)
7) PUCHER M. : *Nukleonik*, 10, 129 (1967)
8) KADOTANI H., IIJIMA, S. : *J. Nucl. Sci. Technol.* (*Tokyo*)., 4, 37 (1967)
9) KRIEGER T.J., NELKIN M.S. : *Phys. Rev.*, 106, 290 (1957)
10) LARSSON K.E., DAHLBORG U. : "Inelastic Scattering of Neutron in Solids and Liquids", Vol. *I*, p. 317 (1963), IAEA, Vienna.
11) IIJIMA S., TOKIZAWA M. : JAERI 1087 (1965).
12) BELL J. : GA-2492 (1962)
13) HAYWOOD B.C. : AERE-R4582 (1964)
14) HAYWOOD B.C. : private communication (1968).
15) SLAGGIE E.L. : *Nucl. Sci. Eng.*, 30, 199 (1967).

16) HARLING O.K., : *Nucl. Sci, Eng.*, 33, 41 (1968).

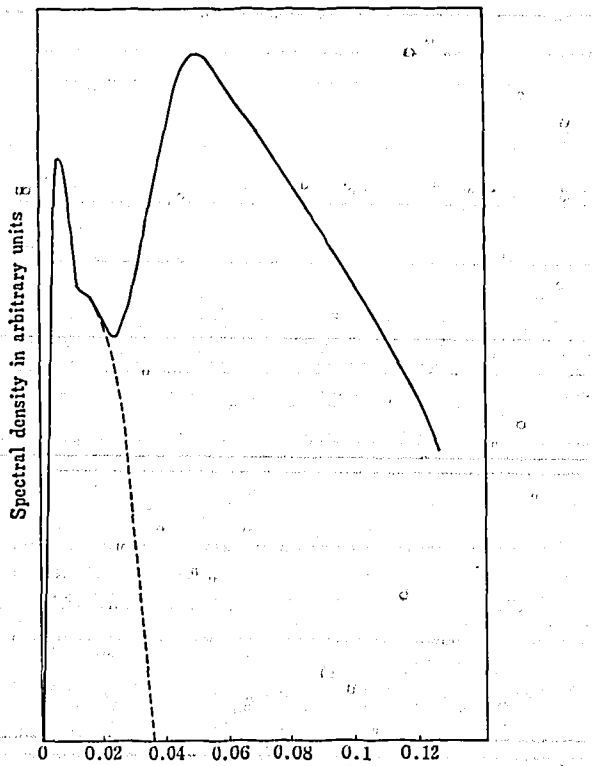

Fig. 1 Spectral density function for D_2O liquid for T=290°K[10].
(Dotted line shows the estimated $\rho^{ac}_{\nu\nu'}(\omega)$)

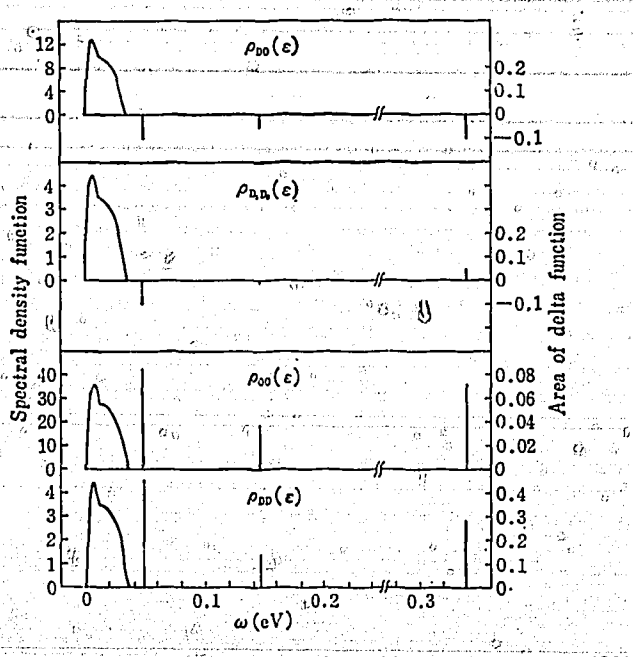

Fig. 2 Spectral density function for D_2O liquid for T=295°K and 423°
(Note change in scale of ordinate)

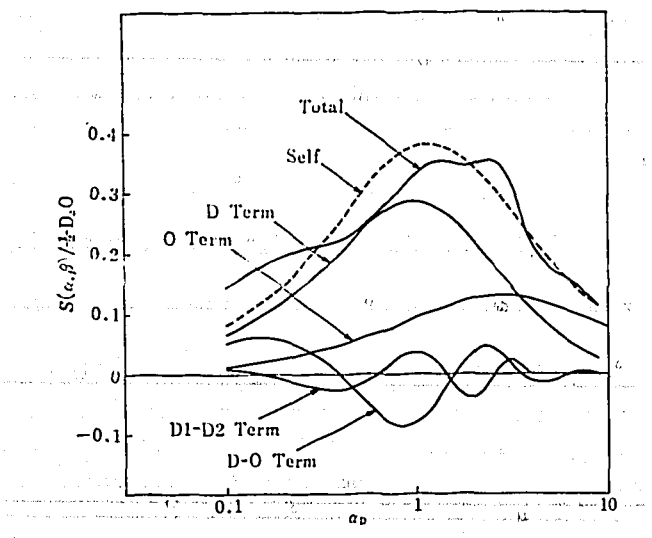

Fig. 3 a Comparision of the different terms contributing to scattering law at $\beta=0.4$ and $T=295°K$.

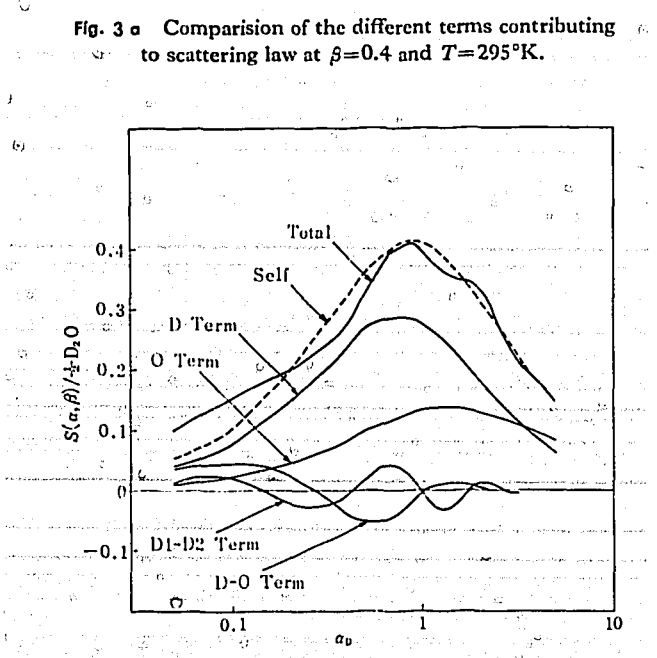

Fig. 3 b Comparision of the different terms contributing to scattering law at $\beta=0.4$ and $T=423°K$.

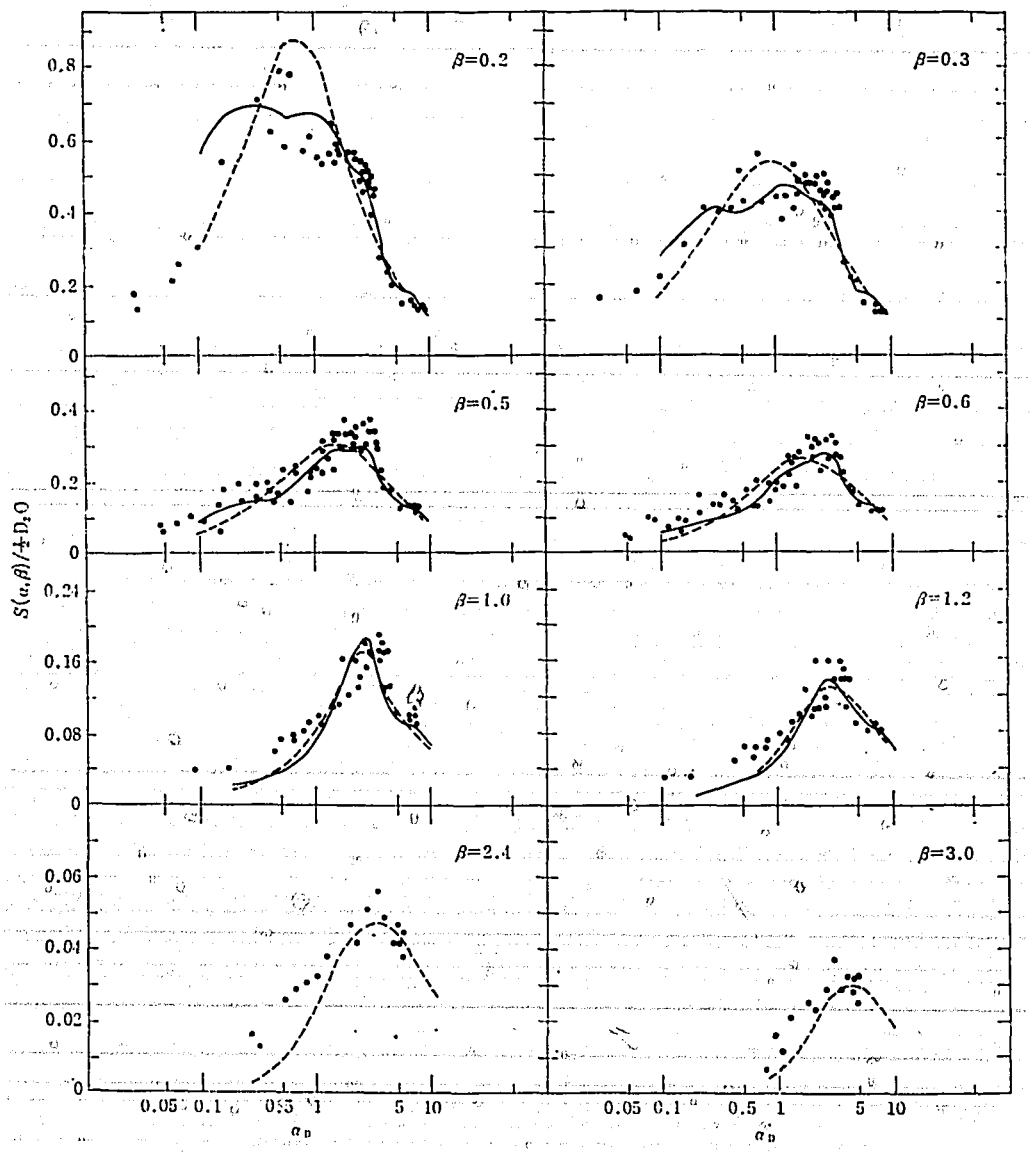

Fig. 4 Comparision of calculated scattering law with experiment[13].
———Total scattering law
·····Self term only

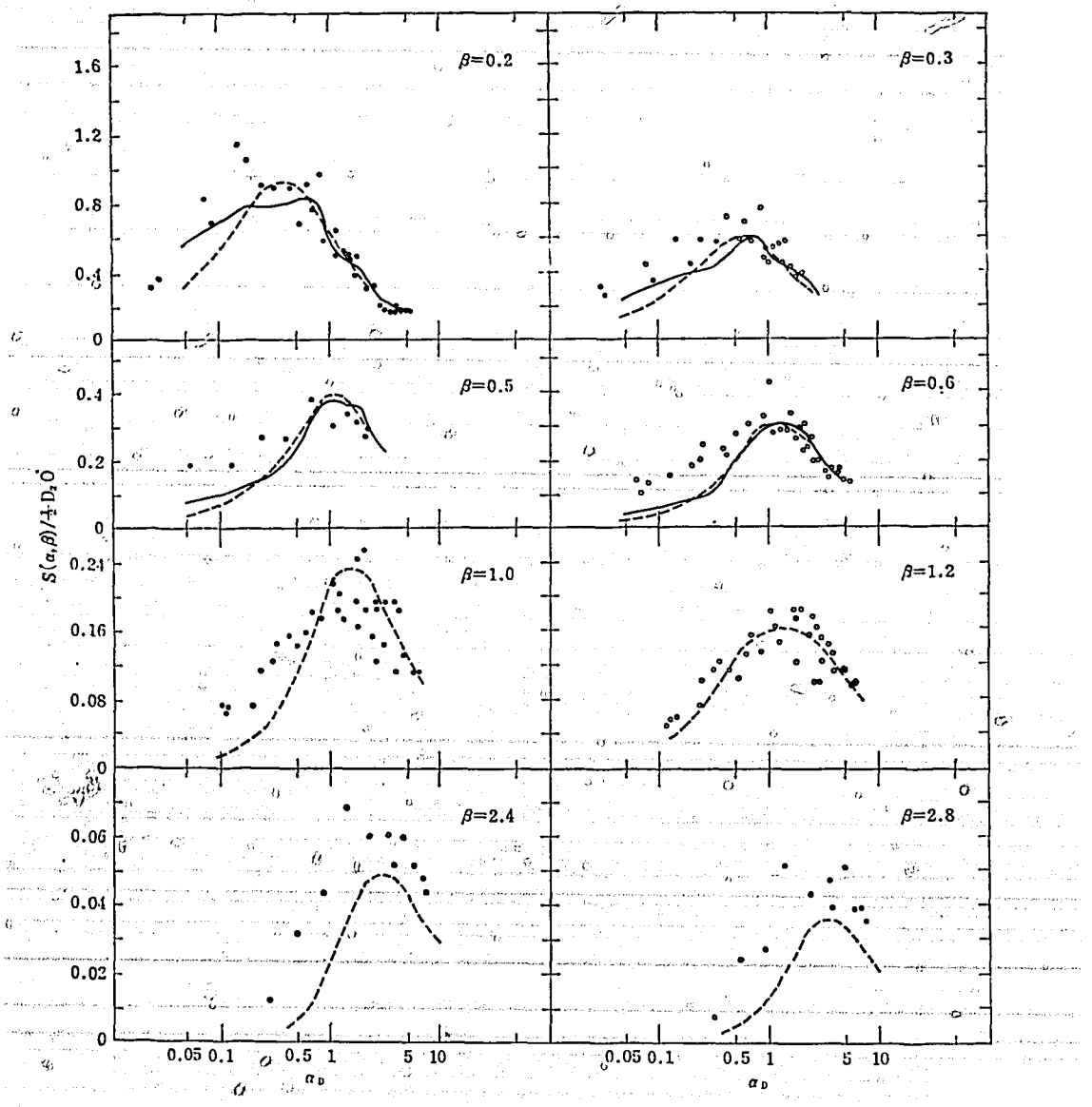

Fig. 5 Comparision of calculated scattering law with experiment[13] at $T=423°K$.
———Total scattering law
·····Self term only

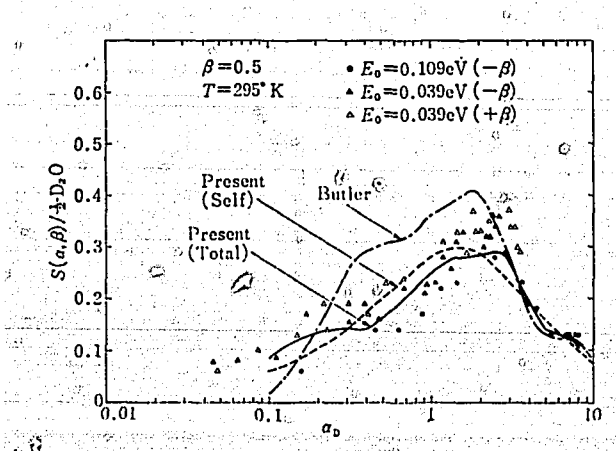

Fig. 6 Comparision of theoretical calculation with experiment at $\beta=0.5$ and $T=295°K$.

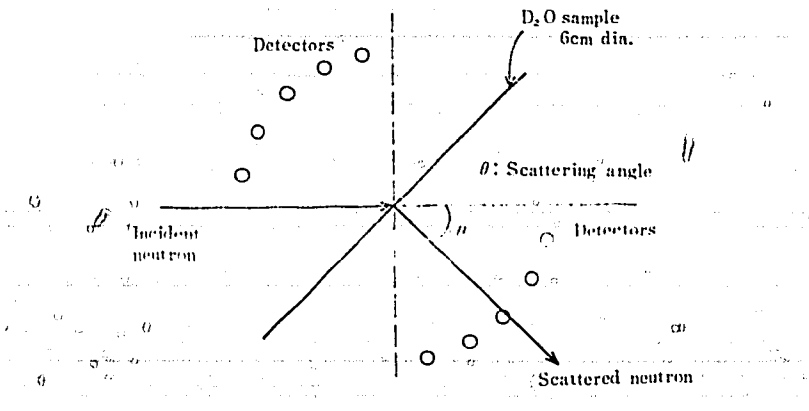

Fig. 7 Experimental geometry for scattering law measurement.

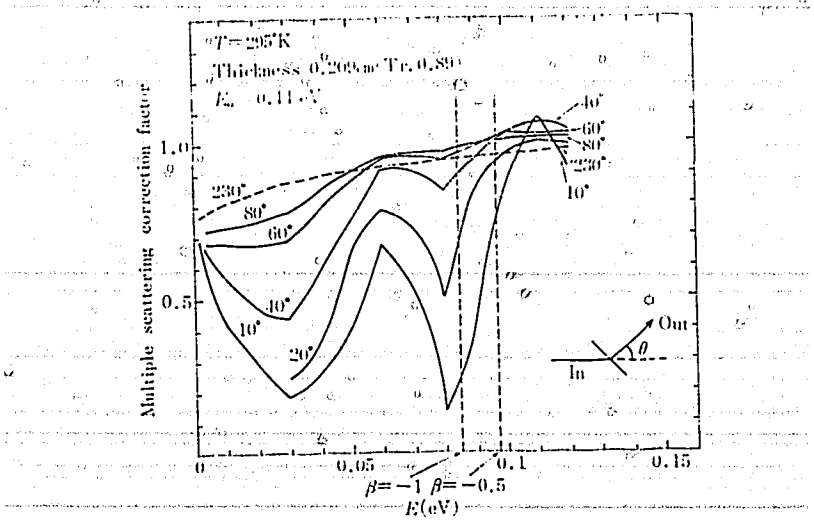

Fig. 8 Multiple scattering correction factor at D_2O in incoherent approx.

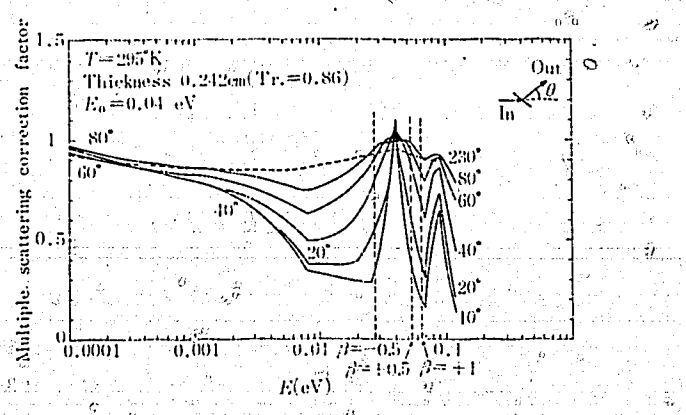

Fig. 9 Multiple scattering correction factor for D_2O in incoherent approx.

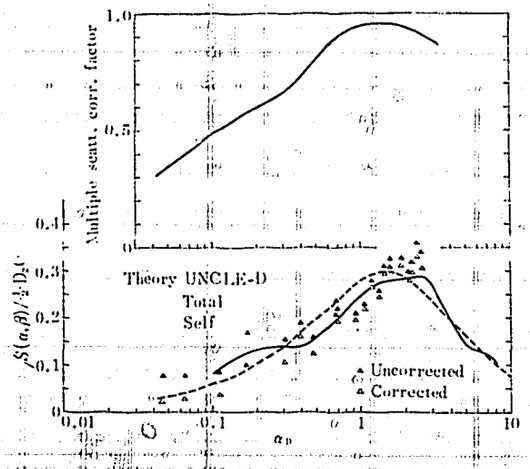

Fig. 10 Multiple scattering correction at $\beta=-0.5$ ($E_0=0.039$eV).

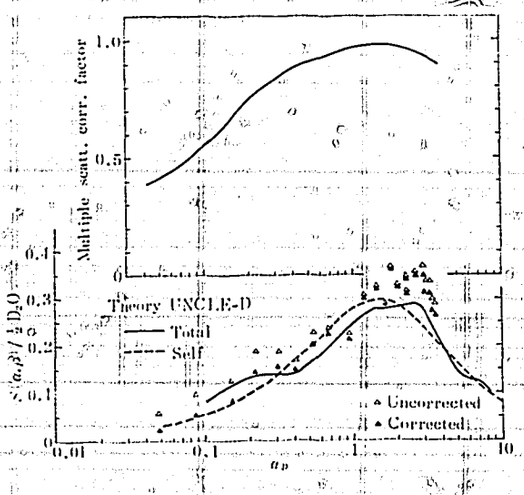

Fig. 11 Multiple scattering correction at $\beta=+0.5$ ($E_0=0.039$ eV).

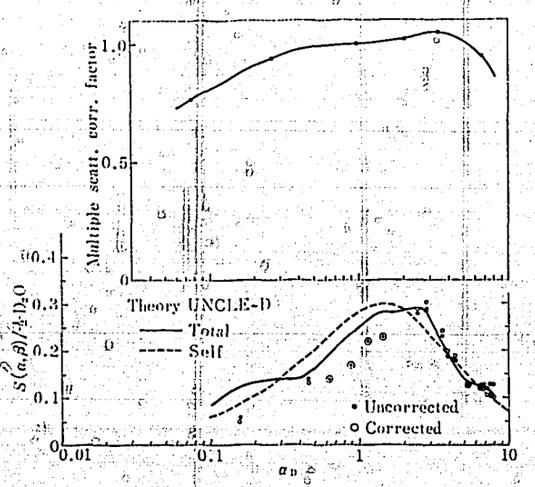

Fig. 12 Multiple scattering correction at $\beta=-0.5$ ($E_0=0.109$ eV).

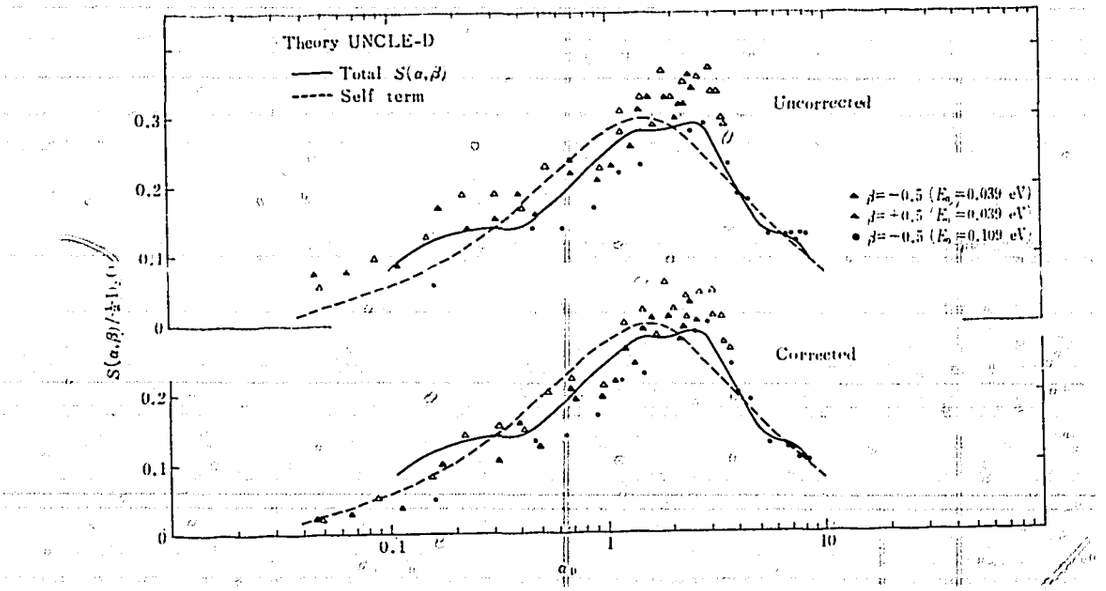

Fig. 13 Multiple scattering correction at $\beta=\pm0.5$

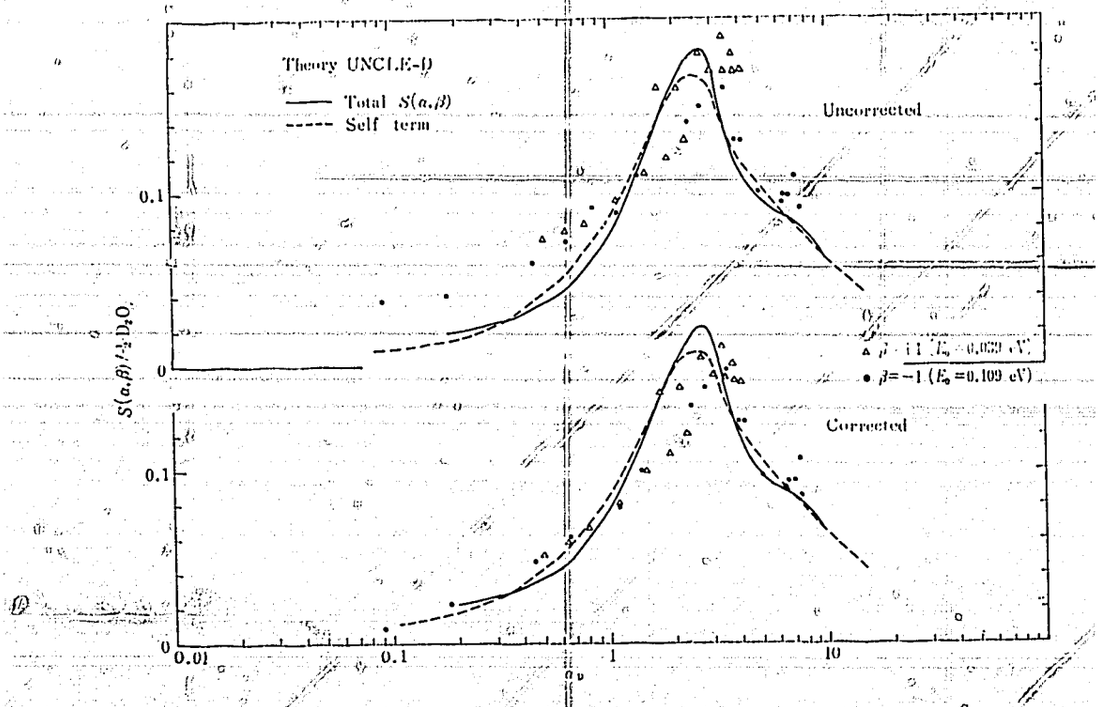

Fig. 14 Multiple scattering correction at $\beta=\pm1$

3.3 Graphite

3.3.1 Graphite

Frequency distributions of lattice vibrations in graphite have been obtained by YOSHIMORI & KITANO[1], YOUNG & KOPPEL[2] and CARVALHO[3]. YOSHIMORI & KITANO calculated the frequency distributions for out-of-plane and in-plane vibrations by means of the Houston's method[4]. The Houston's method solves the one dimensional lattice vibration for the particular wave vectors in the directions of symmetry axes and from

the frequency distributions for one-dimensional lattices the one for three-dimensional lattice is composed analytically. Hence the YKO (YOSHIMORI & KITANO) distribution has spurious singularities inherent in the one dimensional lattice. YOUNG & KOPPEL also used the Yoshimori-Kitano model, but they employed hte root sampling method to obtain the frequency distribution. Thus, YK (YOUNG & KOPPEL) distribution is free from the spurious singularities inherent in the Houston's method. YKO and YK distributions are shown in Fig. 1. CARVALHO performed the extensive measurements on scattering law for graphite at 533°K and determined the frequency distribution by means of the well known extrapolation procedure on $S(\alpha, \beta)/\alpha$. C(CARVALHO) distribution is shown in Fig. 3 in comparison with YK distribution. A remarkable resemblance is seen between them.

Scattering laws for graphite at 22°C calculated from YKO and YK distribution are shown in Fig. 4 in comparison with experimental values compiled by HAYWOOD & SINCLAIR[5]. Agreement with experimental values is better for scattering law calculated from YKO distribution than those from YK. It can not be concluded, however, that YKO distribution is better than YK distribution, because corrections to multiple scattering have not been applied to the experimental scattering law. From the theoretical point of view YK distribution is the best distribution among the available distributions at present.

In Fig. 5 comparisons are made between scattering laws at 300°K calculated from YK and C distribution[3]. There is seen little difference between them. What is effective in the calculation of the scattering cross section is the gross structure of the frequency distribution and the fine structure is rather irrelevant.

Some typical kernels for graphite at room temperature are shown in Fig. 6. These 30 energy point kernels were calculated from the YK distribution. The arrow on the abscissa indicates the incident energy of neutrons.

The incoherent inelastic, elastic (coherent+incoherent) and total scattering cross sections are shown in Fig. 7, together with the total elastic scattering cross section calculated in the incoherent approximation.

In Fig. 8 the transport cross section for graphite at room temperature is illustrated.

Recently PAGE published his experimental data on the scattering law for graphite at 1300°K and 1800°K[6]. PAGE evaluated also the frequency distribution for graphite at 1800°K from the scattering law data[7]. The phenomenological frequency distribution determined by PAGE are compared in Fig. 9 with the YK distribution for room temperature. In spite of the large difference in temperature, overall qualitative features of these distributions bear a remarkable resemblance, except the higher energy cut in the Page's distribution.

For examining the effect of the temperature dependence of the frequency distribution on the scattering cross section, scattering laws for graphite at 1800°K were calculated from the YK distribution at room temperature. These scattering laws are compared with the experimental values obtained by PAGE in Fig. 10. It should be noticed that resolution and multiple scattering corrections are not applied to the measured scattering law. Agreements between calculated and measured values are quite good. Structures seen in the measured scattering law can be attributed mainly to the one-phonon coherent scattering. It may be said from the results shown in Fig. 10 that the YK distribution can be used with reasonable accuracy in calculating the scattering cross section for graphite at high temperature.

Elastic and inelastic scattering cross sections for graphite at 1800°K are shown in Fig. 11 in comparison with those at room temperature. It is remarkable that the inelastic scattering cross section at 1800°K is considerably large in comparison with that at room temperature and has minimum point around 0.015 eV. The inelastic scattering cross section at 1800°K was calculated with UNCLE code from the averaged isotropic frequency distribution, because the execution time of the IBM-7044 computer was estimated to be more than two hours when the anisotropic frequency distribution was used. As for the elastic scattering cross section, the value at high temperature becomes smaller, contrary to the inelastic scattering cross section, than that at room temperature. Below 0.01 eV the temperature effect on the elastic scattering cross section is not large, but above 0.01 eV it is considerably large. For the neutron energy below the Bragg cut BNL 325 contains data on the total cross section at up to 1040°K. If these experimental values are plotted as a function of temperature T, they can be fitted with a linear function of T. The calculated value at 1800°K for the energy below

the Bragg cut lies on this extrapolated straight line. To evaluate the accuracy of the calculated total cross sections in the whole energy range experimental values are needed. We have, however, no available data on the elastic and inelastic (or total) scattering cross sections at 1800°K. It should be noticed that the cross sections at 1800°K were calculated from the YK distribution for graphite at room temperature.

Scattering kernels for graphite at 1800°K are shown in Fig. 12. These kernels were calculated from the isotropic YK frequency distribution.

References

1) Yoshimori A. and Kitano Y. : *J. Phys. Soc. Japan*, 11, 352 (1956).
2) Young J.A. and Koppel J.U. : *J. Chem. Phys.*, 42, 357 (1965).
3) Communicated by Gläser W. : KFK 602 (1967), also "Neutron Thermalization and Reactor Spectra, Vol. 1.", IAEA (1967).
4) Houston W.V. : *Rev. Mod. Phys.*, 20, 161 (1948).
5) Haywood B.C. and Sinclair R.N. : AERE-R 4732 (1964).
6) Page D.I. : AERE-R 5574 (1967).
7) Page D.I. : SM-104/79, IAEA Symposium on Neutron Inelastic Scattering, Copenhagen (1968).

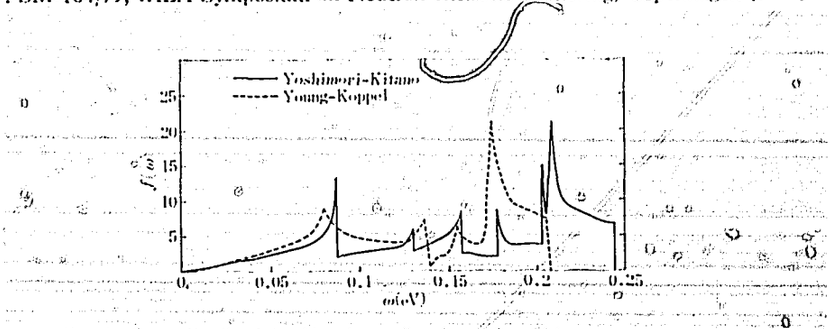

Fig. 1 Frequency distribution of in-plane vibrations of graphite at room temperature. Comparison between Yoshimori-Kitano and Young-Koppel distributions.

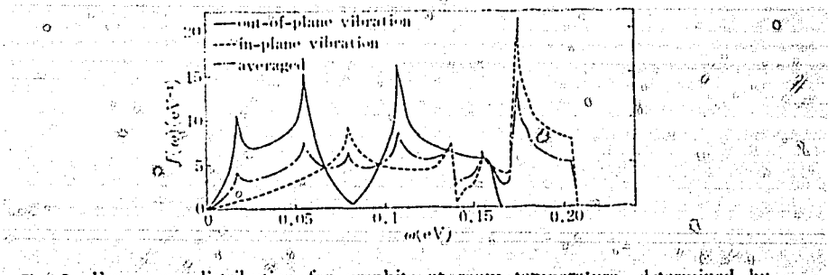

Fig. 2 Frequency distribution for graphite at room temperature, determined by Young and Koppel.

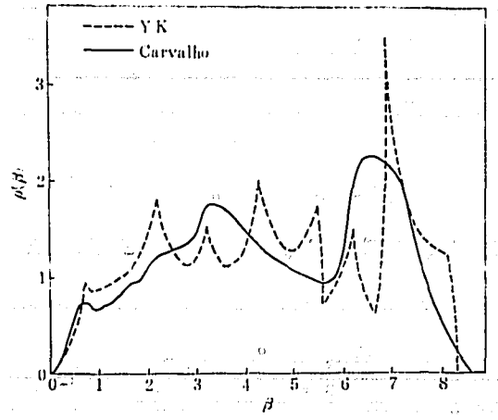

Fig. 3 Comparison between Young-Koppel and Carvalho frequency distributions for graphite at room temperature (in the averaged isotropic form).

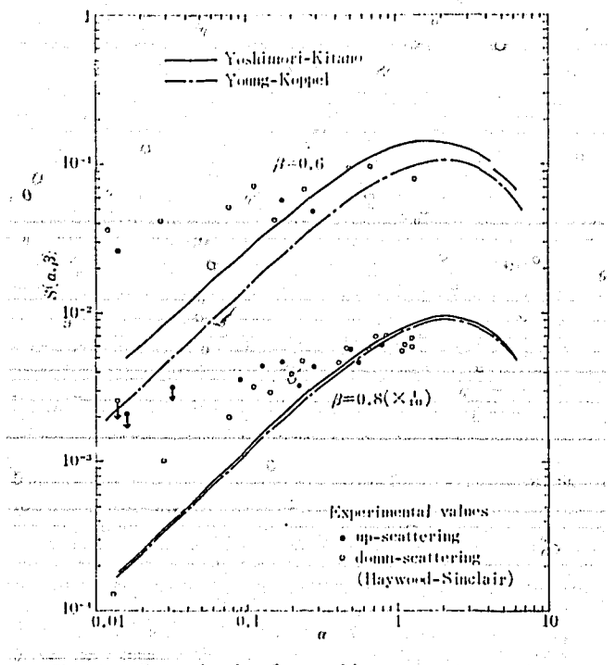

Fig. 4 a Scattering law for graphite at room temperature.

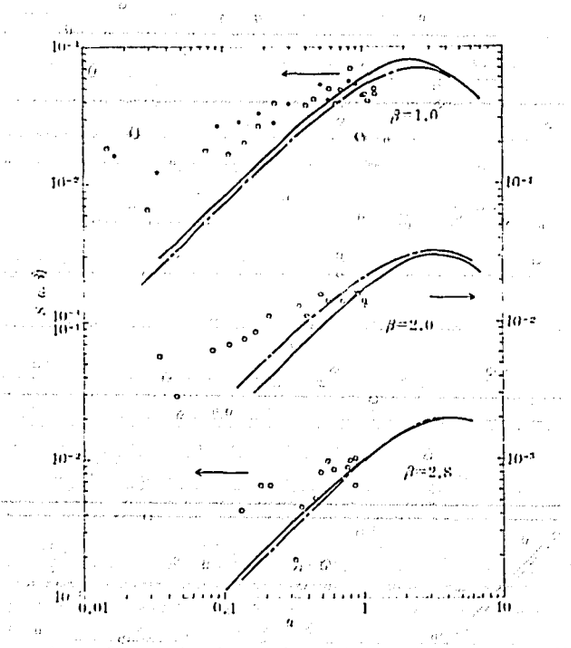

Fig. 4 b Comparison of scattering laws calculated from the anisotropic Yoshimori-Kitano and Young-Koppel frequency distributions.

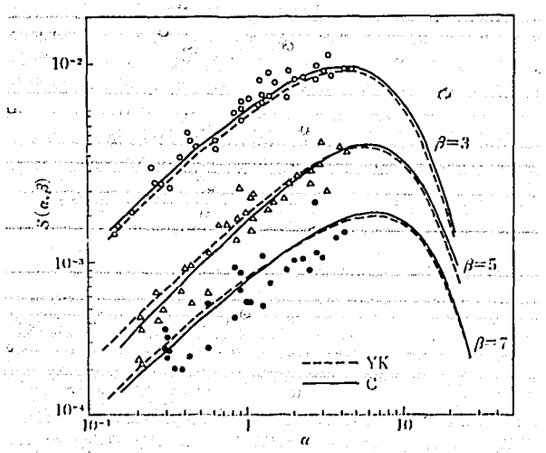

Fig. 5 Comparison of scattering laws calculated from the isotropic Young-Koppel and Carvalho frequency distributions. Experimental values are those obtained by Whittemore.[3]

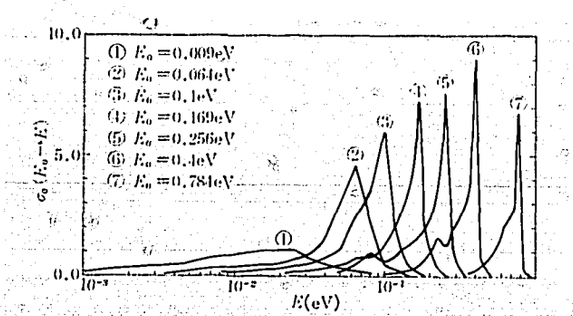

Fig. 6 Scattering kernels for graphite at room temperature, calculated from the anisotropic Young-Koppel frequency distribution.

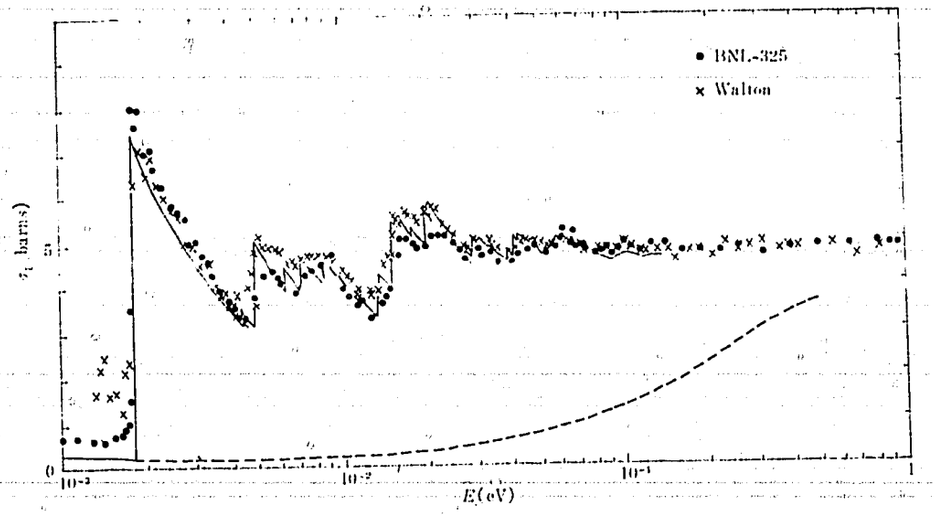

Fig. 7 Inelastic and total scattering cross sections for graphite at room temperature, calculated from the anisotropic Young-Koppel frequency distribution.
—— total, ····· inelastic, × GA-6904(1966)

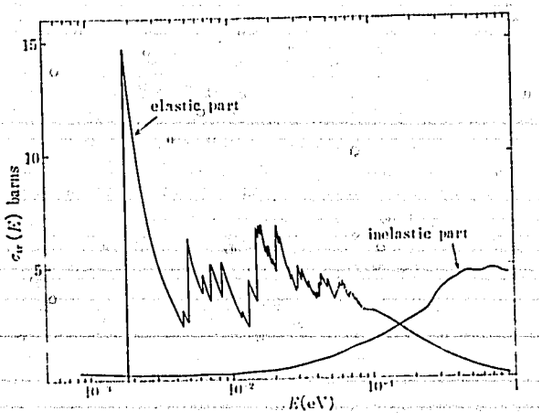

Fig. 8 Transport cross section for graphite at room temperature, calculated from the anisotropic Young-Koppel frequency distribution.

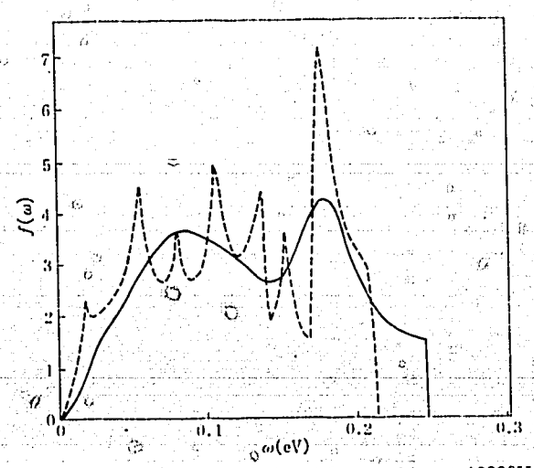

Fig. 9 Frequency distribution (in isotropic form) for graphite at 1800°K, determined by Page from the scattering law data, in comparison with Young-Koppel distribution at room temperature.
—— Page, ····· Young-Koppel

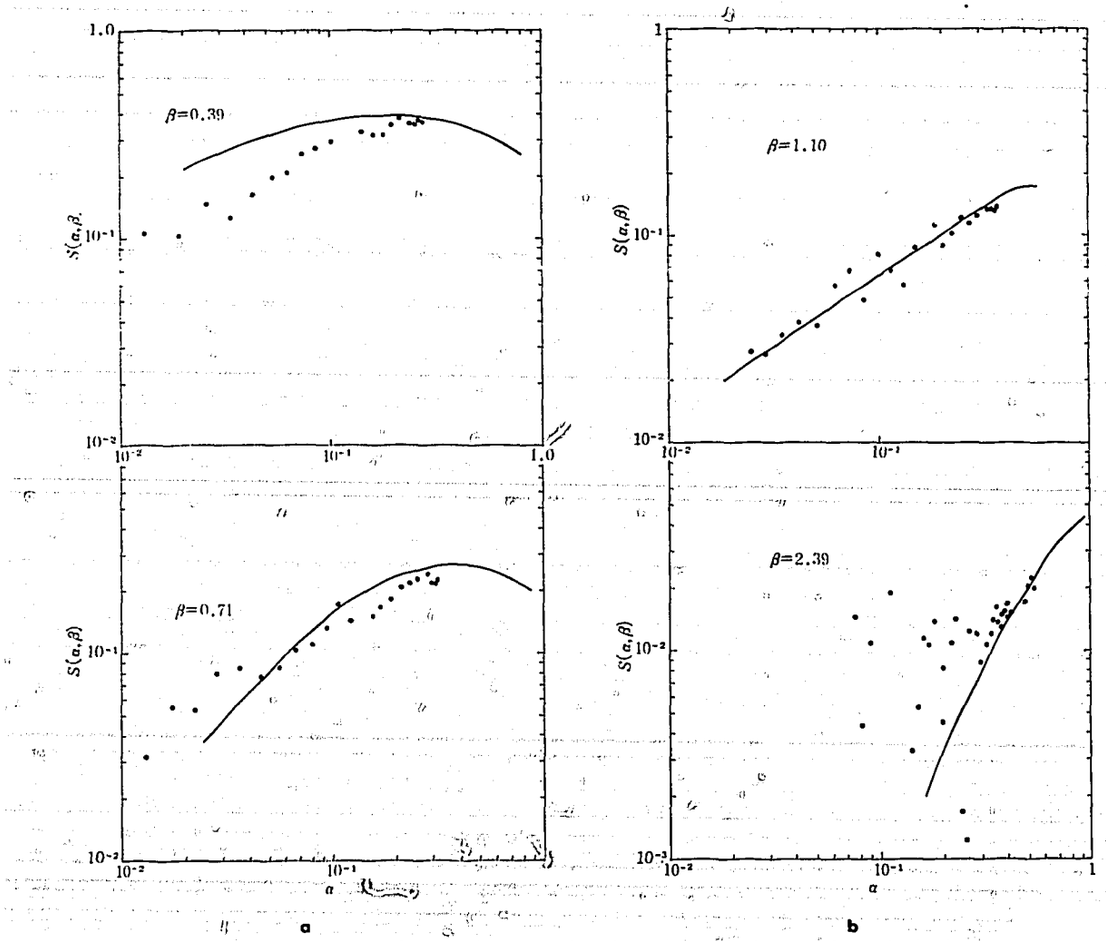

Fig. 10 Scattering law for graphite at 1800°K. Experimental values are those obtained by Page. Theoretical values are calculated from the anisotropic Young-Koppel distribution at room temperature.

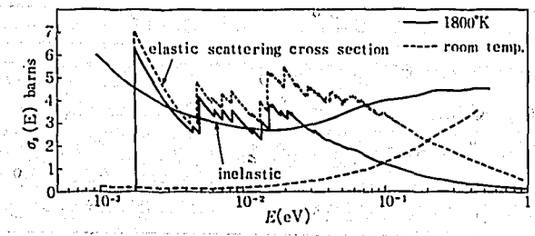

Fig. 11 Elastic and inelastic scattering cross sections for graphite at 1800°K, in comparison with values at room temperature (Cross sections at 1800°K were calculated from the frequency distribution at room temperature).

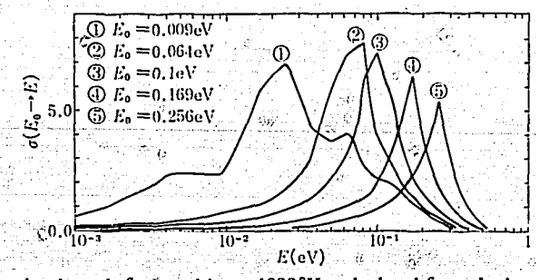

Fig. 12 Scattering kernels for graphite at 1800°K, calculated from the isotropic Young-Koppel distribution.

3. 3. 2 Coherent Inelastic Scattering of Slow Neutrons from Polycrystalline Graphite

Several years ago H. TAKAHASHI made a detailed investigation of one-phonon coherent scattering from graphite by using the root sampling technique. Although the work was reported briefly at the conference on inelastic scattering of neutrons, Nov., 1965, Japan Atomic Energy Reseach Institute and was published in JAERI 1113 ('66), it is felt worth-while to reproduce his work in greater detail in the present evaluation report. Since he is now at BNL on leave from JAERI, the article is presented by one of the editors (S.I.) with permission of H. TAKAHASHI. The writer was informed that TAKAHASHI recalculated the same problem with the force constants determined by YOUNG and KOPPEL, and is preparing the results for publication.

In this paper we present the results of root-sampling calculation for coherent inelastic scattering of neutrons from graphite at room temperature based on Yoshimori-Kitano theory of lattice vibrations.[1] The unsymmetrized one-phonon scattering law $S(\kappa, \omega)$ per atom for polycrystal is expressed by

$$S(\kappa, \omega)=\frac{1}{4\pi}\int d\Omega_{\vec{\kappa}}\, S(\vec{\kappa}, \omega) \tag{1}$$

$$S(\vec{\kappa}, \omega)=\frac{(2\pi)^3}{NV_0}\frac{\hbar}{2M}\sum_{\vec{\tau}}\sum_{s}|g_s(\vec{\kappa})|^2\,\delta(\vec{\kappa}+\vec{q}-\vec{\tau})\frac{1}{\omega_s}\cdot[(n_s+1)\delta(\omega-\omega_s)+n_s\delta(\omega+\omega_s)]. \tag{2}$$

Here $g_s(\vec{\kappa})$ is the dynamical structure factor;

$$g_s(\vec{\kappa})=\sum_{\nu=1}^{4}(\vec{\kappa}, \vec{C}_\nu{}^s)e^{i\vec{\kappa}\vec{r}_\nu}e^{-W_\nu\vec{\kappa}} \tag{3}$$

$s=(\lambda, \vec{q})$ stands for the index for the normal mode and ν is for the basis atom. $\vec{C}_\nu{}^s$, $\vec{r}_\nu$ and $2W_\nu\vec{\kappa}$ are, respectively, the polarization vector, the position in a unit cell and Debye-Waller factor for the ν-th basis atom. The symbols have been defined in § 2.1. Eq. (1) was calculated by the root-sampling technique taking 675 wave vector points in an irreducible segment of the first Brillouin zone for the range of $\alpha=\frac{\hbar^2\kappa^2}{2MT}\leq 1.0$ and $\beta=|\hbar\omega|/T\leq 2$. T is the temperature, in energy unit. An IBM-7044 Fortran IV program, ONE PHONON, was programmed for this purpose. In Yoshimoni-Kitaro theory, the one phonon term in Eq. (1) is split into the sum of the parts corresponding to in-plane vibrations and out-of-plane vibrations.

$$S(\kappa, \omega)=S_{//}(\kappa, \omega)+S_{\perp}(\kappa, \omega) \tag{4}$$

Since in in-plane vibrations the motions of atoms lying on different layers are not coupled, the main physical part of $S_{//}(\kappa, \omega)$, except for Debye-Waller factor, does not depend on κ_z and q_z. Z-axis is taken in the direction of the c-axis.

The calculation proceeds in the following way. A sampling point $\vec{q}$ is taken in the irreducible segment of the first Brillouin zone. Secular equation is solved to obtain $\omega_\nu(\vec{q})$ and $\vec{C}_\nu{}^\lambda(\vec{q})$. $\vec{C}_\nu{}^\lambda(\vec{q})$ is then transformed to $\vec{C}_\nu{}^\lambda(\vec{\kappa})$, where $\vec{\kappa}=\vec{\tau}+\vec{q}$, using crystal symmetry. The range of $\vec{\tau}$ was restricted by $\alpha\leq 1.0$. The intensities of scattering from various $\vec{\tau}$ are collected and classified according to the resulting $|\vec{\kappa}|$ and ω, with intervals $\Delta\alpha=0.01$ and $\Delta\beta=0.1$, respectively. In order to get better statistics, the calculation was done separately for $S_{//}(\kappa, \omega)$ and $S_{\perp}(\kappa, \omega)$. This technique is advantageous, because the out-of-plane vibrations have the higher density of normal modes than that for in-plane vibrations for $\beta\leq 2$, and this implies that a greater number of sampling points are required to calculate $S_{//}(\kappa, \omega)$ with the same accuracy as that for $S_{\perp}(\kappa, \omega)$. The statistics was improved by using the frequency distribution, the density of normal modes, which were calculated with a larger number of sampling points. With the above technique, the present size of sampling points, 675, was not insufficient to make a meaningful comparison between theory and experiment.

Typical results are shown in Figs. 1-4. Plotted together is the multi-phonon contribution calculated in the incoherent approximation using the anisotropic frequency distribution obtained by YOUNG and KOPPEL.[2] Figs. 1 and 2 show the structure of typical $S_{//}(\alpha, \beta)$ and $S_{\perp}(\alpha, \beta)$. In the range of β considered here, $S_{//}(\alpha, \beta)$ exhibits maxima at $\kappa\approx\tau_{//}$ and minima at κ in-between $\tau_{//}$, where $\vec{\tau}_{//}$ is the projection of $\vec{\tau}$ on hexagonal plane. This behavior is understood in closely analogous way to the case of an isotropic crystal,[3] by drawing the momentum conservation diagram in reciprocal lattice space and also by recalling that the density of trans-

verse vibrations is much higher than that of longitudinal vibrations for acoustic branches ($\beta \lesssim 3$) (c.f. Fig. 5).

The structure of $S_\perp(\alpha, \beta)$ is more complicated. When $\beta \sim 0.5$, the minima occur near $\kappa \approx \tau$ and maxima near in-between τ, and the positions of maxima are seen shifted towards larger κ as β increases. When β exceeds somewhat over 0.6, the diffraction-like structure at small α diminishes abruptly, and, at the same time, the phase of minimum and maximum is reversed. These may be interpreted roughly as follows. Firstly, when β is about 0.5 or less, we are observing the accoustic vibrations. In Yoshimori-Kitano theory, the squared frequency of out-of-plane vibrations can be written as

$$\omega^2(\vec{q}) = (\omega^{(1)}(q_z))^2 + (\omega^{(2)}(\vec{q}_{//}))^2 \tag{5}$$

The (central) force constant between the adjacent layers is about only 1/50 of the bending force constant of the plane. Assuming Yoshimori-Kitano's force constants, $\omega^{(1)}(q_z)$ is 11meV at the zone boundary and becomes maximum at the next zone center, 16 meV. The $\omega^{(2)}(\vec{q}_{//})$ is about 80meV at $[10\bar{1}0]$ zone boundary. The equi-frequency surface is therefore not a sphere, but rather, roughly speaking, a cigar type directed to c-axis. The cigar elongates as β increases. For β, say 0.5, the end of the cigar lies near [0001] zone boundary and the lateral surface lies at less than half way to $[10\bar{1}0]$ zone boundary. The density of the modes is high in the direction of c-axis and low in the direction perpendicular to it. Now, in the case $\kappa \approx \tau$ (002), the constant κ sphere crosses the equi-frequency cigar surface at about the middle part of it. There, the density is low. When κ is about $[\tau(002)+\tau(003)]/2$, the κ-sphere glazes the ends of the cigar, where the density is high. This explains the stated results and also the shift of positions of maxima with β. For $\kappa \approx \tau$ (003) and $\approx \tau$ (100), the scattering becomes small either because of the destructive interference or of the orthogonality of $\vec{C}_p$ and $\vec{\kappa}$.

When β exceeds somewhat over 0.6, the equi-frequency surface becomes approximately an infinite cylinder and the bending vibrations (transversal) contribute to the scattering. Since the reciprocal lattice is dense in the direction of c-axis (see Fig. 6 (b)), prominent structure is not expected as κ increases from τ (002) to τ (003). Fig. 6 (a) and (b) also illustrate why the phase of minima and maxima is reversed as β increases from 0.5 to 0.7.

The structure of $S_\perp(\alpha, \beta)$ changes rather rapidly as β increases further, and it depends not only on the geometrical structure and the gross feature of dispersion curves, but also on the polarization vectors.

Figs. 3-5 show the comparison of the calculated scattering law with the experimental data by HAYWOOD and SINCLAIR. For large α, the agreement is satisfactory. The considerable discrepancy at small α may be attributed to the effect of multiple scattering from the sample.

CARVALHO[4] calculated the multiple scattering correction for his measurement of graplite at 533°K. The correction factor was about 0.3 and 0.4 respectively, for $\beta = 2$ and $\beta = 3$ at $\alpha = 0.1$. He also has converted his 533°K results to room temperature, although the procedure may not be very accurate, to compare with the present calculation. Although the fine structures may have been smeared due to the finite angular resolution in the measurement, the agreement between his results and the present calculation is satisfactory.

References

1) YOSHIMORI A. and KITANO Y. : *J. Phys. Soc. Japan*, 11, 352 (1956).

2) YOUG J.A., KOPPEL J.U. : *J. Chem. Phys.* 42, 357 (1964).

3) BRUGGER R. M. : IDO-17063 (1965), SCHMUNK R.E. : *Phys. Rev.* 136, A1303 (1963), IIJIMA S. : *J. Nucl. Sci. Technol.* (*Tokyo*) 3, 164 (1966).

4) CARVALHO F. : EANDC (E) 76 "U" (1966) p. 24, also cited by GLÄSER, W.: Symposium on Neutron Thermalization and Reactor Spectra, IAEA, Ann Arbor, (1967), SM62/1.

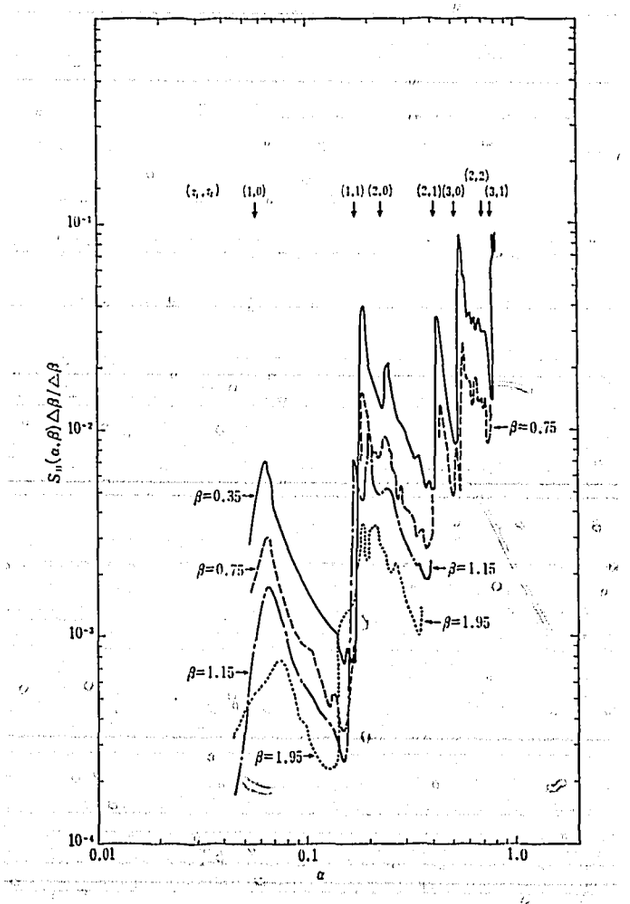

Fig. 1 Typical in-plane one-phonon scattering law $S_{\parallel}(\alpha, \beta)$.

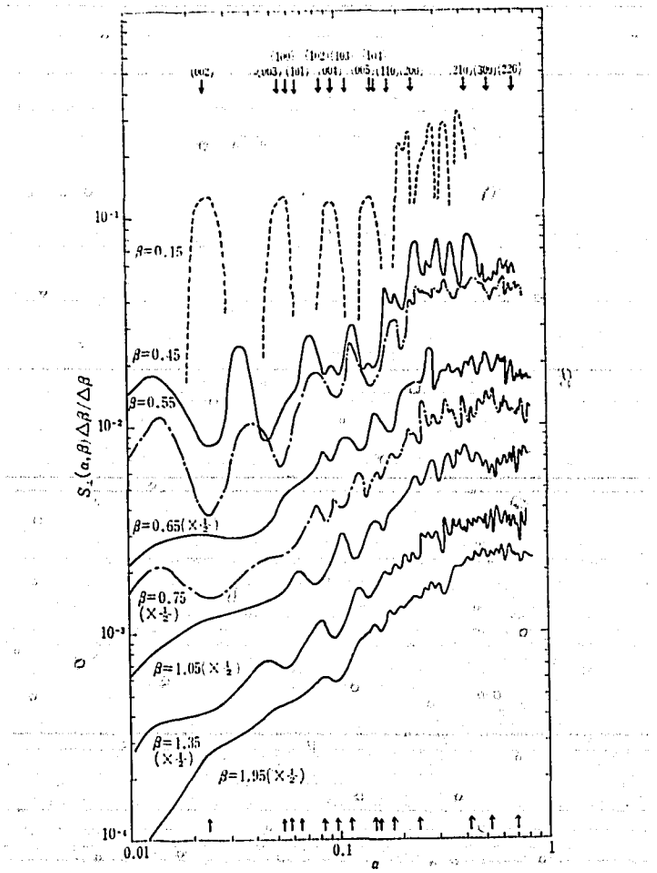

Fig. 2 Typical out-of-plane scattering law $S_\perp(\alpha, \beta)$.

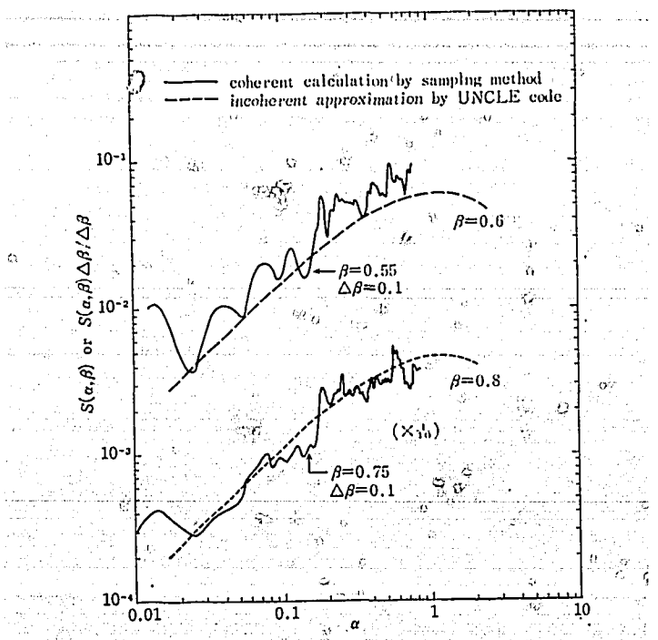

Fig. 3 One-phonon scattering law for graphite at room temperature (1).

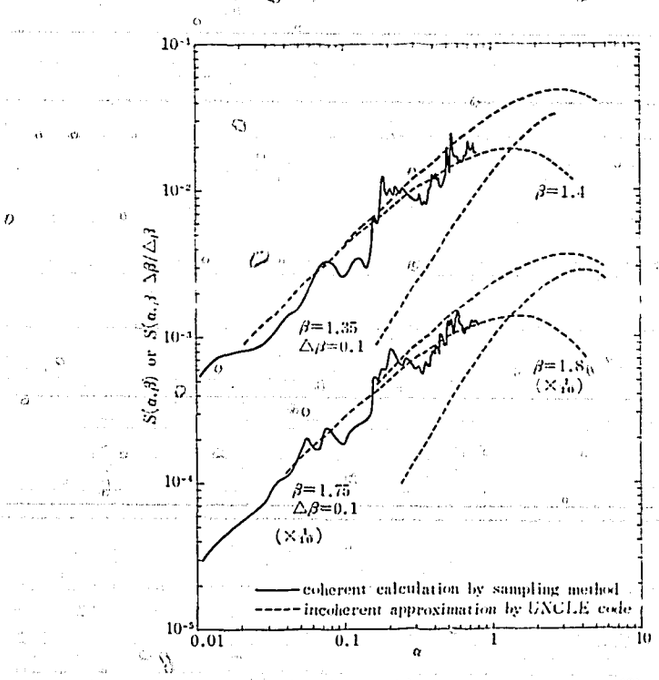

Fig. 4 One-phonon scattering law for graphite at room temperature (2).
……comparison of coherent calculation with incoherent approximation……

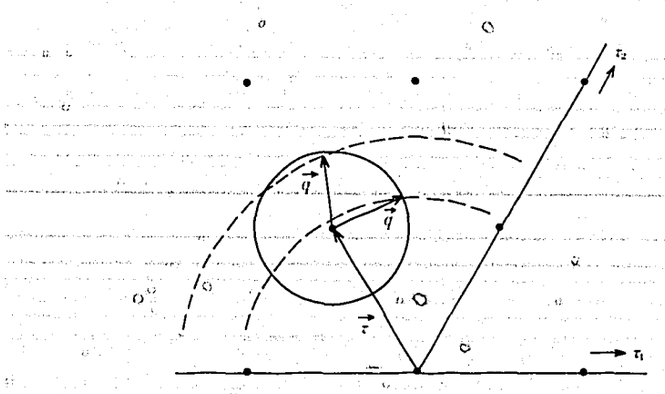

Fig. 5 A schematic drawing of momentum conservation law in reiprocal lattice to illustrate the structure of $S_{\parallel}(\kappa, \omega)$; Dotted semi-circles indicate the constant κ circle. When $\kappa \approx \tau$ (inner circle), transverse vibrations contribute predominantly to $S_{\parallel}(\kappa, \omega)$, while for κ at between τ (outer circle) the longitudinal vibrations are effective. * Solid circle is the equi-frequency surface for in-plane vibrations.

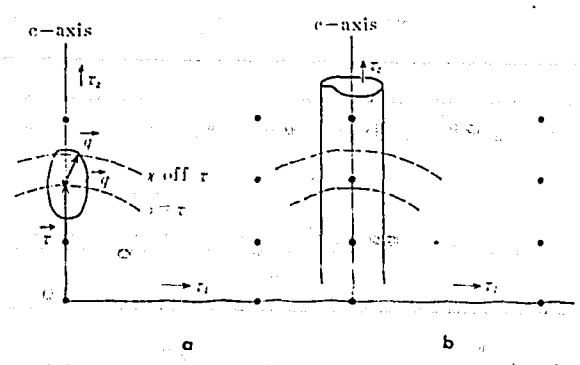

Fig. 6 A schematic draw of momentum coservation law in reciprocal lattice to illustrate the structure of $S_\perp(\kappa, \omega)$; The solid ellipse in Fig. 6a is the equi-frequency surface of $\beta \sim 0.5$ for out-of-plane vibrations. Dotted semi-circles are constant κ spheres. The outer circle crosses the high density part of equi-frequency surface, thus resulting a large scattering cross section. For the inner circle, the situation is opposite. Fig. 6b shows the same illustration for $\beta \sim 0.7$. The equi-frequency surface becomes practically an infinite cylinder. No prominent structure of $S_\perp(\kappa, \omega)$ is expected in this case.

3.4 Beryllium

Frequency distributions of lattice vibrations in beryllium have been obtained by SINCLAIR,[1] YOUNG & KOPPEL[2] and RAUBENHEIMER & GILAT.[3] SINCLAIR measured extensively scattering law for beryllium at 22°C and evaluated the frequency distribution by means of the well known extrapolation procedure on $S(\alpha, \beta)/\alpha$ proposed by EGELSTAFF. YOUNG & KOPPEL and RAUBENHEIMER & GILAT obtained frequency distributions theoretically by means of the root sampling method. YOUNG & KOPPEL used the Schmunk's[4] central force model in which the interactions with up to fifth neighbors are taken into consideration. RAUBENHEIMER & GILAT used the modified axially symmetric model formulated by DEWAMES, WOLFRAN and LEHMAN.[5] All these frequency distributions are shown in Fig. 1 (Note that the normalizations are different for three distributions).

As can be seen from Fig. 1, theoretical distributions have deep valley around $\nu = 15 \times 10^{12}$ sec^{-1}, but experimental one does not. Qualitatively, YK (YOUNG & KOPPEL) distribution resembles S(SINCLAIR) distribution closer than RG (RAUBENHEIMER & GILAT) distribution does, in spite of the fact that the theoretical basis for YK distribution is cruder than that for RG distribution. Phenomenological S distribution, however, can not be said to be precisely true, because the extrapolation procedure has some arbitrariness in eliminating the coherent and multiple scattering contributions from measured scattering law. Therefore, it can not be concluded from Fig. 1 that YK distribution is closer to the truth than RG distribution.

Scattering laws calculated from YK and RG distributions are shown in Fig. 2 in comparison with experimental one determined by SINCLAIR.[6] Agreements are not good for both theoretical values. It may be inferred from Fig. 2 that the true peak in the frequency distribution at the lower frequency exists between the peaks in YK and RG distributions. Scattering laws calculated from S distribution are also shown in Fig. 2. The main peak around $\beta = 2.0$ of the scattering law calculated from S distribution is smaller, whereas those from YK and RG distributions are much larger than experimental values. This may be the reflection of the relative effects of the two main peaks in the frequency distribution. In view of what is said above, experimental data on scattering law were re-evaluated and the final frequency distribution (MOD-2) thus determined is shown in Fig. 3 in comparison with S distribution. MOD-2 distribution is, now, similar to RG distribution qualitatively. This is a reasonable result, since the modified axially symmetric model gives the dispersion relation in excellent agreement with experimental dispersion curve determined by SCHMUNK.[7]

Scattering laws calculated from MOD-2 distribution are shown in Fig. 4. Discrepancy between theoretical and experimental values at small α is mainly due to the coherent and multiple scattering. Theoretical values

have been obtained in the incoherent approximation and the multiple scattering corrections have not been applied to experimental data. At large α where the coherent and multiple scattering effects are unimportant, the agreement is quite good.

Some typical scattering kernels are shown in Fig. 5 for illustration. Numerical values of full kernels are given in Appendices. These 30 energy point kernels were calculated from the MOD-2 frequency distribution.

The incoherent inelastic, elastic (coherent+incoherent) and total scattering cross sections are shown in Figs. 6 and 7. The total elastic scattering cross section calculated in the incoherent approximation is also shown for comparison with the exact elastic scattering cross section. Oscillations seen in the inelastic scattering cross section are due to the structure of the frequency distribution and also dependent upon the energy mesh sizes. If finer energy mesh sizes are used, the amplitudes of the oscillations become smaller and the cross section becomes smoother.

In Fig. 8 the transport cross section for beryllium at room temperature is illustrated. The same explanations as given to the total scattering cross section are also applied to the transport cross section.

Data on thermal neutron scattering from beryllium at high temperature are not available at present. Calculations for beryllium at high temperature have not been performed, because we have no data to compare with calculated cross sections.

References

1) SINCLAIR R.N. : "Neutron Inelastic Scattering in Solids and Liquids", Vol. 2, 199, IAEA (1962).
2) YOUNG J.A. and KOPPEL J.U. : *Nucl. Sci. Eng.*, 19, 367 (1964).
3) RAUBENHEIMER L.J. and GILAT G. : *Phys. Rev.*, 157, 586 (1967).
4) SCHMUNK R.E., BRUGGER R.M., RANDOLPH P.D. and STRONG K.A. : *Phys. Rev.*, 128, 562 (1962).
5) DEWAMES, R.E., WOLFRAN T. and LEHMAN, G.W. : *Phys. Rev.*, 138, A717 (1965).
6) HAYWOOD, B.C. and SINCLAIR R.N. : AERE-R 4732 (1964).
7) SCHMUNK R.E. : *Phys. Rev.*, 149, 450 (1966).

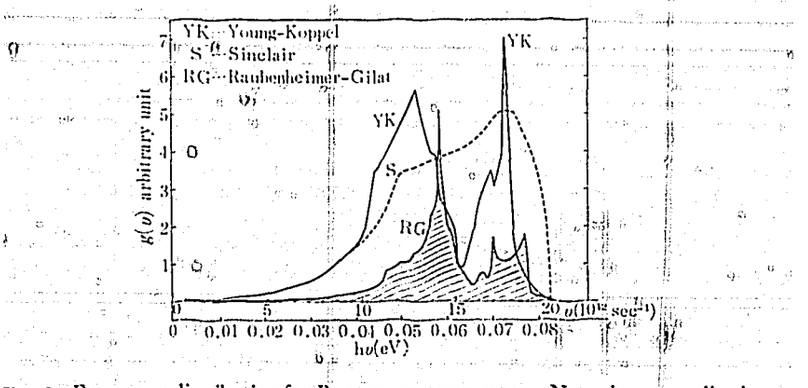

Fig. 1 Frequency distribution for Be at room temperature. Note that normalizations are different for each distribution.

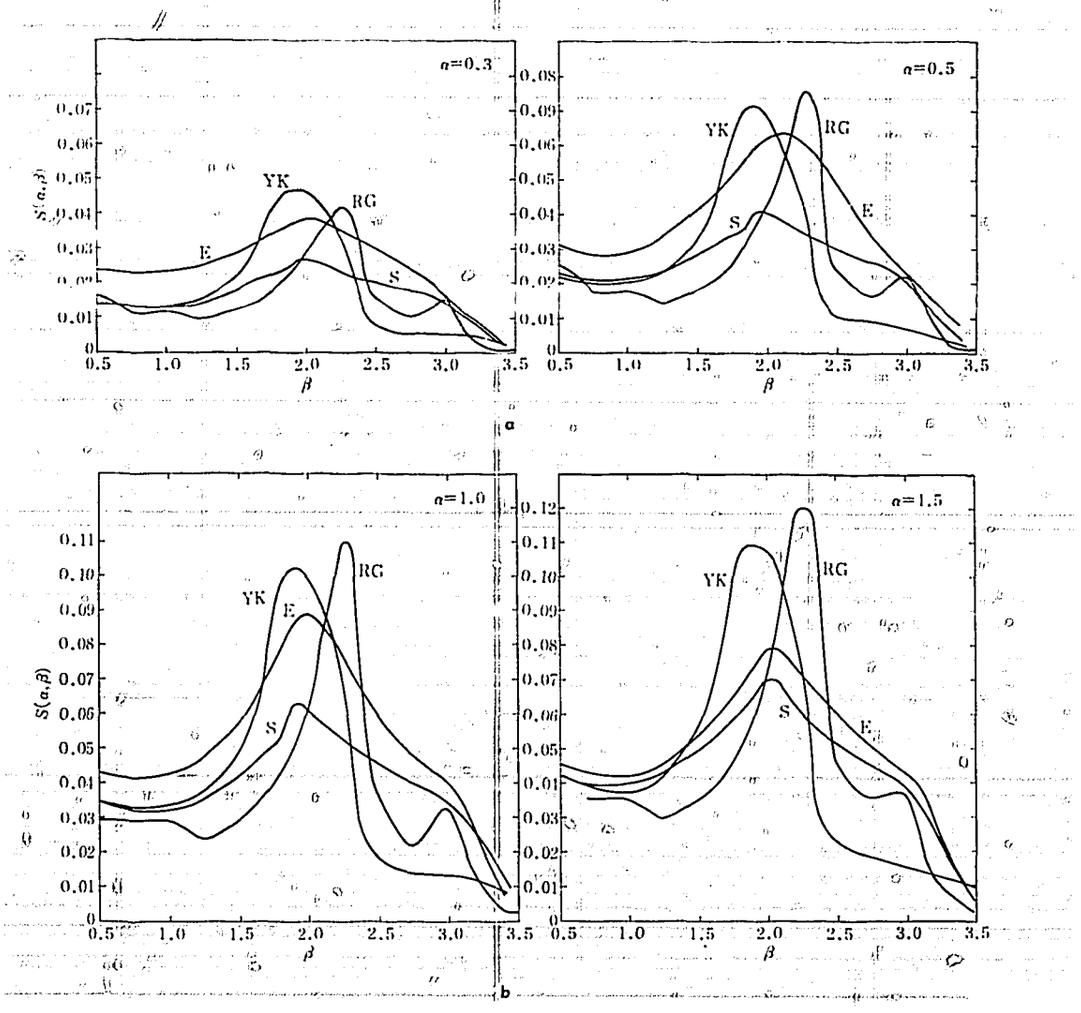

Fig. 2 Scattering law for Be at room temperature. Comparison of scattering laws calculated from the frequency distributions shown in Fig. 1.
YK—Young-Koppel
S—Sinclair
RG—Raubenheimer-Gilat
E—Experimental values

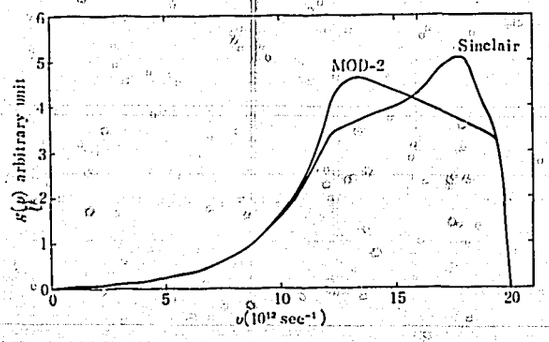

Fig. 3 Evaluated frequency distribution for Be in comparison with Sinclair distribution.

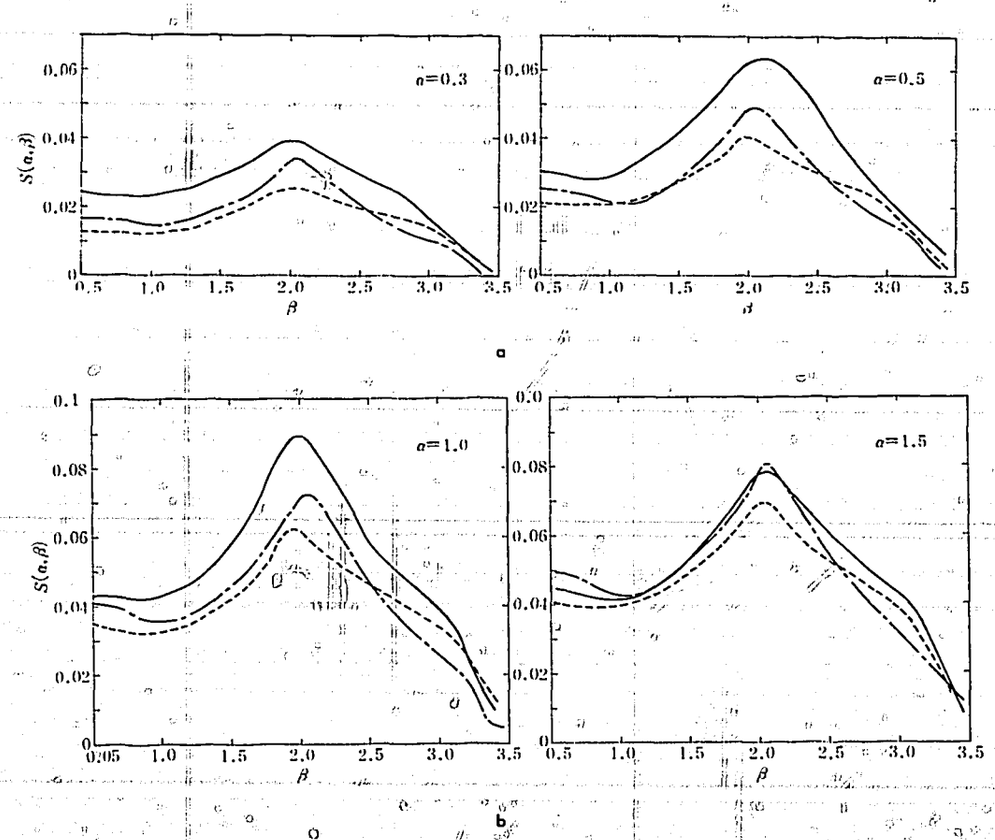

Fig. 4 Scattering law for Be at room temperature, calculated from the MOD-2 distribution, in comparison with those calculated from Sinclair distribution and experimental values.
——— experimental value
····· calculated from the Sinclair's frequency distribution
—·C— calculated from the modified frequency distribution: MOD-2

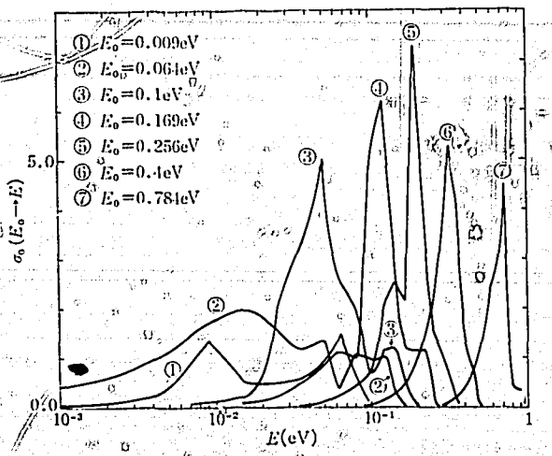

Fig. 5 Scattering kernels for Be at room temperature, calculated from the MOD-2 distribution.

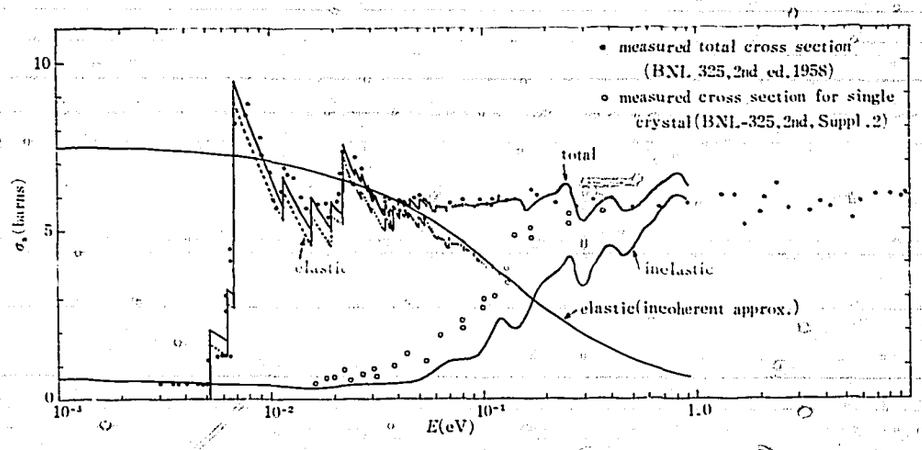

Fig. 6 Elastic, inelastic and total scattering cross sections for Be at room temperature, calculated from Raubenheimer-Gilat distribution.

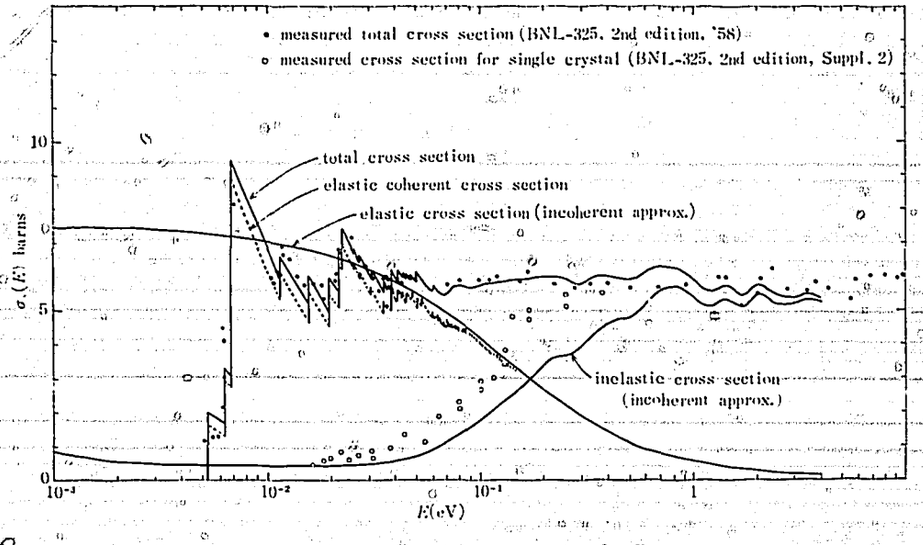

Fig. 7 Elastic, inelastic and total scattering cross section for Be at room temperature, calculated from the MOD-2 distribution.

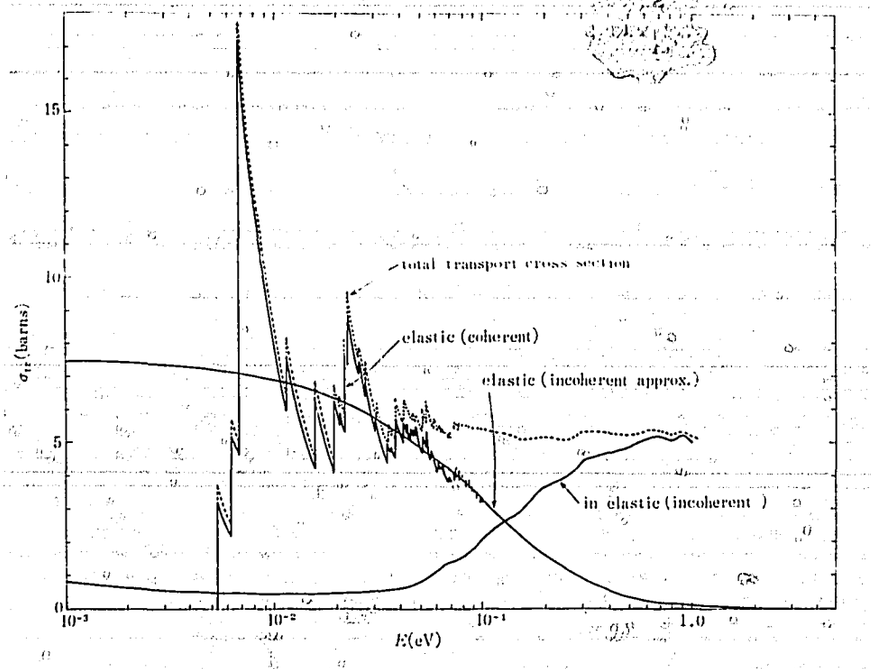

Fig. 8 Transport cross section for Be at room temperature, calculated from the MOD-2 distribution. Elastic and inelastic parts are also shown.

3.5 Beryllium Oxide

The crystal structure of beryllium oxide is wurtzite type, the lattice parameters being c=4.37 Å, c/a=1.623 and the structural parameter u=0.387 at room temperature. The study of lattice dynamics of beryllium oxide is of interest not only because of its use as an important reactor moderator, but also because it is a piczoelectric semiconductor and has a high thermal conductivity and a low electrical conductivity at room temperature.

Sinclair has measured the scattering law at 293°K with incident energy of 0.135 eV.[1] Results were given for the ranges $0.25 \leq \hbar\omega \leq 0.1$ eV and 0.1 Å$<\kappa/2\pi<$ 1 Å. The extrapolation procedure gives the generalized frequency distribution of the form;

$$\rho(\omega) = \rho_{Be}(\omega) + \frac{\sigma_b^0}{\sigma_b^{Be}} \frac{M_{Be}}{M_0} \rho_o(\omega)$$

Since $\rho_{Be}(\omega)$ and $\rho_0(\omega)$ can not be determined separately, the assumption was made that $\rho_{Be}(\omega)=\rho_0(\omega)$ in the analysis of scattering law. The iteration was performed until a reasonable fit was obtained between the calculation and the experiment. The resulting generalized frequency distribution is tabulated in Table 1. and shown graphically in Fig. 1 (a). Fig. 1 (b) shows the phonon dispersion curves recently measured by OSTHELLER *et al.* by neutron scattering technique for wave vectors in [0001] and [10$\bar{1}$0] directions.[2] Also plotted in Fig. 1 (b) are the L-point frequencies measured by LOH from infrared reflection spectra and Raman scattering.[3] The 135 meV LO frequency and 85 meV TO frequency are seen to satisfy Lyddane-Sachs-Teller relation $\omega_{LO}/\omega_{TO}=\sqrt{\varepsilon_0/\varepsilon_\infty}$, where ε_0 and ε_∞ are respectively the static and the high frequency dielectric constants. In comparing Fig. 1 (a) and 1 (b), the critical frequencies are seen to agree well generally in both the generalized frequency distribution and the phonon dispersion curves. The 135 meV LO frequency found by optical measurement has not been observed by neutron scattering measurements. The neutron scattering experiment with a high incident energy or at a high sample temperature will likely to find this mode of vibrations. The critical frequency near 50 meV in the generalized frequency distribution may correspond to the frequency of

about 40 meV of single crystal measurement. This deviation is not significant if the ambiguity of the extrapolation procedure is allowed for.

Figs. 2~6 show the comparison between the calculation and the experiment of scattering law. The agreement is fair at intermediate and large values of α. The discrepancy at small α may be attributed to the presence of the multiple scattering from the sample of the experiment. The measured scattering law exhibits considerable structure with respect to α ,which may presumably be the coherent effect.

The total cross section was calculated and was compared with BNL-325 values in Fig. 7. The calculation agrees well with BNL-325 value for energies above Bragg cut-off. PRYOR and SABINE[4] measured the total cross section of 5 Å neutrons for the temperature range between 100°K-2000°K[3]. Their measurement was compared with the present calculation in Fig. 9. In the calculated range of temperature 300°K-1050°K, the agreement between the calculation and the experiment is seen excellent.

Fig. 8 shows the calculated transport cross section at room temperature, from which diffusion coefficient is calculated to give

$$D_0=\frac{2v_0}{3\sqrt{\pi}}\int_0^\infty \frac{M(E)}{\Sigma_{tr}(E)}dE=1.44\times10^5\text{cm}^2\text{ sec}^{-1} \qquad (1)$$

for the density 2.79 gr/cm³ and at temperature 20°C. Here $v_0=\sqrt{2T/m}$. The experimental values measured by pulsed neutron technique are, in the unit of 10^5 cm²/sec,

D_0=1.18 (24°C); 1.36 (80°C); 1.60 (140°C)

by IYENGAR *et al.*[5] ('57) for a density 2.96 gr/cm³, and

D_0=1.56±0.01 (20°C)

by ZHEZHERUN *et al.*[6] ('64) for a density 2.70 gr/cm³.

The present calculated value is sizeably small compared with the experimental value by ZHEZHERUN *et al.* A part of the discrepancy may be due to the expression of Eq. (1), which is approximate in nature (c.f. section 2.4).

PRYOR and SABINE have measured by neutron diffraction technique the vibrational amplitudes of atoms in beryllium oxide for varying temperatures[5]. Fig. 10 shows the calculation and the experiment of the mean square amplitudes of atoms as functions of temperature. As the present treatment assumes that the frequency distributions are the same for both beryllium and oxygen atoms, the mean square amplitudes of vibrations are given by

$$\langle\vec{u}_\nu^2\rangle_T=3\cdot\frac{\hbar}{2M_\nu}\int_0^\infty\frac{\rho_\nu(\omega)}{\omega}\coth\frac{\hbar\omega}{2T}d\omega$$

Although the measured vibrational amplitudes scatter rather wildly, the calculation definitely underestimates the amplitude of oxygen atom and overestimates that of beryllium, particularly at high temperature. Therefore, the present phenomenological frequency distribution may have to be modified to calculate the high temperature scattering cross section. PRYOR and SABINE calculated the vibrational amplitudes of atoms by assuming Debye-Einstein frequency spectrum, which was determined to fit with specific heat data. They assumed that cation and anion move in unison in acoustic vibrations and move oppositely in optical modes of vibrations. Their result is also plotted in Fig. 6. By using this model, they also calculated the total cross section of 5 Å neutrons, the results plotted in Fig. 5 in comparison with the experiment and with the present calculation.

To conclude, the generalized frequency distribution evaluated in the present report reproduces satisfactorily the observed scattering law and total cross section at room temperature. Theoretical transport cross section underestimates the diffusion coefficient by about 8%, although a transport theoretic calculation of diffusion coefficient may be necessary before drawing the conclusion. Theoretical Debye-Waller factor deviated from the observed values at high temperature, indicating the necessity of the lattice dynamical calculation[7] of spectral density function. This last point will become important in predicting the scattering law at high temperature.

References

1) Sinclair R.N. : "Inelastic Scattering of Neutrons in Solids and Liquids", Chalk River, IAEA (1963) Vol. II.

2) Ostheller G.L., Schmunk R.E., Brugger R.M. and Kearney R.J. : IAEA Symposium on Neutron Inelastic Scattering, Copenhagen, (1968) SM-104/93, c.f. also,
Brugger R.M., Strong K.A. and Carpenter J.M. : *J. Phys. Chem Solid*, 28, 249 (1967).

3) Loh E. : *Phys. Rev.* 166, 673 (1968).

4) Pryor A.W. and Sabine T.M. : *J. Nucl. Materials*, 14, 275 (1964).

5) Iyengar S.B.D. *et al.*, : *Proc. Ind. Acad. Sci.*, 45, 215 (1957).
(cited by Beckurts K.H. : *Nucl. Instr. Method*, 11, 144 (1961).

6) Zhezherun I.F. *et al.*, : 3rd ICPUAE (1964) p. 3262a.

7) c.f. reference 2, see also Nusimovici M.A. and Birman J.L. : *Phys. Rev.*, 156, 925 (1967), Iijima, S. : JAERI 1157 (1968) § 1.7.

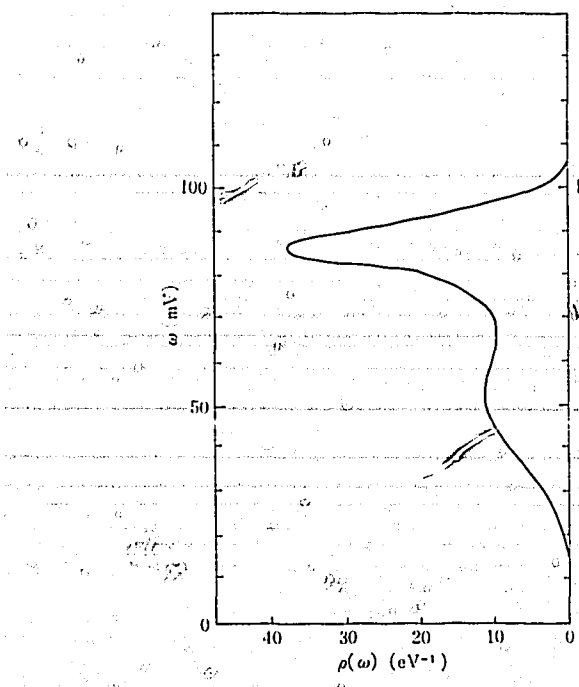

Fig. 1 a The generalized frequency distribution of BeO at room temperature.

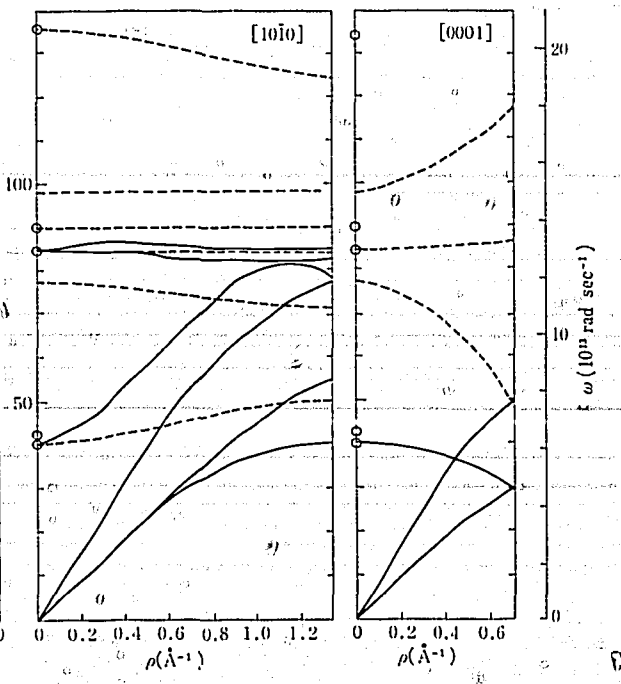

Fig. 1 b The phonon dispersion curves of BeO reproduced from the paper by Ostheller. The solid lines were mapped by neutron scattering techniques. The dashed lines are branches which have not been mapped. The solid points at $q=0$ are the frequencies determined by Loh from optical measurement.

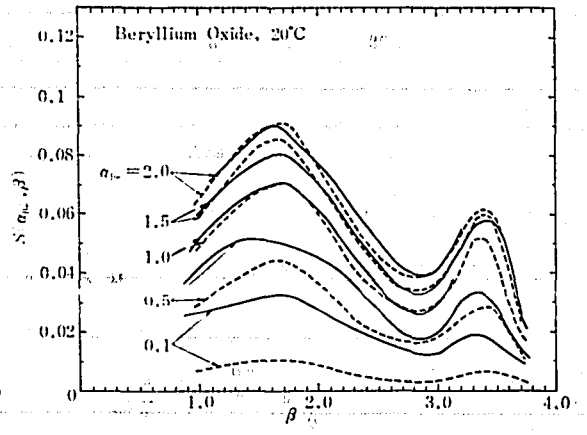

Fig. 2

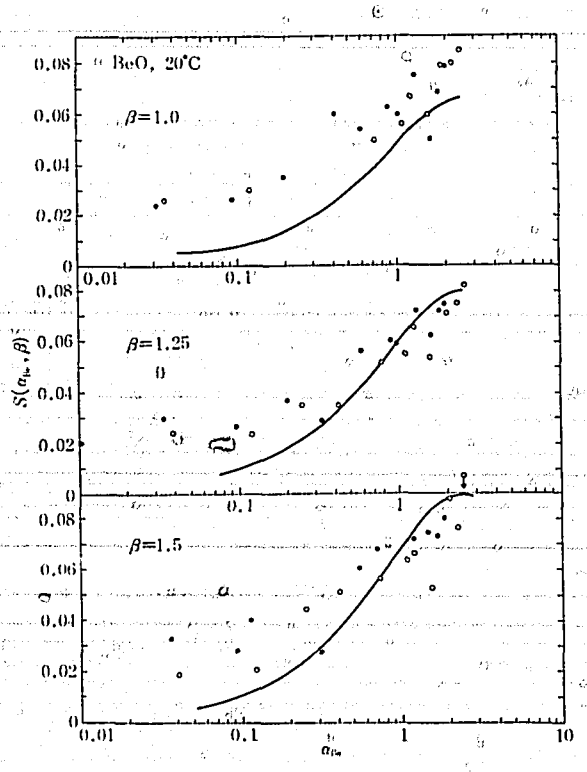

Fig. 3

Fig. 2~Fig. 6 Scattering law of BeO at room temperature. Comparison between calculation and Sinclair's measurement. In Fig. 2, ——calculation, ····· experiment.

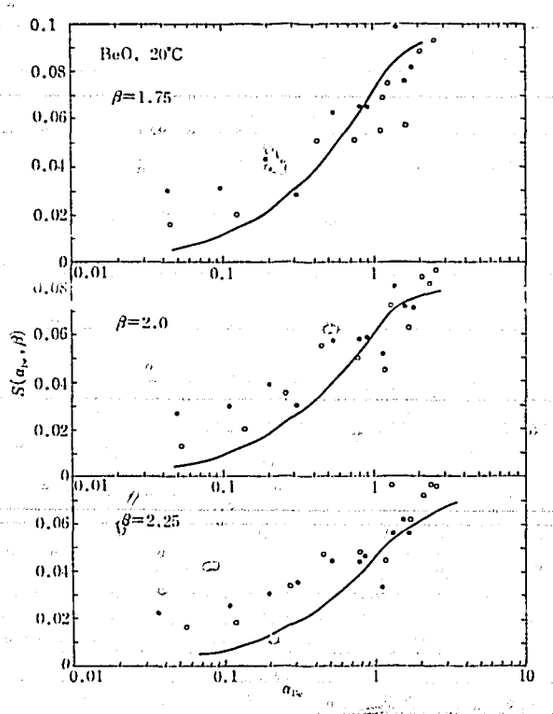
BeO, 20°C
β=1.75
β=2.0
β=2.25
S(α, β)
0.1
0.08
0.06
0.04
0.02
0
0.01
0.1
1
10

Fig. 4

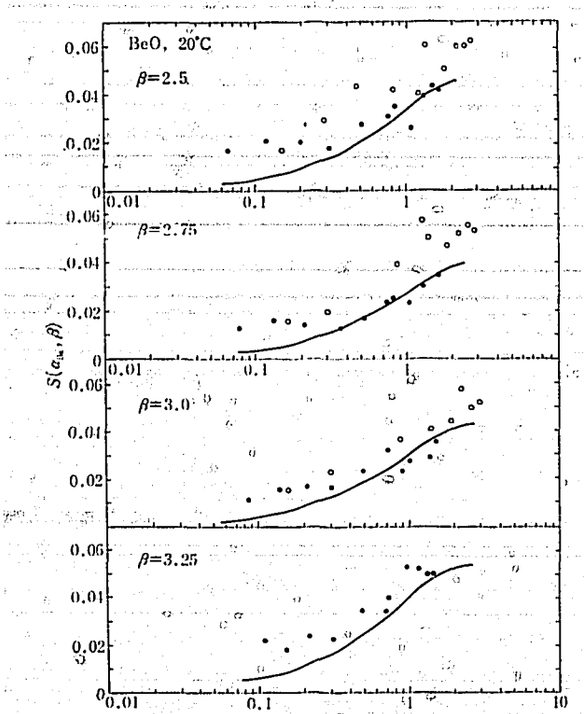
BeO, 20°C
β=2.5
β=2.75
β=3.0
β=3.25
S(α, β)
0.06
0.04
0.02
0
0.01
0.1
1
10

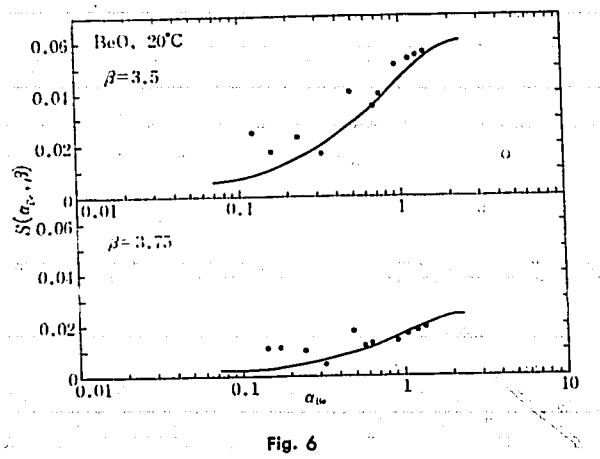

Fig. 6

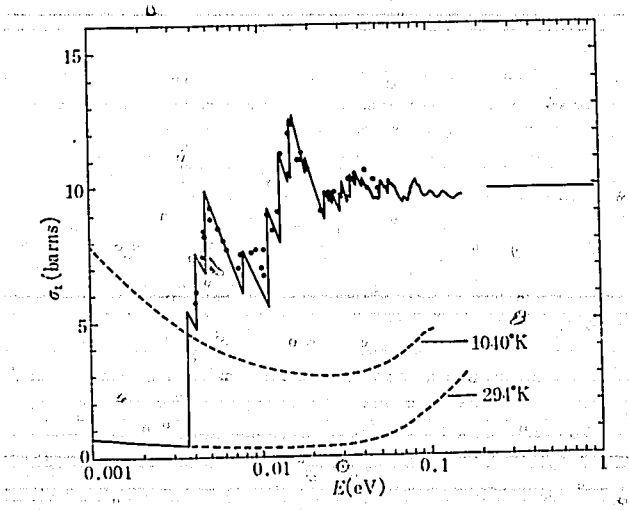

Fig. 7 Total cross section of BeO at room temperature. Comparison of calculation and measurement. The dotted lines are the calculated inelastic cross sections for 294°K and 1044°K. The solid circles are the measured total cross section from BNL-325, while the open circles are Russian measurement.

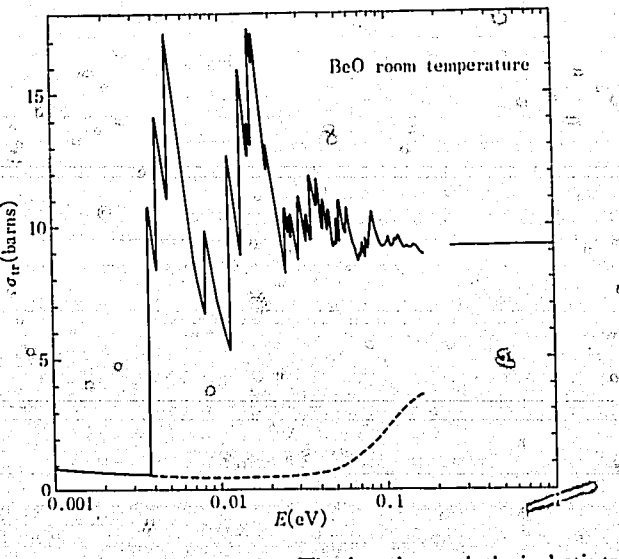

Fig. 8 The calculated transport cross section. The dotted curve is the inelastic transport cross section

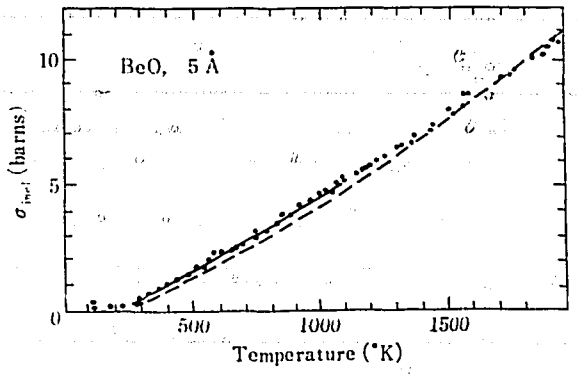

Fig. 9 Total cross section of BeO for 5 Å neutrons versus temperature. The solid line is the present calculation and the dotted line is the calculation by Pryor and Sabine.

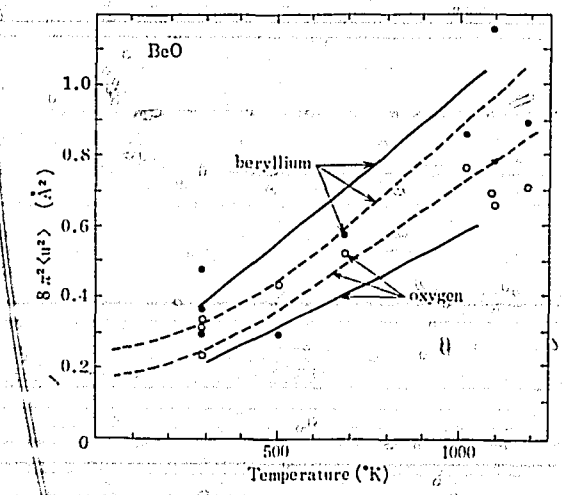

Fig. 10 Comparison of calculation and experiment of the mean square amplitudes of atoms in BeO. The dotted circles and open circles are respectively those for Be and O atoms measured by Pryor and Sabine using neutron diffraction technique. The solid curves are those by present calculation assuming that the spectral density functions are the same for both Be and O atoms. The dotted curves are the ones due to Pryor and Sabine as described in the text.

3.6 Santowax and Diphenyl

Santowax is a mixture of ortho-, meta- and para-terphenyls $(C_6H_5)_2\ C_6H_4$. The melting points of these isomers are 58°C, 89°C and 213°C, and the boiling points are 332°C, 363°C and 250°C, respectively at normal pressure. Diphenyl, $(C_6H_5)_2$, has melting point of 71°C and boiling point of 254.5°C under the same condition.

The scattering law for polyphenyls has been measured by BRUGGER[1] and GLÄSER[2]. Fig. 1 shows the comparison of the measured scattering law for benzene, diphenyl and santowax at room temperature for typical values of β. As seen from the figure, the scattering law per hydrogen atom for diphenyl and santowax are mutually indistinguishable for all the ranges of observed α and β, while the scattering law for benzene is systematically larger than the other two for $0.6 \leq \beta \leq 2.0$. We, therefore, assume the same spectral density functions for diphenyl and santowax of the form;

$$\rho_\nu(\omega, \Omega_\kappa) = \rho_\nu^{acc}(\omega) + \sum_\lambda \frac{|\vec{\kappa} \cdot \vec{C}_\nu^{(\lambda)}|^2}{\kappa^2} \delta(\omega - \omega_\lambda) \qquad (1)$$

where ν stands for either hydrogen or oxygen atom, $\rho_\nu^{acc}(\omega)$ is the acoustic part of the spectral density function, and $\vec{C}_\nu^{(\lambda)}$ and ω_λ are respectively the eigenvectors and the frequencies of internal vibrations of a

molecule. $\rho_\nu^{acc}(\omega)$ is determined by extrapolation-iteration procedure from the observed scattering law. Assuming that atoms move isotropically and in unison in this part of frequencies, we have $\rho_C^{acc}(\omega)=12\ \rho_H^{acc}(\omega)$. Table 1 gives $\rho_\nu^{acc}(\omega)$ determined in this manner. The acoustic part of the spectral density function includes the translation and rotation of a molecule as a whole and also maybe a part of the internal vibrations. The areas are respectively 0.0803 and 0.963 for hydrogen and carbon. Therefore, we expect that the scattering from carbon atom is very much like that from free carbon gas. As the optical vibrations we assume that these are the same as the internal vibrations of a benzene molecule. The eigenvectors and frequencies[3] are tabulated in Table 2. In the actual calculation of the neutron scattering, we have used the isotropic approximation instead of Eq. (1), namely,

$$\rho_\nu(\omega)=\rho_\nu^{acc}(\omega)+\frac{1}{3}\sum_\lambda |\vec{C}_\nu^{(\lambda)}|^2\delta(\omega-\omega_\lambda). \tag{2}$$

In using Eq. (2), $\vec{C}_\nu^{(\lambda)}$'s were renormalized as to give $\int_0^\infty \rho_\nu(\omega)d\omega=1$. This renormalization makes the vibrational amplitudes of carbon atoms incorrect, but, this will not cause significant error in the calculated scattering properties of polyphenyl.

Figs. 3(a)-3(b) show the comparison of the calculated scattering law for santowax at 23°C with the measured values. The agreement between the calculation and the measurement is satisfactory except for small α. Table 3 gives the calculated total cross section and the average cosine of the scattering angle, $\bar{\mu}(E)$, for santowax at 23°C. These were compared with experimental values in Fig. 4 and Fig. 6. The calculated total cross section agrees well with the experimental values by BRUGGER and HOFMYER[4] for santowax, but is considerably larger than that by ANTONINI and PAOLETTI[5] for diphenyl at room temperature. Very recently, SPREVAK[6] calculated the total cross section for liquid diphenyl at 150°C. He assumed a free translation of a molecule as a whole and determined the eigenvectors of internal vibrations of diphenyl molecule by choosing the interatomic force constants so as to give the best fit for the vibrational frequencies measured by optical techniques. The calculated total cross section was in good agreement with the measured value by ANTONINI *et al.* Fig. 5 shows the comparison of the present calculation of total cross section (per hydrogen atom) of santowax at 23°C and 267°C with SPREVAK's calculation for diphenyl at 150°C. It is seen that the present calculation yields definitely larger cross sections than SPREVAK's calculation for the entire range of energy. Since the scattering laws for diphenyl and santowax are indistinguishable as observed previosly, the total cross sections (per hydrogen atom) for both materials are expected to be nearly the same, particularly at low neutron energy. Further measurement of total cross section will be very helpful in clarifying the point.

Fig. 6 shows the comparison of the calculated average cosine of the scattering angle for santowax at 23°C with the measured values for m-terphenyl at room temperature. The agreement is good except at the experimental point at E=0.0225 eV, where the calculated value is larger than the measured one by 40%.

References

1) BRUGGER R.M. : *Phys. Rev.* 126, 29 (1962).
2) GLÄSER W. : *Nucleonik* 7, 64 (1965).
3) SEKIYA Z. : priv. comm., see also BOFFI V.C., MOLINARI V.G. and PARKS D.E., BNL-719 (C-32), Vol. I, P. 69 (1962).
4) HOFMYER C. : *Nucleonik* 7, 286 (1965).
5) ANTONINI B., PAOLETTI A. and GAMBETTA V. : *Physica* 32, 119 (1966).
ANTONINI B. and PAOLETTI B. : *Physica* 30, 1047 (1964).
6) SPREVAK D. : Trans. ANS 11, No. 1, 181 (1968).

Table 1. Acoustic part of the spectral density functions for diphenyl and santowax obtained by extrapolation-iteration procedure.

$A_H=(\rho_H(\varepsilon)/\varepsilon^2)_{\varepsilon=0}=2.07\times10^5(\mathrm{eV}^{-3})$ and $A_C=2.45\times10^6$ (eV^{-3}). Areas are respectively $\int_0^{0.04\mathrm{eV}}\rho_\nu(\varepsilon)d\varepsilon=0.08025$ and 0.963 for hydrogen and carbon.

ε (eV)	$\rho_H(\varepsilon)$ (eV^{-1})	$\rho_C(\varepsilon)$ (eV^{-1})
0.004	2.080	24.96
0.008	3.62	43.44
0.012	2.88	34.56
0.016	2.38	28.56
0.020	2.02	24.24
0.024	1.86	22.32
0.028	1.58	18.96
0.032	1.49	17.90
0.036	1.44	17.98
0.040	1.445	17.33

Table 2. Frequencies and mean squared eigenvectors for internal vibrations of a benzene molecule.

$\langle|C_H^{(j)}|^2\rangle$ e.g., is defined by $\sum_{\nu=1}^{n_H}|\vec{C}_\nu^{(j)}|^2/n_H$

Asterisk denotes the doubly degenerate levels, for which $\langle|C_\nu^{(j)}|^2\rangle$ was given as the summed intensity.

In-plane vibrations			Out-of-plane vibrations		
$\hbar\omega_j$(eV)	$\langle\|C_H^{(j)}\|^2\rangle$	$\langle\|C_C^{(j)}\|^2\rangle$	$\hbar\omega_j$(eV)	$\langle\|C_H^{(j)}\|^2\rangle$	$\langle\|C_C^{(j)}\|^2\rangle$
0.0821*	0.0740	1.198	0.05*	0.1124	0.2254
0.122	0.0218	0.1458	0.0828	0.1847	0.0130
0.125	0.0221	0.1446	0.0868	0.0310	0.1399
0.128*	0.1841	0.1492	0.105*	0.2635	0.0698
0.137	0.1263	0.0403	0.120*	0.2267	0.1069
0.145*	0.2799	0.0534	0.121	0.1347	0.0310
0.164	0.1317	0.0350			
0.183*	0.1268	0.2065			
0.197*	0.0292	0.3042			
0.203	0.0422	0.1244			
0.376*	0.3028	0.0306			
0.378*	0.2956	0.0378			
0.380	0.3009	0.0325			

Table 3. Calculated total cross section and average cosine of scattering angle for santowax at 23°C. $\sigma_s^{(l)}$ is the cross section for the l-th Legendre component of angular distribution.

E (eV)	$\sigma_H^{(0)}/\sigma_{FH}$	$\sigma_C^{(0)}/\sigma_{FC}$	σ_{tot} (barns)	$\sigma^{(1)}$ (barns)	$\bar{\mu}$
0.001	5.62	1.68	1750	−46.5	−0.0266
0.004	4.21	1.31	1310	26.8	0.0204
0.009	3.515	1.161	1100	73.2	0.0664
0.016	3.13	1.112	988	113	0.114
0.0225	2.87	1.082	910	121.5	0.1335
0.036	2.48	1.050	799	146	0.1825
0.044	2.35	1.051	741	156	0.210
0.060	2.06	1.022	675	156	0.231
0.071	1.95	1.028	644	160	0.248
0.090	1.795	1.033	600	166	0.277
0.105	1.694	1.030	571	169	0.297
0.14	1.553	1.028	531	181	0.341
0.20	1.423	1.034	494	190	0.384
0.25	1.357	1.020	474	193	0.408
0.30	1.310	1.016	460	195	0.424

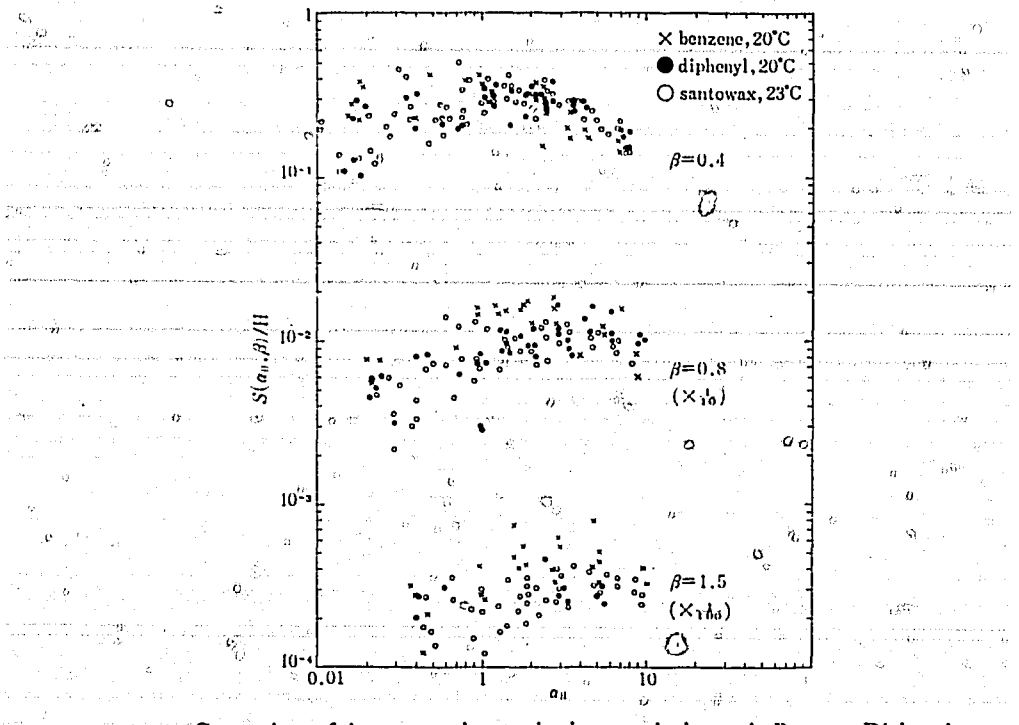

Fig. 1 Comparison of the measured scattering laws per hydrogen in Benzene, Diphenyl and Santowax at room temperature for typical values of β.

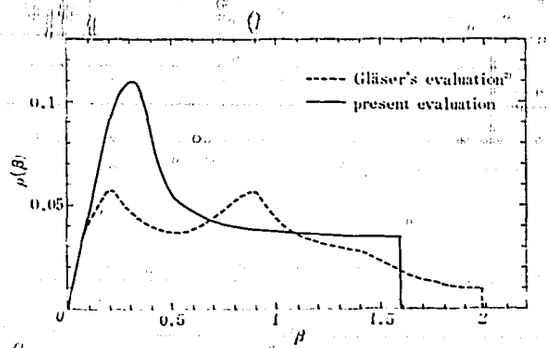

Fig. 2 The acoustic spectral density function for hydrogen atom in Diphenyl and Santowax obtained by extrapolation-iteration procedure from observed scattering law.

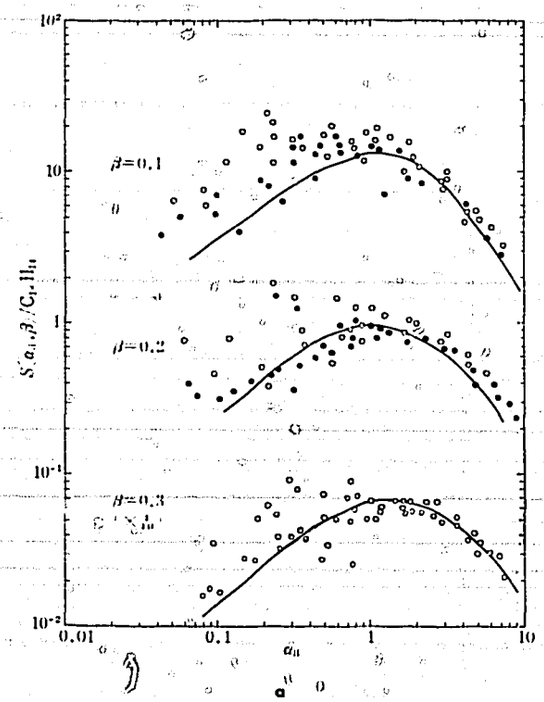

Fig. 3 The scattering law per molecule of Santowax at 23°C. Comparison between calculation and experiment.

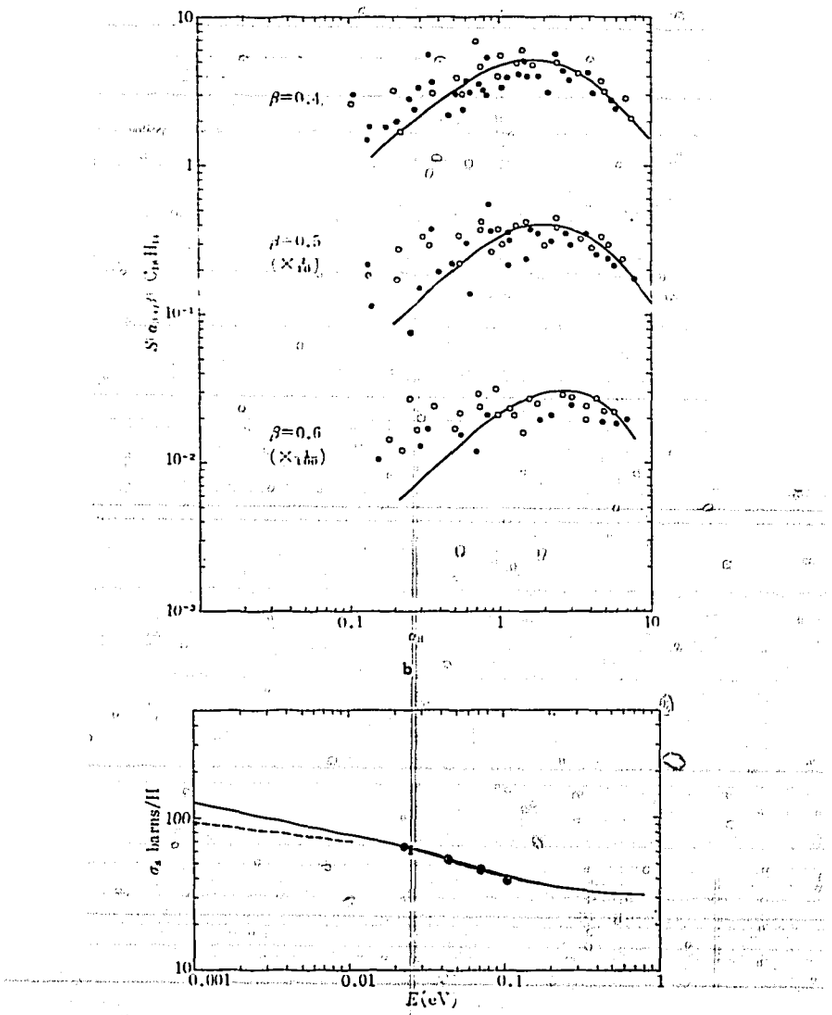

Fig. 4 Total cross section of Santowax at 23°C. Comparison of calculation with experiment. The solid curve is the present calculation. The dashed curve is the least square curve drawn by Antonini *et al.* for the measured scattering cross section for Diphenyl at room temperature.

⊢⊣ : measurement by Brugger for Santowax at 23°C.

⊙ : measurement by Hofmyer fot *m*-terphenyl at 21°C.

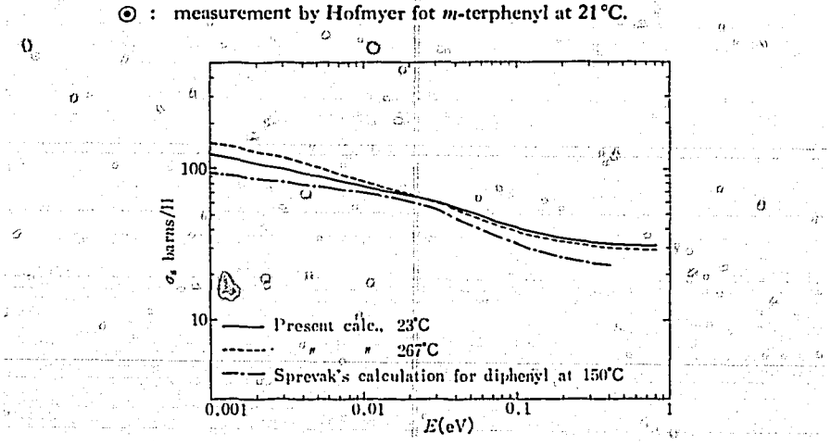

Fig. 5 Comparison of the present calculation of total cross section per hydrogen atom in Santowax at 23°C and 267°C with Sprevak's calculation for Diphenyl at 150°C.

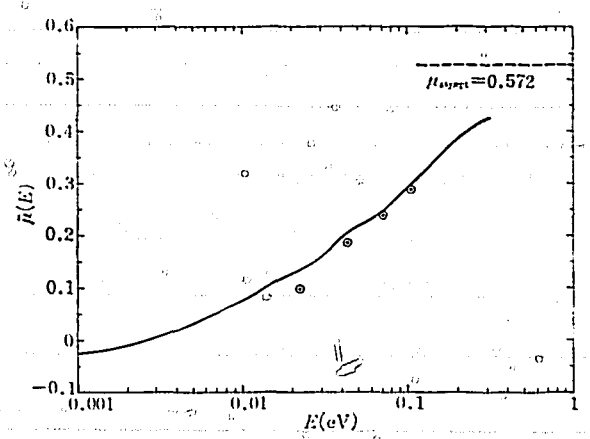

Fig. 6 Average cosine of the scattering angle for Santowax at 23°C. Comparison of calculation with experiment.
⊙ : measurement by Hofmyer for *m*-terphenyl at 21°C.

4. Research Works

Low Frequency Spectra of Organic Moderator Molecules

T. SEKIYA, K. SAKAMOTO and Y. WATARI
Department of Nuclear Engineering,
Osaka University, Suita, Osaka

(1) Introduction

Recently organic materials (usually polyphenyls) are used as moderator and coolant in some types of nuclear reactors by the reason why they have similar number densities of hydrogen to water and low vapor pressure at high temperature. In the light of that, the neutron inelastic scattering data of those organic molecules are growing rapidly[1~4]. As almost all the organic molecules for reactor use contain benzene rings, one of the aims of our research is to determine interaction potentials between benzene rings. In the simplest case of gaseous biphenyl the intramolecular potential has approximately 4-fold symmetry about c-axis and is represented in a form of $H/2(\cos 4\phi - 1)$. The method to determine the barrier height H will be explained in (2). The results suggest that the low frequency peak in neutron scattering data obtained by GLÄSER[2] corresponds to the hindered rotation.

Recently TARINA[3] measured inelastic scattering cross section in the temperature region containing solid-liquid transition point. To catch the physical meaning of these scattering data, we need to be familiar with the dynamical structure of these materials. As cold neutrons have energies comparable to those for rotational, lattice-vibrational and diffusive motions, it is necessary to consider all the degrees of freedom simultaneously from a standpoint of molecular theory. So-called GF Matrix Method has been developed by many authors[5] to analyse Raman and infrared spectrum data[6], [7]. These theories which will be discussed in (3) however, are always limited to solid state. In the temperature range containing solid-liquid transition point, NMR data include not only rotational degrees of freedom but also diffusive one. We will try to connect the results for solid with those for liquid state in (4). In (5) we will discuss results and assumptions, and will give some suggestions for the possible generalizations of conventional methods.

(2) Internal Rotation of Biphenyl Gas[8]

To determine the potential of internal rotation along c-axis of two benzene rings in a biphenyl molecule, we must take into account the competetion between orthogonalizing effect based on H-H repulsions and coplanarizing effect based on π-electrons.

The potential of internal rotation is determined as follows:

In biphenyl molecule shown in Fig. 1 there are two effects competing each other.

(a) Orthogonalizing effect caused by the H-H repulsions between two pairs of hydrogen atoms in ortho-positions. The repulsion potential is a function of H-H distance and the tendency may be investigated by using the data for hydro-carbon given by SIMMONS[9].

(b) Coplanarizing effect caused by π-electrons whose energy has already been evaluated by many authors[10], [11], [12] on the basis of the molecular orbital method.

The H-H repulsion potential curve $R(\phi)$ was calculated by using SIMMONS data, where ϕ is the angle between two planes of benzene rings. The π-electron resonance integral potential curve $S(\phi)$ was calculated by molecular orbital method. As $V(0)=0$, we also have to assume that $S(0)=R(0)$, we get $S(0)=-3$ kcal/mol from the calculation[12] based on the molecular orbital method. This value is also consistent with SIMMONS' $R(0)$ corresponding to the H-H distance.

In the first approximation we will determine H under the assumption that $S(\phi)$ is given by a cosine function. As $R'(\phi)=V(\phi, H)-S(\phi)$ is a linear function of H we can determine H so as to fit the $R'(\phi)$ to $R(\phi)$ at N positions $\phi_1, \phi_2, \cdots\cdots, \phi_N$, in the meaning of the least square method.

Such an optimum H may be determined by the following equation:

$$\frac{d}{dH}\sum_{i=1}^{N}\left\{R'(\phi_i)-R(\phi_i)\right\}^2=0$$

Next we define $R_1(\phi)$ and $S'(\phi)$ by the relations

$$R_1(\phi)=\frac{R(\phi)+R'(\phi)}{2},$$

$$S'(\phi)=V(\phi, H_1)-R_1(\phi),\quad S_2(\phi)=\frac{S(\phi)+S'(\phi)}{2},$$

and determine new H_1 so as to fit $S'(\phi)$ to the real $S(\phi)$ in the meaning of the least square method. In practice, it needs only three repetitions to get the optimum value $H=0.95$(kcal/mol)$=0.042$(eV) within the error limit of 1%. The result is shown in Fig. 2.

We regard the molecule as a symmetric top, then we can get the eigen-values by the method of KOEHLER and DENNISON.

As the barrier height is more than twice of the thermal energies we may use the harmonic approximation which corresponds to replacing the cosine potential curve by a parabola. The level spacing thus obtained is 0.0037 eV at room temperature and it agrees rather well with peak position in frequency distribution obtained by GLÄSER[2].

(3) Normal Vibration of Crystalline Benzene

a) Crystal Structure of Solid Benzene

According to Cox's[13] X-ray analysis of solid benzene, the crystal structure of benzene is orthorhombic bipyramidal and the unit cell contains four molecules which occupy the corners and the face centers of its cell as shown in Fig. 3 The faces of the cell are orthogonal each other and lattice dimensions in a, b, c directions are all different, $a_0=7.034$Å, $b_0=9.666$Å, $c_0=7.460$Å at 270°K. In equilibrium structure all the planes of the rings are approximately parallel to the b-axis and they make an angle of about 40° with (100) planes. This crystal has the symmetry elements of E, C_2^a, C_2^b, C_2^c, i, σ_a, σ_b, and σ_c. In Table 1 the result of the factor group analysis of the crystal is shown.

Table 1. Symmetry species and the character table of crystalline benzene.

D_{2h}^{15}	E	C_2^a	C_2^b	C_2^c	i	σ_a	σ_b	σ_c	infrared	Raman
A_g	1	1	1	1	1	1	1	1		active
A_u	1	1	1	1	−1	−1	−1	−1		
B_{1g}	1	1	−1	−1	1	1	−1	−1		active
B_{1u}	1	1	−1	−1	−1	−1	1	1	active	
B_{2g}	1	−1	1	−1	1	1	1	−1		active
B_{2u}	1	−1	1	−1	−1	1	−1	1	active	
B_{3g}	1	−1	−1	1	1	−1	−1	1		active
B_{3u}	1	−1	−1	1	−1	1	1	−1	active	

By using the bond lengths of benzene molecule:

C-C bond length : 1.397Å

C-H bond length : 1.085Å

and atomic weights:

H=1.00797, C=12.0115,

we may evaluate the moments of inertia along three principal axes shown in Fig. 3:

$$I_x=I_y=1,476\times10^{-38}\text{gcm}^2,$$
$$I_z=2,952\times10^{-38}\text{gcm}$$

b) Normal Coordinates and Frequency Spectrum

Let $\vec{X}_i$ and $\vec{Y}_i$ be 36 dimensional displacement vectors of all the atoms in i-th molecule (i=1, 2, 3, 4) whose Cartesian components are taken along coordinate axes fixed on the molecule and the crystal respectively. They are connected with each other by the transformation matrix $\boldsymbol{T}_i$:

$$\vec{Y}_i=\boldsymbol{T}_i\vec{X}_i \tag{1}$$

The kinetic and the intramolecular potential energies are straightforwardly expressed by $\vec{X}$'s:

$$T=\frac{1}{2}\sum_{\lambda=1}^{4}\dot{\tilde{\vec{X}}}_i\boldsymbol{M}\dot{\vec{X}}_i, \tag{2}$$

$$V_0=\frac{1}{2}\sum_{i=1}^{4}\tilde{\vec{X}}_i\boldsymbol{F}_0\vec{X}_i, \tag{3}$$

where $\boldsymbol{M}$ and $\boldsymbol{F}_0$ are the diagonal mass matrix and the potential energy matrix, respectively. The intermolecular potential energy V' is easily expressed by $\vec{Y}$'s:

$$V'=\frac{1}{2}\sum_{i,j=1}^{4}\tilde{\vec{Y}}_j\boldsymbol{F}'_{ij}\vec{Y}_j \tag{4}$$

By using equations (1), (3), and (4), the total potential energy is written as follows:

$$V=V+V'=\frac{1}{2}\sum_{i=1}^{4}\tilde{\vec{X}}_i\boldsymbol{F}_0\vec{X}_i+\frac{1}{2}\sum_{i,j}^{4}\tilde{\vec{X}}_i\tilde{\boldsymbol{T}}_i\boldsymbol{F}'_{ij}\boldsymbol{T}_j\vec{X}_j. \tag{5}$$

For the molecular crystal the intermolecular potential energy can be treated as a perturbation term. We choose unperturbed coordinates $\vec{Q}$ by using the normal coordinates as follows: In addition to usual intramolecular normal coordinates six coordinates $\vec{Q}^{TR}$ corresponding to the over-all translation and rotation of molecules are included in $\vec{Q}$, and $\vec{Q}$, $\vec{Q}^{TR}$ are connected with $\vec{X}$, $\vec{X}^{TR}$ by the relation $\vec{X}=\boldsymbol{L}\vec{Q}$, $\vec{X}^{TR}=\boldsymbol{L}^{TR}\vec{Q}^{TR}$ respectively. The elements of $\boldsymbol{L}^{TR}$ for benzene molecule are given in Table 2.

Table 2. The elements of $\boldsymbol{L}^{TR}$ for benzene molecule.

	Q^{Tx}	Q^{Ty}	Q^{Tz}	Q^{Rx}	Q^{Ry}	Q^{Rz}
x_j^{TR}	$\frac{1}{\sqrt{M}}$	0	0	0	0	$\frac{-b_j}{\sqrt{I_z}}$
y_j^{TR}	0	$\frac{1}{\sqrt{M}}$	0	0	0	$\frac{a_j}{\sqrt{I_z}}$
z_j^{TR}	0	0	$\frac{1}{\sqrt{M}}$	$\frac{b_j}{\sqrt{I_x}}$	$\frac{-a_j}{\sqrt{I_y}}$	0

In this table Q^{Tx} is the normal coordinate expressing the over-all translation in the x direction and other elements have similar meanings. x_j, y_j and z_j are the Cartesian coordinate of the j-th atom and a_j, b_j and c_j are the equilibrium values. When the cross terms in the potential function between the lattice vibrations and the intramolecular vibrations are small, we can approximately separate the two types of motion. In this case kinetic and potential energies of the lattice vibration are expressed by

$$T=\frac{1}{2}\sum_{i=1}^{4}\dot{\tilde{\vec{Q}}}_i^{TR}\dot{\vec{Q}}_i^{TR}$$

$$V=\frac{1}{2}\sum_{i,j=1}^{4}\tilde{\vec{Q}}_i\tilde{L}^{TR}\tilde{T}_iF''_{ij}T_jL^{TR}\vec{Q}_j. \tag{7}$$

Accordingly the eigenvalues and eigenvectors of the 24 dimensional matrix:

$$F^{TR}\equiv(\tilde{L}^{TR}\tilde{T}_iF''_{ij}T_jL^{TR})$$

give the frequency spectrum and the vibrational modes of the optically active lattice vibrations. The matrix F^{TR} is further reduced to smaller matrices due to the symmetry of the Bravais cell using the symmetry coordinates given in Table 3.

Table 3. The symmetry coordinates for the lattice vibrations of benzene.

A_{1g}	$S_1=\frac{1}{2}(Q_1^{Tz}+Q_2^{Tz}+Q_3^{Tz}+Q_4^{Tz})$	A_{1u}	$S_{13}=\frac{1}{2}(Q_1^{Ty}-Q_2^{Ty}+Q_3^{Ty}-Q_4^{Ty})$
	$S_2=\frac{1}{2}(Q_1^{Tx}+Q_2^{Tx}+Q_3^{Tx}+Q_4^{Tx})$		$S_{14}=\frac{1}{2}(Q_1^{Rz}-Q_2^{Rz}+Q_3^{Rz}-Q_1^{Rz})$
	$S_3=\frac{1}{2}(Q_1^{Ry}+Q_2^{Ry}+Q_3^{Ry}+Q_4^{Ry})$		$S_{15}=\frac{1}{2}(Q_1^{Rx}-Q_2^{Rx}+Q_3^{Rx}-Q_4^{Rx})$
B_{2g}	$S_4=\frac{1}{2}(Q_1^{Tz}-Q_2^{Tz}+Q_3^{Tz}-Q_4^{Tz})$	B_{2u}	$S_{16}=\frac{1}{2}(Q_1^{Ty}+Q_2^{Ty}+Q_3^{Ty}+Q_4^{Ty})$
	$S_5=\frac{1}{2}(Q_1^{Tx}-Q_2^{Tx}+Q_3^{Tx}-Q_4^{Tx})$		$S_{17}=\frac{1}{2}(Q_1^{Rz}+Q_2^{Rz}+Q_3^{Rz}+Q_4^{Rz})$
	$S_6=\frac{1}{2}(Q_1^{Ry}-Q_2^{Ry}+Q_3^{Ry}-Q_4^{Ry})$		$S_{18}=\frac{1}{2}(Q_1^{Rx}+Q_2^{Rx}+Q_3^{Rx}+Q_4^{Rx})$
B_{1u}	$S_7=\frac{1}{2}(Q_1^{Tz}-Q_2^{Tz}-Q_3^{Tz}+Q_4^{Tz})$	B_{1g}	$S_{19}=\frac{1}{2}(Q_1^{Ty}+Q_2^{Ty}-Q_3^{Ty}-Q_4^{Ty})$
	$S_8=\frac{1}{2}(Q_1^{Tx}-Q_2^{Tx}-Q_3^{Tx}+Q_4^{Tx})$		$S_{20}=\frac{1}{2}(Q_1^{Rz}+Q_2^{Rz}-Q_3^{Rz}-Q_4^{Rz})$
	$S_9=\frac{1}{2}(Q_1^{Ry}-Q_2^{Ty}-Q_3^{Ry}+Q_4^{Ry})$		$S_{21}=\frac{1}{2}(Q_1^{Rx}+Q_2^{Rx}-Q_3^{Rx}-Q_4^{Rx})$
B_{3u}	$S_{10}=\frac{1}{2}(Q_1^{Tz}+Q_2^{Tz}-Q_3^{Tz}-Q_4^{Tz})$	B_{3g}	$S_{22}=\frac{1}{2}(Q_1^{Ty}-Q_2^{Ty}-Q_3^{Ty}+Q_4^{Ty})$
	$S_{11}=\frac{1}{2}(Q_1^{Tx}+Q_2^{Tx}-Q_3^{Tx}-Q_4^{Tx})$		$S_{23}=\frac{1}{2}(Q_1^{Rz}-Q_2^{Rz}-Q_3^{Rz}+Q_4^{Rz})$
	$S_{12}=\frac{1}{2}(Q_1^{Ry}+Q_2^{Ry}-Q_3^{Ry}-Q_4^{Ry})$		$S_{24}=\frac{1}{2}(Q_1^{Rx}-Q_2^{Rx}-Q_3^{Rx}+Q_4^{Rx})$

c) Determination of Rotational Barrier Heights from NMR Data and Calculation of Rotational Frequencies.

In 1953 ANDREW and EADES[14] measured the nuclear magnetic resonance absorption spectrum and the spin-lattice relaxation time of benzene in polycrystalline form between 75°K and 278°K. As the intramolecular contribution of the second moment decreased about one-fourth of the total second moment between 90°K and 120°K they concluded that the reorientations of the molecules about each hexad axis were caused near this temperature. In general the potential barrier hight H of such a hindered rotation of atomic assemblies is given by the following equation;

$$\tau_c=\tau_0\exp\left(\frac{H}{RT}\right), \tag{8}$$

where τ_c ; correlation time of thermal motion,
R ; gas constant,
T ; absolute temperature.

In solid case the spin lattice relaxation time T_1 of such a motion was derived by BLOEMBERGEN[15] and is expressed by ;

$$\frac{1}{T_1}=C\left[\frac{\tau_c}{1+\omega^2\tau_c^2}+\frac{2\tau_c}{1+4\omega^2\tau_c^2}\right], \tag{9}$$

where C is a constant and ω is an angular frequency of the magnetic field. So, by measuring the spin lattice relaxation time T_1, it is possible to decide the H value from the slope of log τ_c against $\frac{1}{T}$. From the data given by ANDREW and EADES, we get two lines (see Fig. 4),—the one between 90°K and 240°K, the other between 240°K and the melting point—whose slopes are decided by the least square method and the resulting barrier heights are;

$$H=\begin{cases} 3.7\pm0.2\text{kcal/mol} & (\ 90°\text{K}\leqq T\leqq 240°\text{K}) \\ 10.5\pm0.2\text{kcal/mol} & (240°\text{K}\leqq T\leqq 270°\text{K}) \end{cases} \tag{10}$$

The linearity between 90°K and 240°K depends on the decrease of correlation time about hexad axis with temperature increase. On the other hand, it seems that the rotation about two-fold axis which has been interrupted by neighbouring molecules becomes free by the thermal expansion and so τ_c changes its slope abruptly at 240°K. Therefore the former corresponds to hexad axis rotation and the latter to mainly two-fold ones.

Usually the rotational energy about m-fold axis is given by

$$\text{potential energy;}\quad V=\frac{H}{2}(1-\cos m\varphi), \tag{11}$$

and

$$\text{kinetic energy ;}\quad K=-\frac{\hbar^2}{2I}\frac{d^2}{d\varphi^2}, \tag{12}$$

where φ is a rotational angle and I is the moment of inertia. The Schrödinger equation in this case is expressed as follows:

$$\frac{d^2u}{d\varphi^2}+\frac{2I}{\hbar^2}\left\{E-\frac{H}{2}(1-\cos m\varphi)\right\}u=0, \tag{13}$$

where u is the eigenfunction, and E is the eigenvalue. The potential barrier heights determined from NMR data are rather higher than the thermal energies, so we can write approximately Eq. (13) as follows:

$$\frac{d^2u}{d\varphi^2}+(\lambda-\xi^2\varphi^2)\,u=0, \tag{14}$$

where

$$\kappa=\frac{2IE}{\hbar^2},\quad \xi^2=\frac{m^2H}{2I} \tag{15}$$

As (14) is the equation for the well-known harmonic oscillator, wave functions may be expressed by Hermite functions;

$$u_n=\exp\left(-\frac{\xi}{2}\varphi^2\right)\mathrm{H}_n(\sqrt{\xi}\varphi),\quad \lambda=(2n+1)\xi, \tag{16}$$

and the corresponding eigenvalue is

$$E=\left(n+\frac{1}{2}\right)m\hbar\sqrt{\frac{H}{2I}}. \tag{17}$$

By substituting the values given in a) and c) into Eq. (17) the level space of hexad axis rotation is calculated:

$$\Delta E_6=(8.2\pm0.2)\times10^{-3}\text{eV}.$$

If the second barrier height in Eq. (10) is mainly caused by two-fold axis rotation, the level spacing is:

$$\Delta E_2=(6.3\pm0.1)\times10^{-3}\text{eV}.$$

d) Comparison between These Calculated Values and Observed Ones.

In Table 4 the frequency spectrum evaluated from *GF* Matrix Method is compared with Raman and infrared spectrum. We also give neutron scattering data in Table 5.

Table 4. Lattice vibrational frequencies of benzene molecule.

(meV)

	Solid			Liquid	
	GF method by Shimanouchi (−3°C)	Raman spectrum by Fruhling (0°C)	Rot. // axis	Raman spectrum by Blatz (26°C)	Infrared spectrum by Stanevich (10°C)
A_g	3.5	4.3 (ν_1)	z		
	7.1	7.8 (ν_2)	y		
	9.8	...	x		
B_{1g}	4.1	4.3 (ν_1)	z		
	8.7	...	y		
	12.6	13.0(ν_4)	x		
B_{2g}	6.9	7.8 (ν_2)	y	9.3	
	8.6	8.6 (ν_3)	z		
	9.4	...	x		
B_{3g}	7.4	...	y		
	8.9	8.6 (ν_3)	z		
	12.4	13.0 (ν_4)	x		
A_u	3.2				
	6.1				
	7.2				
B_{1u}	4.2				
	7.2				
B_{2u}	3.8				6.8
	7.1				
B_{3u}	3.7				
	5.5				

Table 5. Neutron scattering data of liquid benzene.

(meV)

Zemlyanov (20°C)	Gläser (20°C)	Ross (20°C)	Rush (23°C)
1.8			
3.7 (ν_1)			
5.8 (ν_2)	≃ 10	≃ 7.5	≃ 9.9
7.6 (ν_3)			
12.1 (ν_4)			

Table 6. Pressure variation of rotational relaxation time.

Pressure (atm)	1	200	400	600	700
$\log \tau_c$	−11.60	−11.24	−11.14	−11.06	−11.03

Table 7. Extrapolated rotational relaxation time in Fig. 4.

Temperature (°K)	304.8	278.7
$\log \tau_c$	−11.74	−11.04

(4) Quasi-crystalline Structure of Liquid Benzene.

Boss and STEJSKAL[16] measured the pressure variation of rotational relaxation time in liquid benzene at 304.8°K. These values are given in Table 6.

In Table 7 we show the values of $\log \tau_c$ at 304.8°K and at the melting point (278.7°K) by extrapolating the line between 240°K and 270°K in Fig. 4.

By comparing these two tables, we find that, within the limit of experimental errors, $\log \tau_c$ of liquid benzene is just upon the extrapolated straight line of solid benzene in Fig. 4 and by pressurizing the liquid benzene, the relaxation time approaches gradually to that of solid at the melting point. So we may expect that the rotational barrier heights of liquid benzene are approximately equal to those of solid near the room temperature and its rotational structure is nearly the same as solid one.

Moreover self diffusion seems to exist in liquid state. In such a motion NMR spin echo method[17] is very useful to measure the self diffusion coefficient D and to determine the potential barrier height from it using the following equation:

$$D=D_0 \exp(-\beta V_0/V_F) \exp\left(-\frac{H}{RT}\right),$$

where β ; geometrical factor between 0.5 and 1,
V_0 ; specific volume for closest packing,
V ; specific volume,
$V_F=V-V_0$; free volume.

From this point of view, R. HAUSER, G. MAIER and F. NOACK determined the potential barrier height of self diffusion in liquid benzene from room temperature up to the critical point. We assume here that the potential curve is given by

$$V(X)=\frac{H}{2}\left(1-\cos\pi\frac{x}{\lambda}\right), \quad (\lambda\text{ ; period of the potential curve}).$$

By using the barrier height $H=2.0$ kcal/mol which is given by above method, we get the level spacing ΔE;

$$\Delta E=2.3\times10^{-3}\text{ eV} \quad (\lambda=6\text{Å})$$

(5) Discussion and Conclusion

① In (2) we treated intramolecular rotation in biphenyl gas and in (3) we explained the conventional theories which were developed to treat crystalline system, especially solid benzene. We stress here that, by combining above two methods, they may be generalized to treat the biphenyl crystal which include intramolecular rotation.

② As shown in Table 4 BLATZ stressed that, in both cases of Raman and infrared experiments, the average values over all active frequencies except lowest two agree rather well with the peak positions of liquid benzene. Strictly speaking these agreements cannot be accepted straightforwardly, because he compared averages for crystal with the peak positions for liquid. On the contrary we treated solid benzene in (3). Our result for hexad axis rotational level from NMR data shows a good agreement with the above-mentioned average value. And this also proves the validity of neglect of two levels.

③ Although it becomes possible to explain the general tendency of inelastic scattering of neutron from above discussions, many problems about fine structure of scattering cross section are remained to be clarified. For example we found that the lowest level 1.8 meV in Table 5 is the same order as our level spacing for diffusion motion obtained in (4). From above discussion we may conclude that in the quasi-crystalline structure of liquid benzene both the degree of freedoms of solid and liquid states coexist.

References

1) Zemlyanov M.G. and Chernoplekov H.A. : *Atomnaya Energiya* 14, 257 (1963).
2) Gläser W. : *Nucleonik* 7, 64 (1965).
3) Tarina V. : *J. Chem. Phys.*, 46, 2273 (1967).
4) Ross D.K., Szabo F.P. and Sanalan Y. : Symposium on Neutron Thermalization and Reactor Spectra SM 96/1 (1967).
5) Harada I. and Shimanouchi T. : *J. Chem. Phys.*, 46, 2708 (1967), *J. Chem. Phys.*, 44, 2016 (1966).
6) Ito M. and Shigeoka T. : *Spectrochim. Acta* 22, 1029 (1966).
7) Fruhling A. : *Ann. de Phys.*, 12, 26 (1951).
8) Sekiya T., Sakamoto K. and Nishida C. : *Tech. Repts. Osaka Univ.*, 16, 431 (1966).
9) Simmons H.E. and Williams J.K. : *J. Am. Chem. Soc.* 86, 3222 (1964).
10) Suzuki H. : *Bull. Chem. Soc. Japan* 32, 1340 (1959).
11) Adrian F.J. : *J. Chem. Phys.* 28, 608 (1958).
12) Coulson C.A. and Streitwieser Jr. A. : "Supplemental Tables of Molecular Orbital Calculations Vol. 2, Dictionary of π-electron Calculation", Pergamon Press Inc. (1965).
13) Cox E.G. : *Rev. Mod. Phys.*, 30, 159 (1958).
14) Andrew E.R. and Eades R.G. : *Proc. Roy. Soc. London*, A, 218, 537 (1953).
15) Bloembergen N., Purcel E.M. and Pound P.V. : *Phys. Rev.* 73, 679 (1948).
16) Boss B.D., Stejskal E.O. : *J. Chem. Phys.*, 45, 81 (1966).
17) Hauser R., Maier G. and Noack F. : *Z. Naturforschg*, 21 a, 1410 (1966).

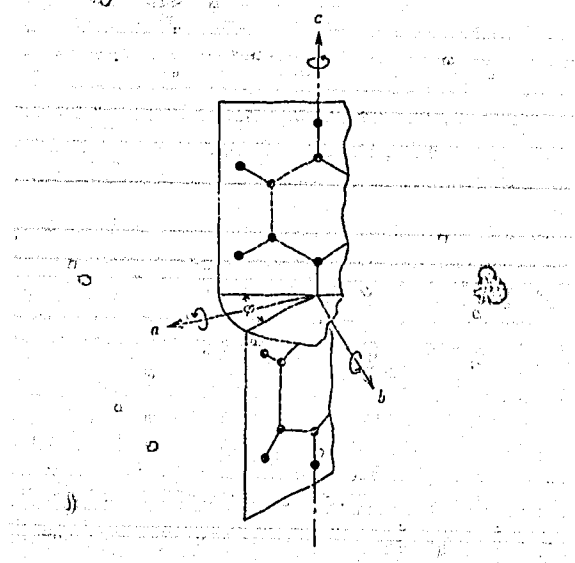

Fig. 1 Principal axes of biphenyl molecule.

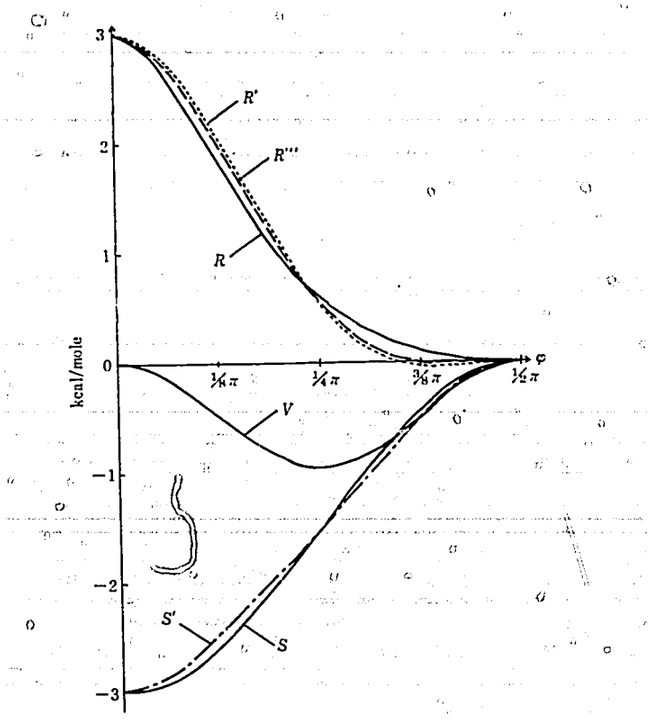

Fig. 2 Determination of potential barrier height.

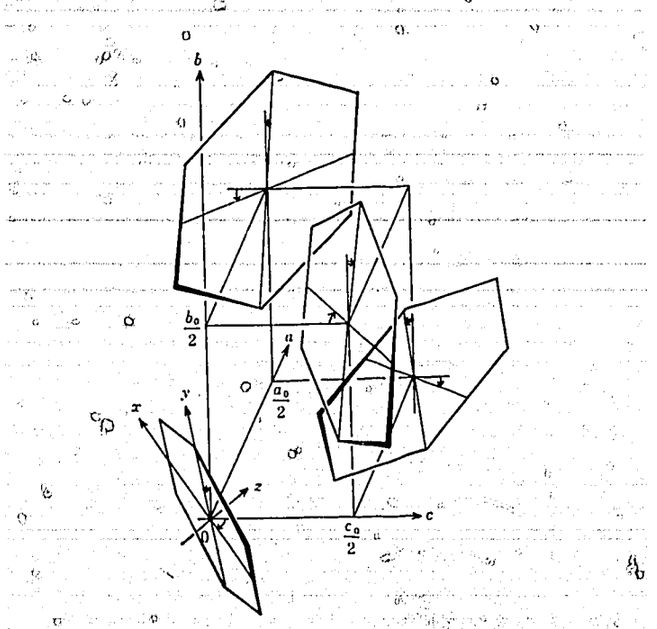

Fig. 3 Crystalline structure and principal axis of benzene molecule.

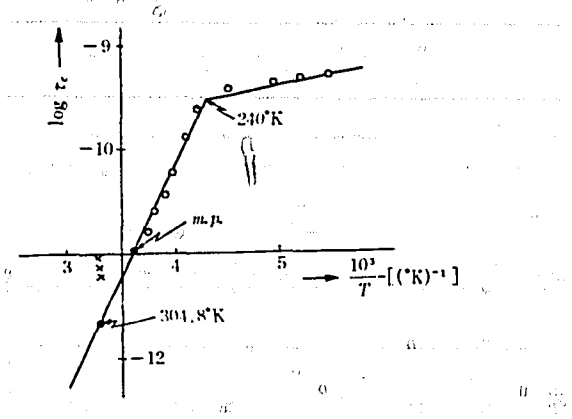

Fig. 4 Plot of $\log_{10} \tau_c$ against $10^3/T$ for benzene,
where ○; Andrew's data
●; extrapolated values
×; Boss' data

Theory of Multiple Scattering of Slow Neutron

T. Nishigori, S. Yamasaki and S. Sunakawa (*Prog. Theor. Phys.* 39(1968) 37)
Department of Nuclear Engineering,
Faculty of Engineering,
Osaka University
Suita, Osaka

When the wavelength of a neutron is very long, the neutron interacts with the target system as a whole rather than with the individual atoms, and the effect of multiple scattering becomes important. The Van Hove formula[1] for neutron scattering fails to describe such a process. In the previous paper[2], the Van Hove formula is generalized to include the effect of the multiple scattering. On account of the drastic approximations adopted in the paper, however, the formula proposed does not satisfy the condition of detailed balance. The purpose of the present paper is to remedy this defect.

The scattering of a neutron is described by a scattering operator T, which can be rearranged in the following form,

$$T=\sum_{\alpha}T_{\alpha}+\sum_{\alpha}\sum_{\beta\neq\alpha}T_{\alpha}GT_{\beta}+\sum_{\alpha}\sum_{\beta\neq\alpha}\sum_{\gamma\neq\beta}T_{\alpha}GT_{\beta}GT_{\gamma}+\cdots\cdots, \tag{1}$$

$$T_{\alpha}=V_{\alpha}+V_{\alpha}GV_{\alpha}+V_{\alpha}GV_{\alpha}GV_{\alpha}+\cdots\cdots, \tag{2}$$

and

$$G=\frac{1}{E_i-H_A-H_n+i\varepsilon}\ , \tag{3}$$

where G refers to the propagator of the neutron, and H_A and H_n stand for the Hamiltonians of the target atoms and the neutron, respectively. The scattering operator T_α describes the scattering of a neutron by a single atom α in the target system through the interaction potential $V_\alpha=V(\boldsymbol{r}_n-\boldsymbol{r}_\alpha)$, where $\boldsymbol{r}_n$ and $\boldsymbol{r}_\alpha$ are the position operators of the neutron and the atom α, respectively.

In the present formalism, two approximations will be introduced. The first is that the propagators G in the single scattering operator T_α are replaced by that of the free neutron $G_0=(\varepsilon_i-H_n+i\varepsilon)^{-1}$, although the propagators G in (1) are treated exactly. By virtue of the fact that the propagators G in (1) is retained as it is, the recoil effect to the intermediate neutron is taken into account and the condition of detailed balance is satisfied. The second approximation is

$$<\boldsymbol{k}_f|t(\varepsilon_i)|\boldsymbol{k}_i>\simeq\frac{2\pi\hbar^2}{m}a\ , \tag{4}$$

where $t(\varepsilon_i)$ is the scattering operator which describes scattering of a neutron by a target atom fixed at the origin and ε_i is the incident energy of the neutron.

Under these two assumptions, we obtain the following expression for the scattering cross section;

$$\frac{d^2\sigma}{d\Omega d\varepsilon_f}=\sum_{m=0}^{\infty}\sum_{n=0}^{\infty}a^2\frac{k_f}{k_i}\int_{-\infty}^{\infty}\frac{dt}{2\pi\hbar}\,e^{i(\varepsilon_f-\varepsilon_i)t/\hbar}\int_{-\infty}^{\infty}dt_1'\cdots dt_n'\,dt_1\cdots dt_n$$
$$\times\int d\boldsymbol{x}_0'\,d\boldsymbol{x}_1'\cdots d\boldsymbol{x}'_m\,d\boldsymbol{x}_i\,d\boldsymbol{x}_1\cdots d\boldsymbol{x}_n\,e^{i\boldsymbol{k}_f(\boldsymbol{x}_0'-\boldsymbol{x}_0)}\,e^{-i\boldsymbol{k}_i(\boldsymbol{x}_m'-\boldsymbol{x}_n)}$$
$$\times K_i^{(-)}(\boldsymbol{x}'_m-\boldsymbol{x}'_{m-1},t'_m-t'_{m-1})\cdots K_i^{(-)}(\boldsymbol{x}_1'-\boldsymbol{x}_0',t_1'-0)\cdot K_i^{(+)}(\boldsymbol{x}_0-\boldsymbol{x}_1,0-t_1)$$
$$\cdots K_i^{(+)}(\boldsymbol{x}_{n-1}-\boldsymbol{x}_n,t_{n-1}-t_n)G(\boldsymbol{x}'_m,t'_m;\boldsymbol{x}'_{m-1},t'_{m-1};$$
$$\cdots;\boldsymbol{x}'_0,0\,|\,\boldsymbol{x}_0,t;\boldsymbol{x}_1,t+t_1;\cdots;\boldsymbol{x}_n,t+t_n),$$

where the $(m+n+2)$—particle space-time correlation function G is defined by

$$G(\boldsymbol{x}'_m,t'_m;\boldsymbol{x}'_{m-1},t'_{m-1};\cdots;\boldsymbol{x}'_0,t'\,|\,\boldsymbol{x}_0,t,\ ;\boldsymbol{x}_1,t+t_1;\cdots;\boldsymbol{x}_n,t+t_n)$$
$$=\sum_{\alpha'}\cdots\sum_{\nu'\neq\mu'}\sum_{\alpha}\cdots\sum_{\nu\neq\mu}\ll\delta(\boldsymbol{x}'_m-\boldsymbol{r}_{\nu'}(t'_m))\,\delta(\boldsymbol{x}'_{m-1}-\boldsymbol{r}_{\mu'}(t'_{m-1}))\cdots\delta(\boldsymbol{x}'_1-\boldsymbol{r}_{\beta'}(t_1'))$$
$$\times\delta(\boldsymbol{x}'_0-\boldsymbol{r}_{\alpha'}(0))\cdot\delta(\boldsymbol{x}_0-\boldsymbol{r}_\alpha(t))\,\delta(\boldsymbol{x}_1-\boldsymbol{r}_\beta(t+t_1))\cdots\delta(\boldsymbol{x}_n-\boldsymbol{r}_\nu(t+t_n))\gg,$$

and the propagation functions $K_i^{(\pm)}(\boldsymbol{r},t)$ are given by

$$K_i^{(\pm)}(\boldsymbol{r},t)=\pm\frac{i}{\hbar}\theta_\pm(t)K_i(\boldsymbol{r},t), \tag{7}$$

and

$$K_i(\boldsymbol{r},t)=\frac{2\pi\hbar^2}{m}a\int\frac{d\boldsymbol{k}}{(2\pi)^3}e^{i(\varepsilon_i-\varepsilon k)t/\hbar}\,e^{i\boldsymbol{k}\boldsymbol{r}},$$

$$\theta_\pm(t)=\begin{cases}e^{-\varepsilon|t|/\hbar} & \text{for } t\gtrless 0\\ 0 & \text{for } t\lessgtr 0.\end{cases} \tag{8}$$

The time-dependence of $K_{i\pm}(\boldsymbol{r},t)$ is caused by the recoil effect of the neutron.

The first term in the right-hand side of (5) is the contribution from the single scattering and coincides with the Van Hove formula. The other terms describe the effect of the multiple scattering. A method obtaining a classical approximation for this multiple scattering cross section is studied along the line of reasoning of the previous paper[3].

References

1) Van Hove : *Phys. Rev.* 95, 249 (1954).

2) Sunakawa S., Fukui Y. and Nishigori T. : *Prog. Theor. Phys.* 35, 228 (1966).

3) Sunakawa S., Yamasaki S. and Nishigori T. : *Prog. Theor. Phys.* 37, 1051 (1967).

Quasi-classical Theory of Slow Neutron Scattering

T. NISHIGORI and S. SUNAKAWA (to be published in *Prog. Theor. Phys.*)
Department of Nuclear Engineering,
Faculty of Engineering,
Osaka University,
Suita, Osaka

Several years ago, VINEYARD[1] proposed a prescription of a classical approximation to the Van Hove formula[2] for the scattering of a slow neutron. The Vineyard's classical formula for the cross section, however, does not satisfy the condition of detailed balance, because of the obvious defect that the recoil effect of the scattered neutron is completely discarded. In order to correct this defect, great efforts have been made by many authors,[3),4)] but these results still have some unsatisfactory features. In the previous paper,[5] a new method for obtaining a classical approximation of the scattering cross section is proposed. In this treatment, the recoil effect of the scattered neutron is fully taken into consideration. The condition of detailed balance, however, is not satisfied rigorously, since the effect of the quantum mechanical thermal average is discarded. The aim of the present note is to remedy this defect and to obtain a well-defined classical formula which satisfies the condition of detailed balance rigorously.

For this purpose, we reformulate the quantum-mechanical formula for the scattering cross section so as to be quite adequate to get the classical formula. By making use of the generalized cumulant expansion method[6], and with the aid of the fluctuation-dissipation theorem for the cumulant function $K_{\alpha\beta}(\boldsymbol{p}, t)$ defined below, we can transform the scattering cross section into the following form

$$\frac{d^2\sigma}{d\Omega d\varepsilon_f}=\left(\frac{m}{2\pi\hbar^2}\right)^2 |<\boldsymbol{p}_f|t(\varepsilon_i)|\boldsymbol{p}_i>|^2 \frac{p_f}{p_i} e^{-\beta\varepsilon/2} \sum_{\alpha,\beta} \int_{-\infty}^{\infty} \frac{dt}{2\pi\hbar} e^{i\varepsilon t/\hbar} A_{\alpha\beta}(\boldsymbol{p}, t), \tag{1}$$

where the scattering function $A_{\alpha\beta}$ is defined by

$$A_{\alpha\beta}(\boldsymbol{p}, t)=\exp\left[-\left\{\left(\operatorname{cosec}\frac{\beta\hbar}{2}\frac{d}{dt}\right) \operatorname{Im} K_{\alpha\beta}(\boldsymbol{p}, t)+C(\boldsymbol{p})\right\}\right], \tag{2}$$

and m, $\boldsymbol{p}_i$ and $\boldsymbol{p}_f$ are the mass, the initial momentum and the final one of the neutron, respectively. The momentum transfer $\boldsymbol{p}$ and the energy transfer ε are denoted by $\boldsymbol{p}=\boldsymbol{p}_f-\boldsymbol{p}_i$, and $\varepsilon=\varepsilon_f-\varepsilon_i$. The cumulant function $K_{\alpha\beta}(\boldsymbol{p}, t)$ (2) is defined by

$$K_{\alpha\beta}(\boldsymbol{p}, t)=<\exp_s\left[\frac{i}{\hbar}(pA_1(t)+p^2A_2(t)+p^3A_3(t)+\cdots\cdots)\right]-1>_{cum}, \tag{3}$$

where

$$\begin{aligned}
&A_1(t)=r_{\alpha p}(0)-r_{\beta p}(t),\\
&A_2(t)=\frac{1}{2i\hbar}[r_{\alpha p}(0),\ r_{\beta p}(t)],\\
&A_3(t)=\frac{1}{12}\left(\frac{1}{i\hbar}\right)^2([[r_{\alpha p}(0),\ r_{\beta p}(t)], r_{\beta p}(t)]-[[r_{\beta p}(t),\ r_{\alpha p}(0)], r_{\alpha p}(0)]),\\
&\cdots\cdots\cdots\cdots
\end{aligned} \tag{4}$$

The bracket $<\cdots>_{cum}$ designates a cumulant average and $\exp_s$ indicates the symmetrized exponential. The operator $r_{\alpha p}$ in (4) refers to the component of $\boldsymbol{r}_\alpha$ in the direction of $\boldsymbol{p}$. The constant of integration $C(\boldsymbol{p})$ in (2) is determined by the initial condition

$$C(\boldsymbol{p})=\operatorname{Re}K_{\alpha\beta}(\boldsymbol{p}, 0)+\left[\left(\cot\frac{\beta\hbar}{2}\frac{d}{dt}\right)\operatorname{Im}K_{\alpha\beta}(\boldsymbol{p}, t)\right]_{t=0}. \tag{5}$$

The condition of detailed balance is of course satisfied in the quantum mechanical formula (1) owing to the extra factor $\exp(-\beta\varepsilon/2)$ and to the following property of the scattering function $A_{\alpha\beta}$:

$$A_{\alpha\beta}(\boldsymbol{p}, t)=A_{\alpha\beta}(-\boldsymbol{p}, -t), \tag{6}$$

which is valid under the condition that the Hamiltonian of the target system is invariant under space reflection

and time-reversal operation. Since the scattering function $A_{\alpha\beta}$ is written in terms of the commutators A_n, the formula (1) involves the recoil effect of the neutron explicitly, and it will be quite convenient to obtain a well-defined classical formula.

As already mentioned in the previous paper[5], all terms in the exponent of the right-hand side of (3) should be retained in the classical limit by replacing the commutators by the classical Poisson brackets $\{\cdots\}_c$. Thus the classical limit of (1) is given by

$$\frac{d^2\sigma^c}{d\Omega d\varepsilon_f}=\left(\frac{m}{2\pi\hbar^2}\right)^2 |<\boldsymbol{p}_f|\, t(\varepsilon_i)|^2\, \boldsymbol{p}_i> e^{-\beta\varepsilon/2}\, \frac{p_f}{p_i}\sum_{\alpha,\beta}\int_{-\infty}^{\infty}\frac{dt}{2\pi\hbar}\, e^{i\varepsilon t/\hbar}\, A_{\alpha\beta}{}^c(\boldsymbol{p},t), \tag{7}$$

where

$$A_{\alpha\beta}{}^c(\boldsymbol{p},t)=\exp\left[-\left\{\left(\operatorname{cosec}\frac{\beta\hbar}{2}\frac{d}{dt}\right)[\mathrm{Im}\,K_{\alpha\beta}(\boldsymbol{p},t)]_{\mathrm{classical}}+C^c(\boldsymbol{p})\right\}\right], \tag{8}$$

$$[\mathrm{Im}\,K_{\alpha\beta}(\boldsymbol{p},t)]_{\mathrm{classical}}=\mathrm{Im}\ll\exp\left[\frac{i}{\hbar}\,(pA_1{}^c(t)+p^2A_2{}^c(t)+p^3A_3{}^c(t)\cdots)\right]-1\gg_{cum}, \tag{9}$$

and

$$C^c(\boldsymbol{p})=[\mathrm{Re}K_{\alpha\beta}(\boldsymbol{p},0)]_{\mathrm{classical}}+\left[\left(\cot\frac{\beta\hbar}{2}\frac{d}{dt}\right)[\mathrm{Im}\,K_{\alpha\beta}(\boldsymbol{p},t)]_{\mathrm{classical}}\right]_{t=0}. \tag{10}$$

The bracket $\ll\cdots\gg_{cum}$ indicates the classical cumulant average, and $A_1{}^c(t)$, $A_2{}^c(t)$ ... are defined by

$$\begin{aligned}
A_1{}^c(t)&=r_{\alpha p}{}^c(o)-r_{\beta p}{}^c(t),\\
A_2{}^c(t)&=\frac{1}{2}\,\{r_{\alpha p}{}^c(0),\ r_{\beta p}{}^c(t)\}_c,\\
A_3{}^c(t)&=\frac{1}{12}(\{\{r_{\alpha p}{}^c(o),\ r_{\beta p}{}^c(t)\}_c,\ r_{\beta p}{}^c(t)\}_c,\ -\{\{r_{\beta p}{}^c(t),\ r_{\alpha p}{}^c(o)\}_c,\ r_{\alpha p}{}^c(o)\}_c),\\
&\cdots\cdots\cdots.
\end{aligned} \tag{11}$$

The function $r_{\alpha p}{}^c(t)$ is a solution of the classical equation of motion of the target atom.

On the basis of the condition that the Hamiltonian is invariant under space reflection and time-reversal operation, we can show classicaly that $A_{\alpha\beta}{}^c$ has the symmetric property :

$$A_{\alpha\beta}{}^c(\boldsymbol{p},t)=A_{\alpha\beta}{}^c(-\boldsymbol{p},-t), \tag{12}$$

The classical expression of the scattering cross section (7), therefore, does satisfy the condition of detailed balance, and furthermore the recoil effect is taken into consideration.

When the motions of the atoms are described by linear equations, the Poisson bracket $A_2{}^c(t)$ becomes independent of the statistical average, and the Poisson brackets $A_3{}^c(t)$, $A_4{}^c(t)$,... vanish. In this case, the self-part of the scattering function $A_s{}^c$ has the simple Gaussian form:

$$A_s{}^c(\boldsymbol{p},t)=\exp\left[-p^2\left\{\left(\operatorname{cosec}\frac{\beta\hbar}{2}\frac{d}{dt}\right)[\mathrm{Im}\,\lambda_2{}^s(t)]_{\mathrm{classical}}-\left(\cot\frac{\beta\hbar}{2}\frac{d}{dt}\right)[\mathrm{Im}\,\lambda_2{}^s(t)]_{\mathrm{classical}}]_{t=0}\right\}\right], \tag{13}$$

where

$$[\mathrm{Im}\,\lambda_2{}^s(t)]_{\mathrm{classical}}=\frac{1}{2\hbar}\,\{r_{\alpha p}{}^c(o),\ r_{\beta p}{}^c(t)\}_c. \tag{14}$$

Finally, we shall apply the new classical formula to a simple illustrative example. Consider a system composed of independent isotropic harmonic oscillators with an identical frequency ω and a mass M. The dynamical motion of an atom α in this system is described by

$$\boldsymbol{r}_\alpha{}^c(t)=\boldsymbol{r}_\alpha{}^c(o)\cos\omega t+\frac{\boldsymbol{p}_\alpha{}^c(o)}{M\omega}\sin\omega t, \tag{15}$$

and then the scattering function $A_s{}^c$ has the Gaussian form. In (15), $\boldsymbol{r}_\alpha{}^c(o)$ and $\boldsymbol{p}_\alpha{}^c(o)$ are the initial position and momentum of the atom α, respectively. Substituting (15) into (14), we have

$$[\mathrm{Im}\,\lambda_2{}^s(t)]_{\mathrm{classical}}=\frac{1}{2M\hbar\omega}\sin\omega t, \tag{16}$$

and obtain the classical incoherent scattering cross section

$$\frac{d^2\sigma_{inc}}{d\Omega d\varepsilon_f}=a^2{}_{inc}\frac{p_f}{p_i}\,e^{-\beta\varepsilon/2}\,e^{-p^2/M\beta\hbar\omega^2}\sum_{n=-\infty}^{\infty}I_n(z)\delta(\varepsilon+n\hbar\omega), \tag{17}$$

where

$$\frac{1}{\beta'}=\frac{\hbar\omega}{2}\coth\frac{\beta\hbar\omega}{2}\ ,$$

and

$$\varkappa=\frac{p^2}{M\beta'\hbar^2\omega^2}\sqrt{1-(\beta'\hbar\omega/2)^2}\ .$$

Since $[\mathrm{Im}\,\lambda_2^2(t)]_{\mathrm{classical}}$ has the same form as the quantum mechanical one, the result (17) based on the present classical formula coincides precisely with that obtained in quantum-mechanical way.

The details of the present work will be published in the near future.

References

1) Vineyard G.H. : *Phys. Rev.* 110, 999 (1958).
2) Van Hove L. : *Phys. Rev.* 95, 249 (1954).
3) Schofield P. : *Phys. Rev. Letters* 4, 239 (1960).
4) Rahman A. : *Phys. Rev.* 130, 1334 (1963).
5) Sunakawa S., Yamasaki S. and Nishigori T. : *Prog. Theor. Phys.* 37, 1051 (1967).
6) Kubo R. : *J. Phys. Soc. Japan* 17, 1100 (1962).

Phonon Spectrum and Thermal Neutron Scattering in Light Water Ice

Y. NAKAHARA (*J. Nucl. Sci. Eng.* 5, 31, '68)
Japan Atomic Energy Research Institute

Ice is a hexagonal crystal, belonging to D^4_{6h}, over the temperature range about −100~0°C[1]. The unit cell contains four H_2O molecules. Each oxygen atom is arranged in the crystal ice as shown in Fig. 1 and is surrounded by four neighboring oxygen atoms in tetrahedral arrangement. We assume that point molecules with mass of H_2O molecules are arranged at the positions of oxygen atoms. In other words, we consider that the lattice vibrations are not affected by molecular rotations and vibrations.

We calculated the phonon spectrum of light water ice at 0°C by means of the root sampling method for a sampling of 1,050 points in an irreducible sampling region of the first Brillouin zone. The force model used in our computation is a non-central force model formulated by FORSLIND, in which interactions with only the nearest neighbors are taken into consideration[2]. The number of the atomic force constants introduced as model parameters is seven. The values of force constants have been determined by FORSLIND from the experimental values of the elastic constants obtained by JONA and SCHERRER:

$\alpha = 379$ $\theta = 2830$
$\beta = 4445$ $\varepsilon = 1616$
$\gamma = 3600$ $\kappa = 21549$
$\delta = 2830$ in dyne/cm²

The cell dimensions at 0°C are

a=4.5226 Å,
c=7.3670 Å.

The phonon spectrum of ice at 0°C and dispersion relations in the crystallographic a- and c- axis are shown in Fig. 2.

So far we have neglected the effects of intramolecular motions. The complete frequency distribution for ice can be given approximately by superimposing frequency distributions of hindered molecular rotations and intramolecular vibrations upon the phonon spectrum obtained above by the root sampling method. We approximate frequency distributions of molecular rotations and vibrations by descrete δ-type levels (Fig. 3).

The characteristic frequencies for molecular rotations and vibrations of H_2O molecules in ice are known from the infrared and Raman spectrocopic investigations[1]:

rotation $\omega_r = 0.0756$ eV,
vibrations $\omega_v^1 = 0.2033$ eV,
$\omega_v^2 = 0.3896$ eV,
$\omega_v^3 = 0.4030$ eV.

Although intensities of these discrete modes will be somewhat different from the values for liquid water, we use the same values as those obtained by NELKIN for liquid water[3]. The effective masses for molecular rotations and vibrations are

$m_r = 2.32$,
$m_v = 1.95$.

We used the GASKET code written by KOPPEL *et al.*[4] to evaluate the scattering law for ice. The double differential scattering cross section and the scattering law for thermal neutron scattering in light water ice at 268°K have been measured by HARLING[5]. The calculated values of the scattering law for ice at 0°C are shown in Figs. 4~10, together with the experimental values at −5°C by HARLING. Our calculations resulted in good agreement with the neutron scattering measurements.

The author is indebted to Dr. H. Takahashi for the initial suggestion of this problem and for the most

helpful guidance and encouragement.

References

1) Seki S. : "Bussei Butsurigaku Koza" (Series in Solid State Physics, written in Japanese), Vol. 11, Chap. 6, ed. Ariyama K. *et al.*, Kyoritsu Pub. Co. Ltd., Tokyo (1954).

2) Forslind E. : Proc. No. 21, Swedish Cement and Concrete Res. Inst. at Royal Inst. of Technology, Stockholm (1954).

3) Nelkin M. : *Phys. Rev.*, 119, 741 (1960).

4) Koppel J.U., Triplett J. R. and Naliboff Y. D. : GASKET: A Unified Code for Thermal Neutron Scattering, GA-7417 (Rev.) (1967).

5) Harling O.K. : Compilation of Doubly Differential Cross Section and the Scattering Law for H_2O and D_2O at 299°K and for H_2O at 268°K, BNWL-436 (1967).

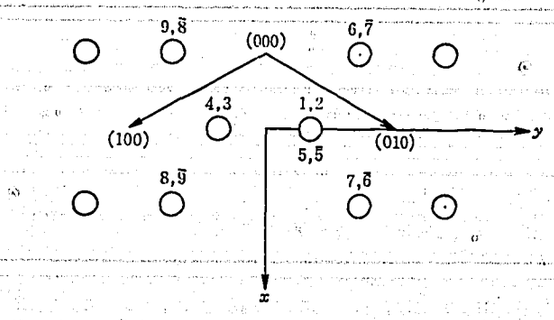

Fig. 1 Projection on the basis plane of cells containing interacting molecules. Molecules 1~4 are contained in the same unit cell.

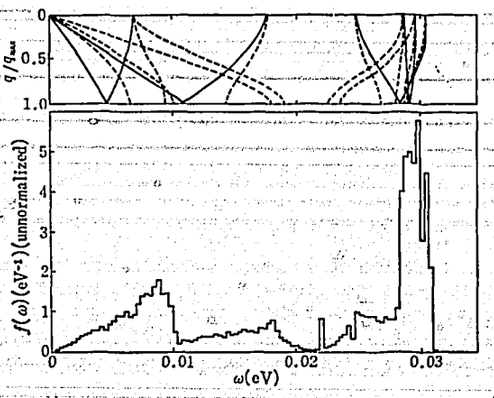

Fig. 2 Dispersion relation and the unnormalized phonon spectrum of light water ice at 0°C. The upper figure shows dispersion relations along the crystallographic *c*-axis (——) and *a*-axis (·····).

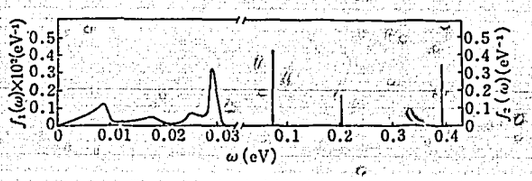

Fig. 3 The full frequency distribution of ice used to compute the scattering law for ice. The continuous part $f_2(\omega)$ is normalized to 1/18 and the disceret $f_1(\omega)$ to 17/18.

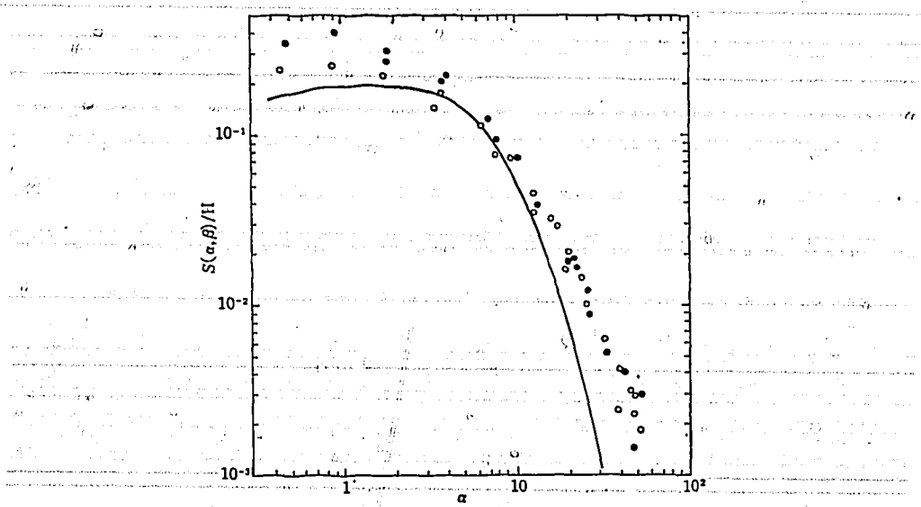

Fig. 4 Scattering law (per H) for light water ice: β=0.5 The solid curve is the calculated value at 0°C. Experimental values are from Harling: • for up-scattering, ○ for down-scattering.

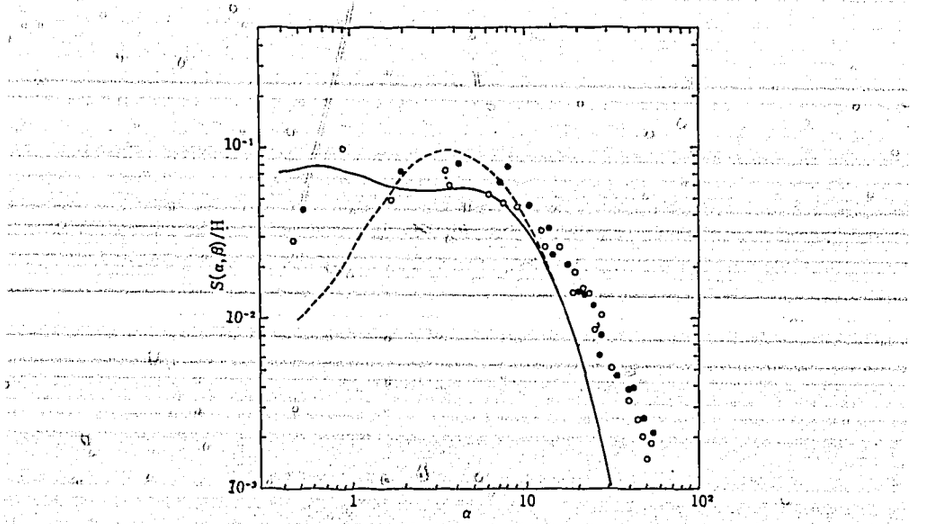

Fig. 5 Scattering law (per H) for ice: β=1.0. The dotted curve is the calculated scattering law for liquid water at room temperature (based on the Haywood model). Experimental values are from Harling. Also in Figs. 6—10.

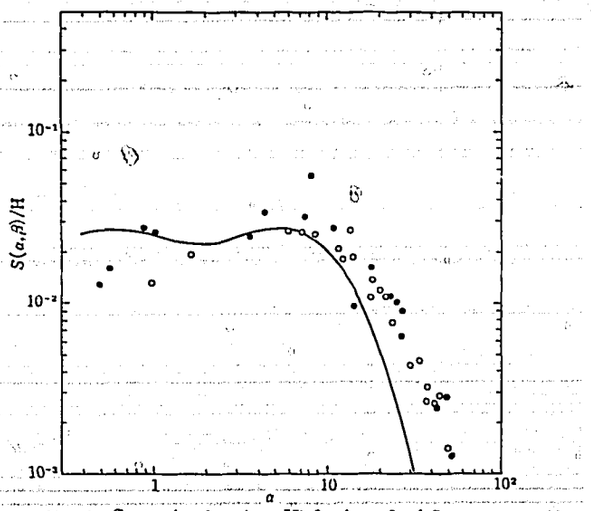

Fig. 6 Scattering law (per H) for ice: β=1.5.

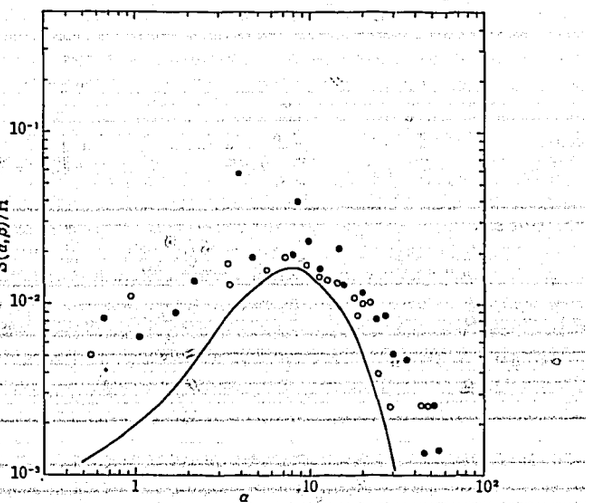

Fig. 7 Scattering law (per H) for ice: β=2.0.

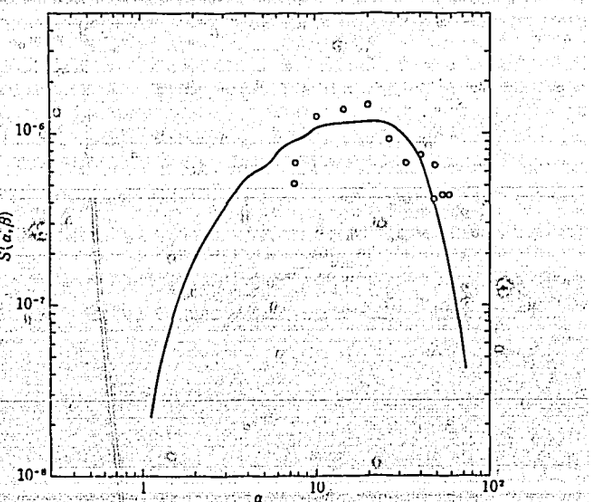

Fig. 8 Scattering law (per H) for ice: β=4.0.

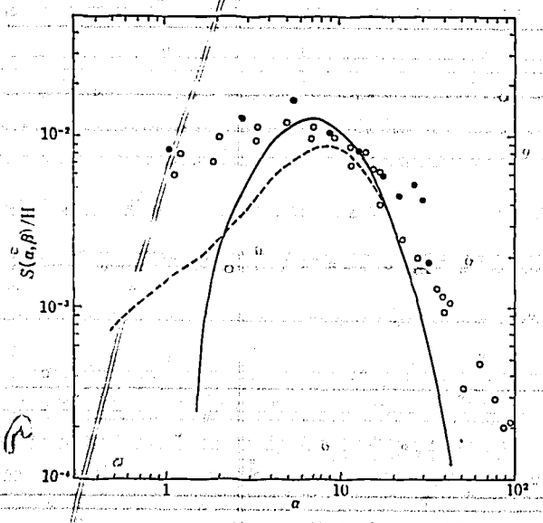

Fig. 9 Scattering law (per H) for ice: $\beta=10$.
The dotted curve is the scattering law when the value 0.06 eV (the value for liquid water) is used for ω_r.

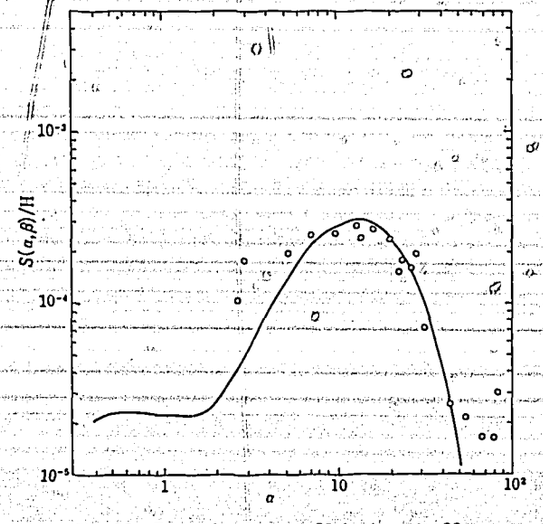

Fig. 10 Scattering law per H for ice: $\beta=20$.

Appendices

Tables of Frequency Spectra and Scattering Kernels

Frequency Specta of H_2O

The following lists (supplied by GASKET code) are the spectra of dynamical modes of the scatterer: Mode 1.... Free translation (gas), Mode 2.... Diffusive or Brownian motion, Mode 3....Harmonic isotropic vibrations with continuous frequency spectrum, Mode 4... Harmonic anisotropic vibrations with continuous frequency spectrum, Mode 5.... Harmonic isotropic vibrations with discrete frequency spectrum. W1-W5 means the weight of each mode. The frequency (RHO) of mode 3 and the values (OPHON) which is deduced multiplying the frequency by the factor of $e^{\frac{\omega}{2T}}/2\omega \sinh \frac{\omega}{2T}$ are tabulated as a function of OMEGA (ω, eV). The frequencies of discrete oscillators are given in eV with weights and maximum number of phonon terms calculated for the corresponding oscillators.

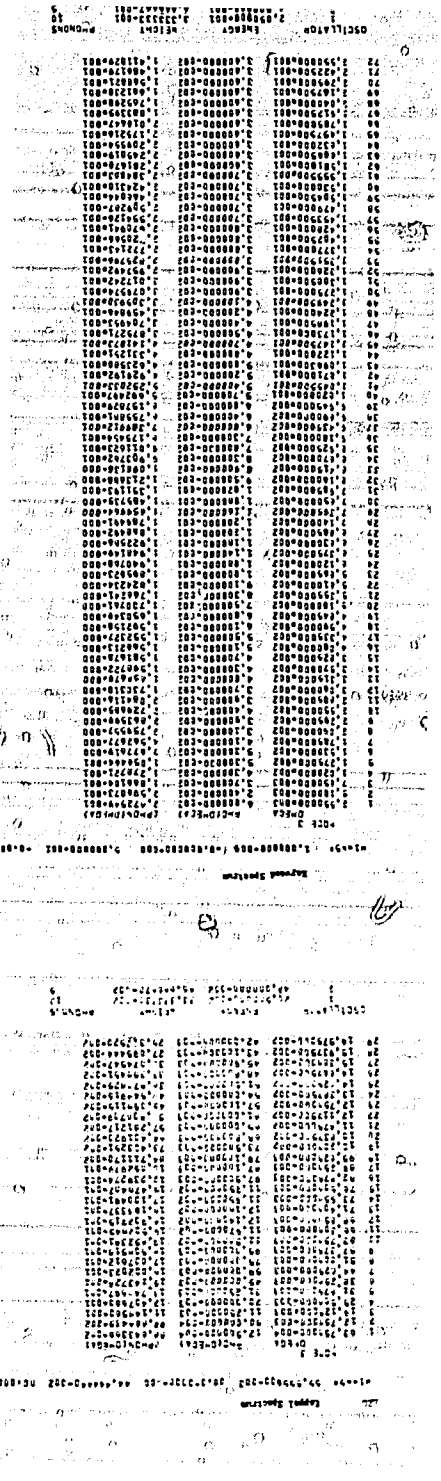

Frequency Distribution of Graphite

The numerical values of the frequency distribution of graphite, which must be supplied as input to the UNCLE code, are given below. The physical meanings of the symbols are as follows.

RHOJI=$\rho_j^i(\omega_k)$= The low (I=1) and the high (I=2) frequency part of the density of modes for the out-of-plane (J=1) and in-plane (J=2) vibrations for equally spaced values of frequencies ω_k.

K= The mesh number of frequencies.

THETA(J, I)= The maximum value of ω for which RHOJI is given.

$A(J,I)=\lim_{\omega^2\to 0}[\rho_j^i(\omega)/\omega^2]$

NUM= The number of $\rho_j^i(\omega_k)$ to be read in.

ω_k = (THETA/NUM)× k.

Graphite
UNCLE

RHOJ1 NUM= 17 THETA(J,I)= 0.425000E-01 A(J,I)= 0.760000E 05

K	RHOI(K,J,I)	K	RHOI(K,J,I)	K	RHOI(K,J,I)	K	RHOI(K,J,I)	K	RHOI(K,J,I)
1	0.1625nF 00	2	0.6350nE n0	3	0.1000OE 01	4	0.1650nF 01	5	0.2650OF 01
6	0.3750OF 01	7	0.5200E 01	8	0.4000E 01	9	0.3250OF 01	10	0.2700OF 01
11	0.2300OF 01	12	0.1900EE 01	13	0.1550OL 01	14	0.1150OF 01	15	0.7500OF 00
16	0.3500nF 00	17	0.						

RHOJ2 NUM= 24 THETA(J,I)= 0.160000E 00 A(J,I)= 0.160000E 04

K	RHOI(K,J,I)	K	RHOI(K,J,I)	K	RHOI(K,J,I)	K	RHOI(K,J,I)	K	RHOI(K,J,I)
1	0.	2	0.1000nF-01	3	0.4000OE-01	4	0.2700OF 00	5	0.6400OF 00
6	0.6200OF 00	7	0.8400OF 00	8	0.1100OF 01	9	0.1400OF 01	10	0.1850OF 01
11	0.2200OF 01	12	0.2600nF n1	13	0.3000OE 01	14	0.3500OF 01	15	0.4050OF 01
16	0.4600OF 01	17	0.5300OF 01	18	0.5500OL 01	19	0.5750OF 01	20	0.6100OF 01
21	0.7300OF 01	22	0.8950nF 01	23	0.8050OL 01	24	0.6350OF 01	25	0.5700OF 01
26	0.5700OF 01	27	0.5950nF n1	28	0.2300OL 01	29	0.1800OF 01	30	0.1350OF 01
31	0.8500OF 00	32	0.4000OE u0	33	0.2000OL 00	34	0.3800OF 00	35	0.8000OF 00
36	0.1500OF n1	37	0.1900OF n1	38	0.2450OF 01	39	0.3100OF 01	40	0.3900OF 01
41	0.4450OF n1	42	0.7800nF n1	43	0.1040OL 02	44	0.8100OF 01	45	0.7050OF 01
46	0.6100OF 01	47	0.5780OF n1	48	0.5200nE 01	49	0.4950OF 01	50	0.4800OF 01
51	0.4400OF n1	52	0.4480nF n1	53	0.4360OE 01	54	0.4220OF 01	55	0.4060OF 01
56	0.3950OF 01	57	0.3880nF n1	58	0.3750OE 01	59	0.3700OF 01	60	0.3600OF 01
61	0.3480OF 01	62	0.2330OF 01	63	0.9000OE 00	64	0.		

RHOJ1 NUM= 17 THETA(J,I)= 0.425000E-01 A(J,I)= 0.600000E 04

K	RHOI(K,J,I)	K	RHOI(K,J,I)	K	RHOI(K,J,I)	K	RHOI(K,J,I)	K	RHOI(K,J,I)
1	0.3750OE-n1	2	0.1500nE n0	3	0.2000OE 00	4	0.2500OF 00	5	0.2950OF 00
6	0.2800OF 00	7	0.2900OE 00	8	0.3000OE 00	9	0.3000OF 00	10	0.3000OF 00
11	0.2900OF 00	12	0.2700OF 00	13	0.2400OF 00	14	0.2000OF 00	15	0.1500OF 00
16	0.1000OE 00	17	0.						

RHOJ2 NUM= 63 THETA(J,I)= 0.2075nE 00 A(J,I)= 0.600000F 03

K	RHOI(K,J,I)	K	RHOI(K,J,I)	K	RHOI(K,J,I)	K	RHOI(K,J,I)	K	RHOI(K,J,I)
1	0.3750OE-n2	2	0.1500nF-n1	3	0.3375OE-01	4	0.6000OF-01	5	0.1100OF 00
6	0.1800OE 00	7	0.2500nE n0	8	0.3400OE 00	9	0.4400OF 00	10	0.5500OF 00
11	0.7000OF 00	12	0.8700nE n0	13	0.9400OE 00	14	0.1100OF 01	15	0.1250OF 01
16	0.1430OF 01	17	0.1650OE n1	18	0.1720OE 01	19	0.1810OL 01	20	0.1920OF 01
21	0.2040OE 01	22	0.2190nF n1	23	0.2310OE 01	24	0.2450OF 01	25	0.2610OF 01
26	0.2880OE n1	27	0.3000OF n1	28	0.3330OE 01	29	0.3400OF 01	30	0.4010OF 01
31	0.4500OE 01	32	0.5330nF n1	33	0.5200OL 01	34	0.4470OF 01	35	0.3900OF 01
36	0.3490OE 01	37	0.3400nE n1	38	0.3250OE 01	39	0.3100OF 01	40	0.2980OF 01
41	0.2890OF n1	42	0.2820nF n1	43	0.2800OE 01	44	0.2750OF 01	45	0.2700OF 01
46	0.2690OE 01	47	0.2690nF 01	48	0.2720OE 01	49	0.2730OF 01	50	0.2820OF 01
51	0.2940OE 01	52	0.3130nF n1	53	0.3470OE 01	54	0.4210OF 01	55	0.4250OF 01
56	0.3750OF 00	57	0.1740nE n1	58	0.1410OE 01	59	0.1920OF 01	60	0.1530OF 01
61	0.2850OE 01	62	0.3800nF 01	63	0.3220OE 01	64	0.2810OF 01	65	0.2760OF 01
66	0.2450OE n1	67	0.2250nF n1	68	0.6700OE 01	69	0.1150OF 02	70	0.1250OF 02
71	0.1070OE n2	72	0.9050nE n1	73	0.7050OE 01	74	0.6490OF 01	75	0.6050OF 01
76	0.5730OE n1	77	0.5550nF n1	78	0.5400OE 01	79	0.5270OF 01	80	0.5070OF 01
81	0.4950OF n1	82	0.4900nF n1	83	0.				

Frequency Distributions of Be and BeO

The numerical values of the frequency distributions of Be and BeO, which must be supplied as input to the UNCLE code, are given below. In the case of an isotropic crystal, or when lattice vibrations are assumed to be isotropic, the J=1 set is eliminated and RHO21 gives the isotropic frequency distribution.

Beryllium
UNCLE

RHO21 NUM= 80 THETA(J,I)= 0.661600E-01 A(J,I)= 0.500000E 01

K	RHOI(K,J,I)	K	RHOI(K,J,I)	K	RHOI(K,J,I)	K	RHOI(K,J,I)	K	RHOI(K,J,I)
1	0.100000E-01	2	0.200000E-01	3	0.300000E-01	4	0.400000E-01	5	0.500000E-01
6	0.700000E-01	7	0.100000E 00	8	0.120000E 00	9	0.140000E 00	10	0.170000E 00
11	0.200000E 00	12	0.240000E 00	13	0.270000E 00	14	0.300000E 00	15	0.350000E 00
16	0.400000E 00	17	0.450000E 00	18	0.500000E 00	19	0.600000E 00	20	0.750000E 00
21	0.870000E 00	22	0.108000E 01	23	0.125000E 01	24	0.145000E 01	25	0.165000E 01
26	0.195000E 01	27	0.225000E 01	28	0.260000E 01	29	0.155000E 01	30	0.265000E 01
31	0.425000E 01	32	0.450000E 01	33	0.440000E 01	34	0.465000E 01	35	0.455000E 01
36	0.447000E 01	37	0.445000E 01	38	0.430000E 01	39	0.420500E 01	40	0.410000E 01

RHO22 NUM= 51 THETA(J,I)= 0.663800E-01 A(J,I)= 0.

K	RHOI(K,J,I)	K	RHOI(K,J,I)	K	RHOI(K,J,I)	K	RHOI(K,J,I)	K	RHOI(K,J,I)
1	0.	2	0.	3	0.	4	0.	5	0.
6	0.	7	0.	8	0.	9	0.	10	0.
11	0.	12	0.	13	0.	14	0.	15	0.
16	0.	17	0.	18	0.	19	0.	20	0.
21	0.	22	0.	23	0.	24	0.	25	0.
26	0.	27	0.	28	0.	29	0.	30	0.
31	0.	32	0.	33	0.	34	0.	35	0.
36	0.	37	0.	38	0.	39	0.	40	0.
41	0.405000E 01	42	0.495000E 01	43	0.460000E 01	44	0.485000E 01	45	0.760000E 01
46	0.360000E 01	47	0.350000E 01	48	0.410000E 01	49	0.253000E 01	50	0.
51	0.								

BeO
UNCLE

RHO21 NUM= 79 THETA(J,I)= 0.725000E-01 A(J,I)= 0.400000E 02

K	RHOI(K,J,I)	K	RHOI(K,J,I)	K	RHOI(K,J,I)	K	RHOI(K,J,I)	K	RHOI(K,J,I)
1	0.500000E-02	2	0.400000E-01	3	0.120000E-01	4	0.900000E-02	5	0.750000E-02
6	0.100000E-01	7	0.150000E-01	8	0.200000E-01	9	0.300000E-01	10	0.450000E-01
11	0.600000E-01	12	0.800000E-01	13	0.110000E-00	14	0.140000E-00	15	0.180000E-00
16	0.170000E-00	17	0.270000E-00	18	0.210000E-00	19	0.270000E-00	20	0.280000E-00
21	0.275000E-00	22	0.270000E-00	23	0.260000E-00	24	0.250000E-00	25	0.240000E-00
26	0.240000E-00	27	0.240000E-00	28	0.240000E-00	29	0.		

RHO22 NUM= 69 THETA(J,I)= 0.625000E-00 A(J,I)= 0.

K	RHOI(K,J,I)	K	RHOI(K,J,I)	K	RHOI(K,J,I)	K	RHOI(K,J,I)	K	RHOI(K,J,I)
1	0.100000E-10	2	0.100000E-10	3	0.100000E-10	4	0.100000E-10	5	0.100000E-10
6	0.100000E-10	7	0.100000E-10	8	0.100000E-10	9	0.100000E-10	10	0.100000E-10
11	0.100000E-10	12	0.100000E-10	13	0.100000E-10	14	0.100000E-10	15	0.100000E-10
16	0.100000E-10	17	0.100000E-10	18	0.100000E-10	19	0.100000E-10	20	0.100000E-10
21	0.100000E-10	22	0.190000E-10	23	0.100000E-10	24	0.100000E-10	25	0.100000E-10
26	0.100000E-10	27	0.100000E-10	28	0.100000E-10	29	0.275000E-00	30	0.320000E-00
31	0.490000E-00	32	0.470000E-00	33	0.270000E 00	34	0.910000E-00	35	0.490000E 00
36	0.410000E 00	37	0.430000E-00	38	0.350000E-00	39	0.190000E-00	40	0.600000E-01
41	0.300000E-01	42	0.	43	0.	44	0.	45	0.
46	0.	47	0.	48	0.	49	0.		

H2O SIGMA(EI, EF) FOR KOPPEL SPECTRUM

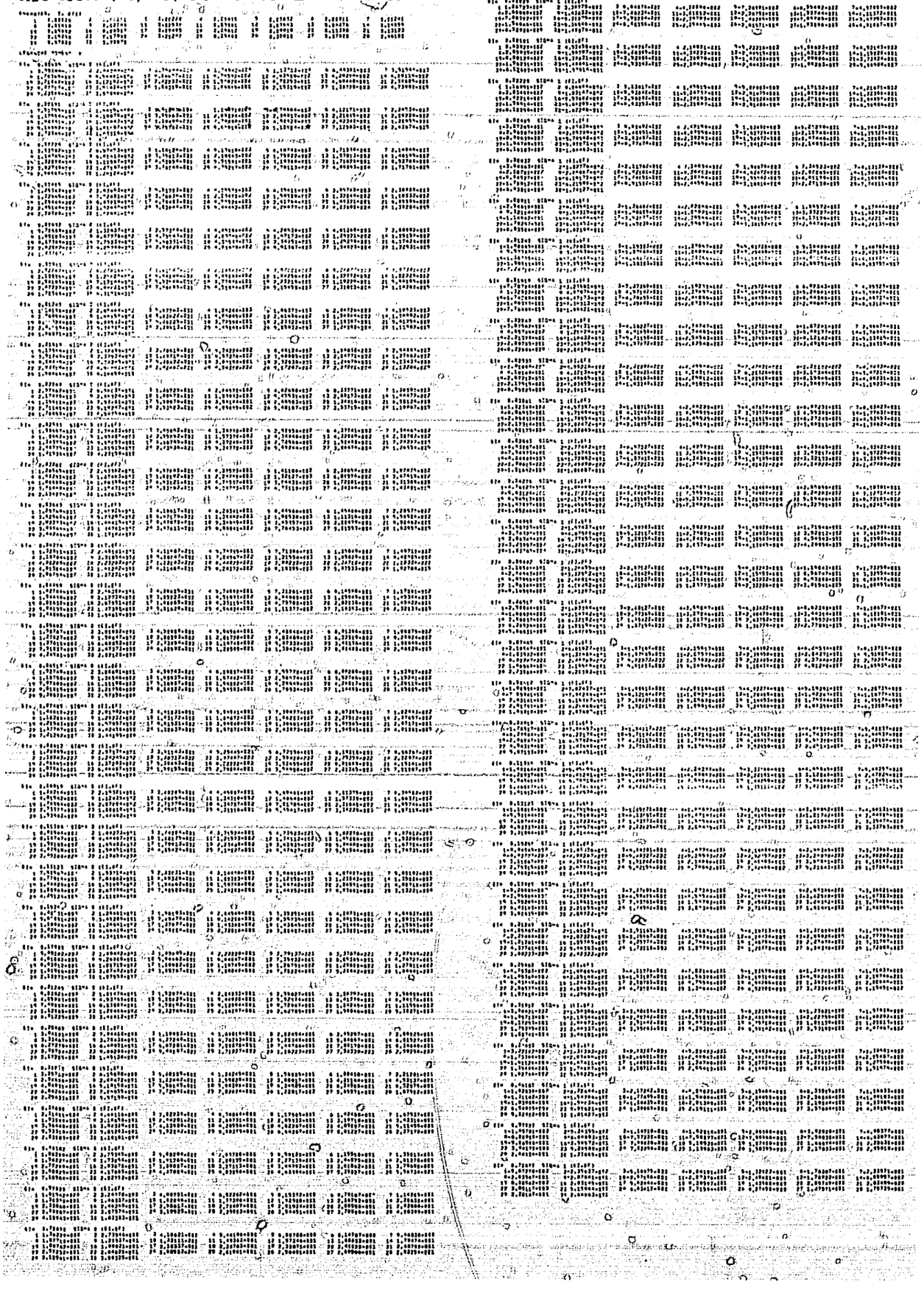

H20 SIGMA(EI, EF) FOR MODEL-2 SPECTRUM

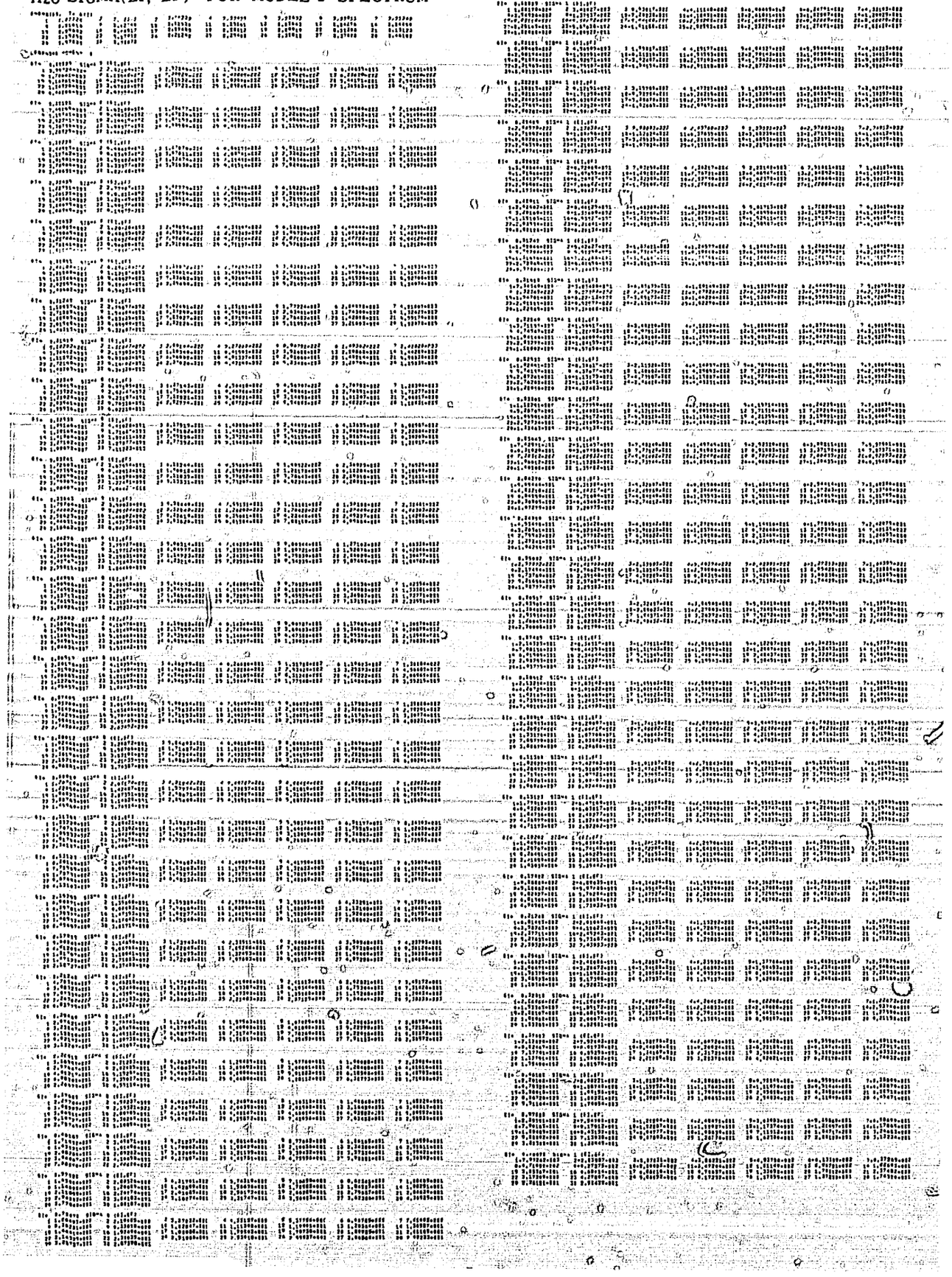

$\sigma_0(E_0 \rightarrow E)$ for A Deuteron in D_2O (Cross section for 0-phonon process is included in diagonal elements)

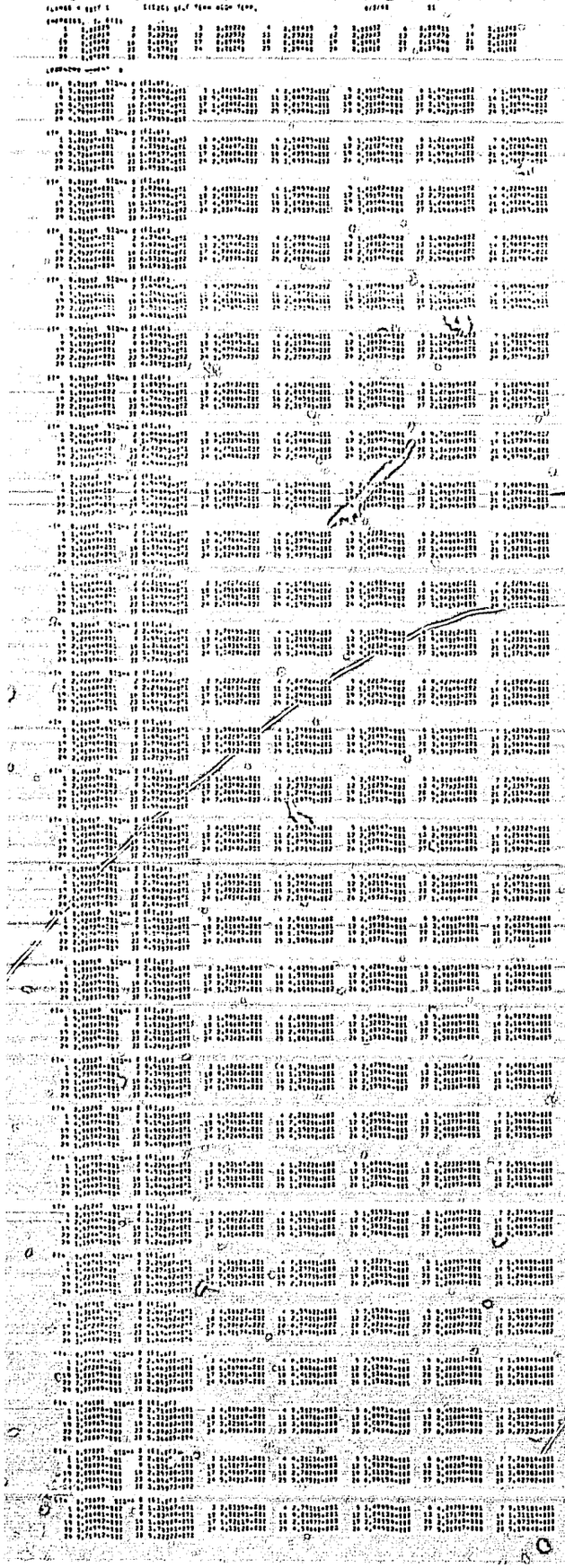

$\sigma_1(E_0 \rightarrow E)$ for A Deuteron in D_2O

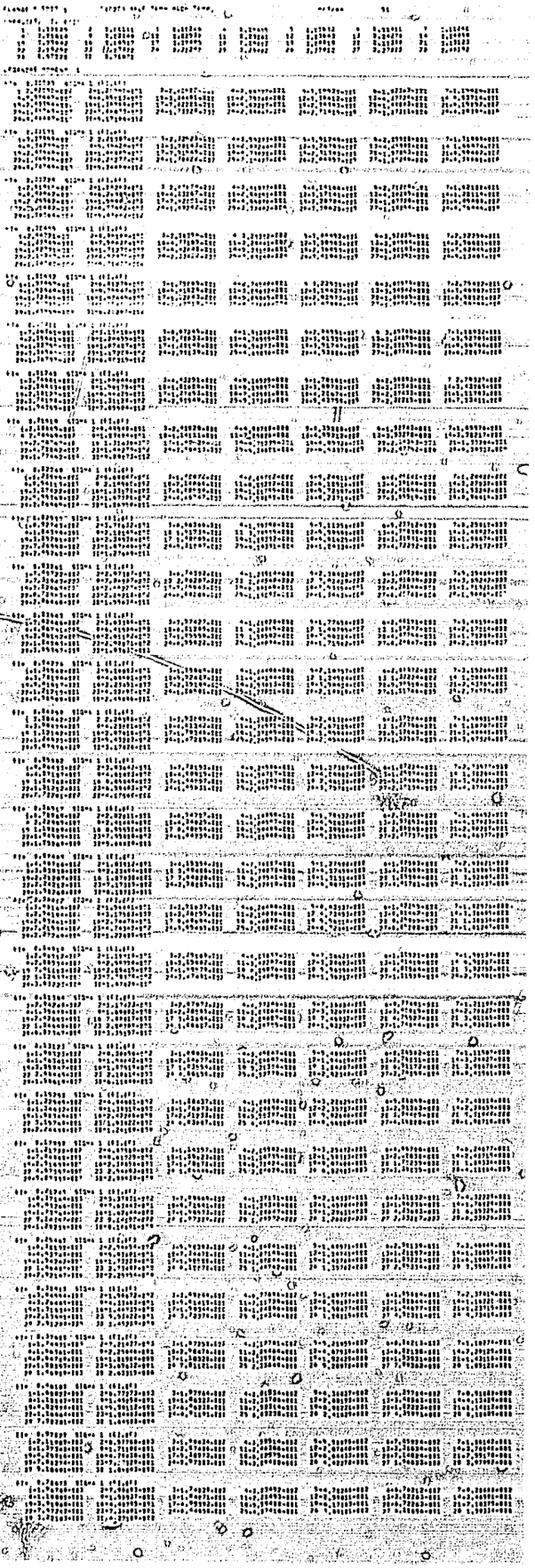

$\sigma_0(E_0 \rightarrow E)$ for An Oxygen in D_2O

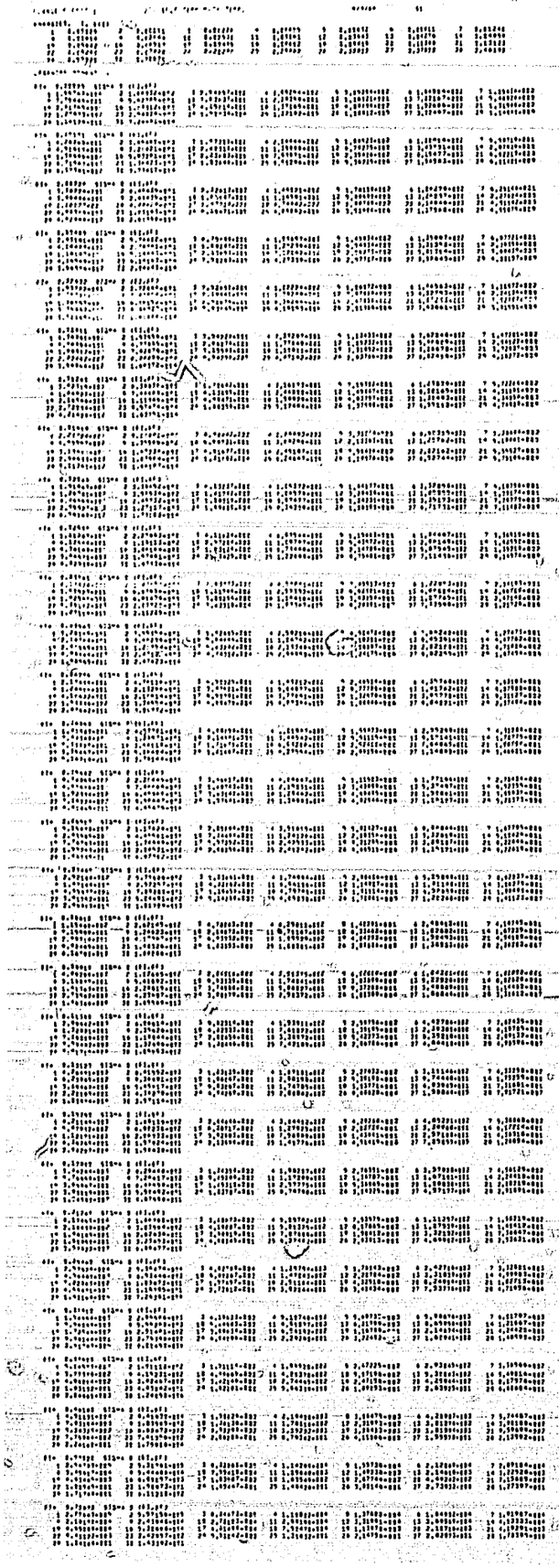

$\sigma_1(E_0 \rightarrow E)$ for An Oxygen in D_2O

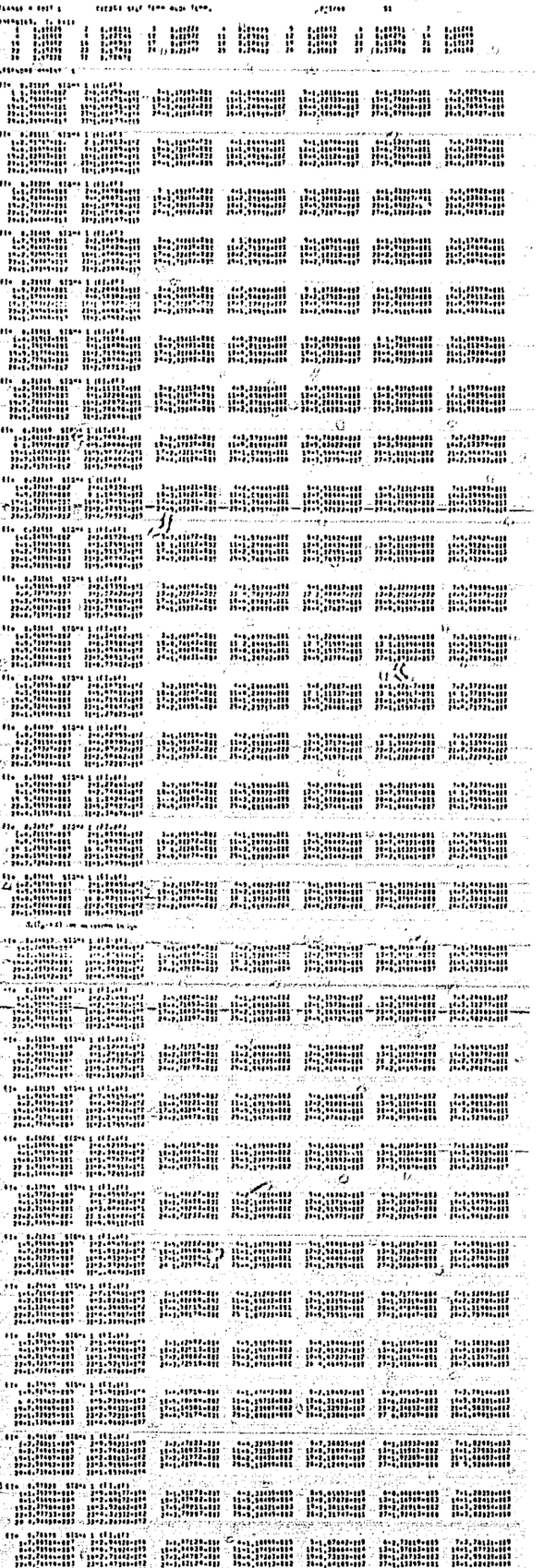

THERMOS kernel

The following lists are original 30 points THERMOS input data. These values are obtained as follows

$$P_{oij} = 4\pi(0.0253)\, v_i\, v_j \int_{-1}^{1} d\mu\, P_0(\mu) \frac{d\sigma(E_i \leftarrow E_j,\ \mu)}{dE} \Delta v_j$$

THERMOS uses only the P_0 kernel. Data format is defined as (6 E 12. 5).

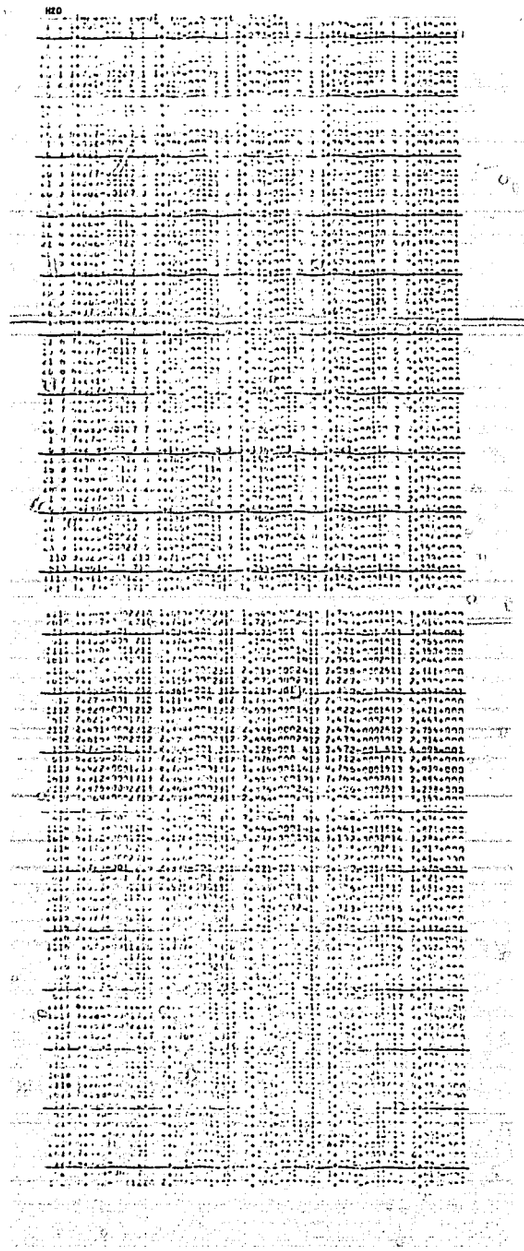

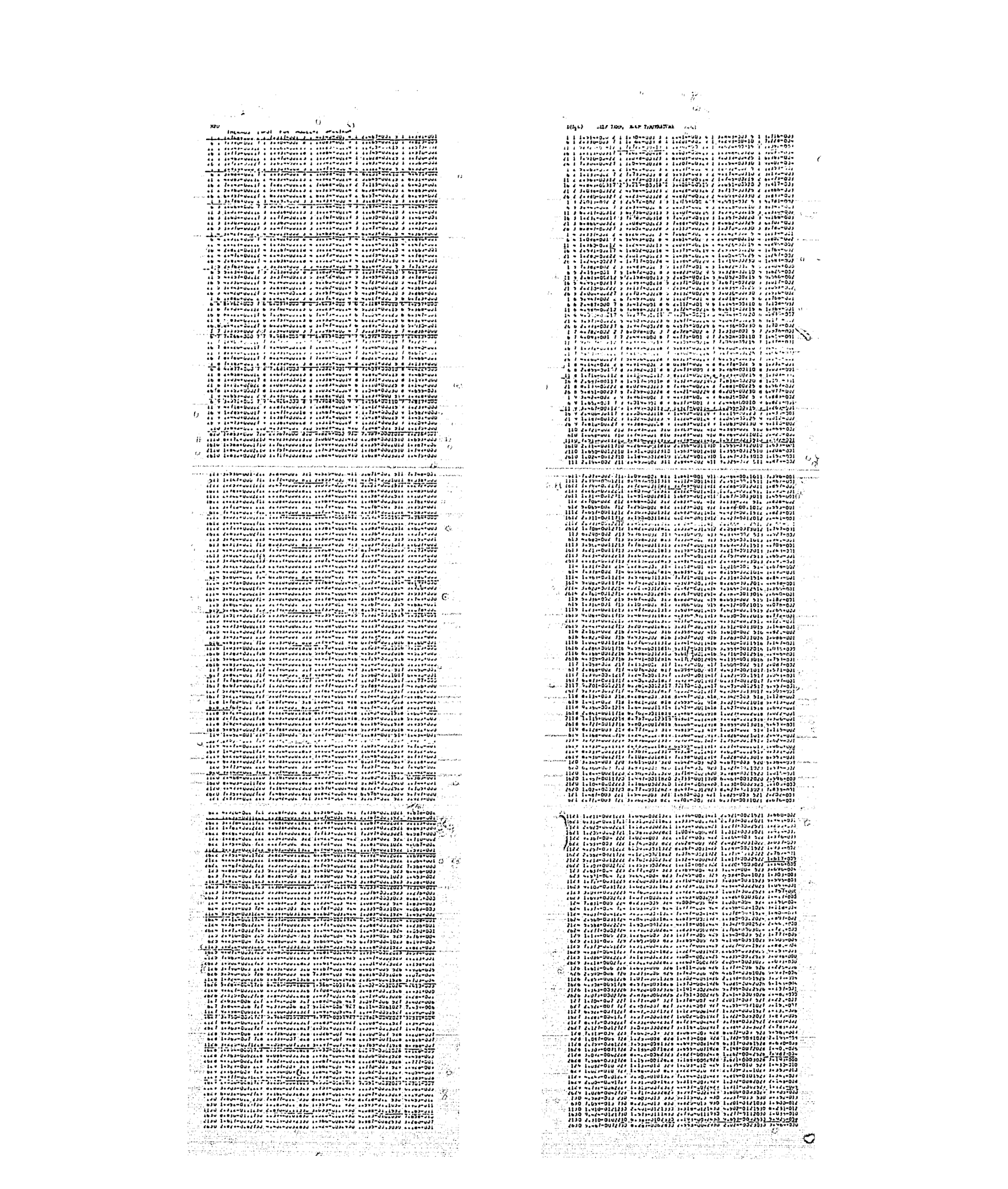

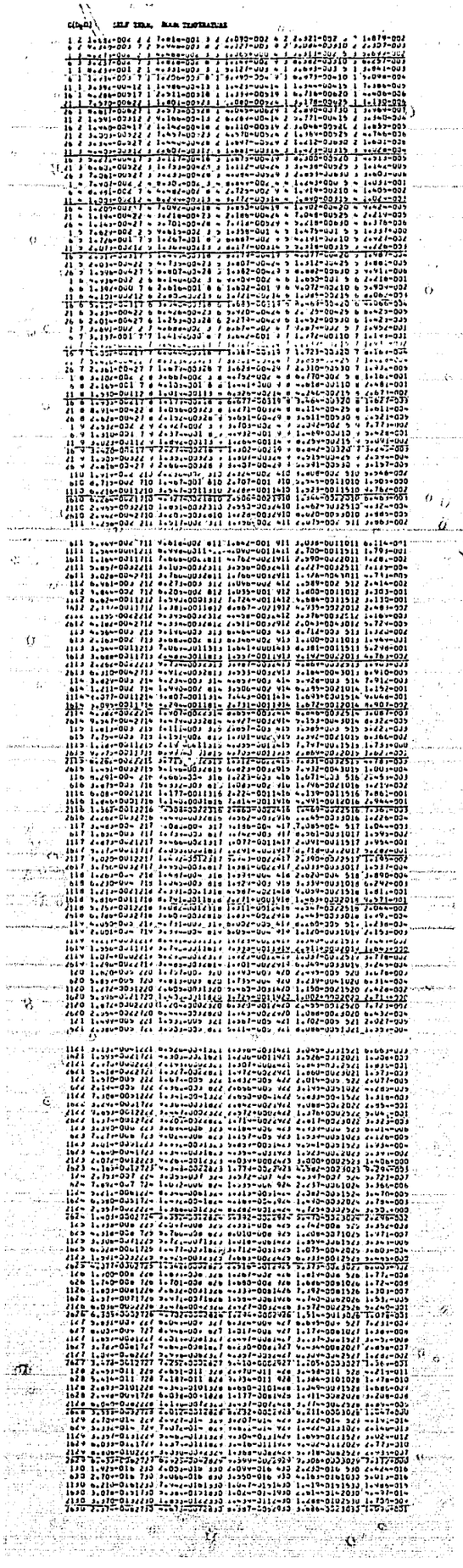

UNCLE kernels $\sigma_l(E_0 \rightarrow E)$

The numerical values of the 30 group full kernels, calculated with the UNCLE code, are listed below. The form of representation is as follows.

$ij \quad \sigma_{ij} \quad i+1,j \quad \sigma_{i+1,j} \cdots\cdots \sigma_{i+5,j}\ \ell \ m$

$E_0 = E_j = j$ and $E = E_i = i$ are the energies of the incident and scattered neutrons, respectively. The $\sigma_{ji} = \sigma(E_0 \rightarrow E)$ are listed 5 per line. The order of the Legendre moments of kernels is designated by $\ell\,(=0, 1)$ in columns 74-76. Columns 77-80 contain the card number.

Energy meshes are given in ev, each energy value corresponds to the neutron velocity equally spaced between 0.001eV~0.9eV.

	Input Energy				
K	E(K)	K	E(K)	K	E(K)
1	0.001	11	0.121	21	0.441
2	0.004	12	0.144	22	0.484
3	0.009	13	0.169	23	0.529
4	0.016	14	0.196	24	0.576
5	0.025	15	0.225	25	0.625
6	0.036	16	0.256	26	0.676
7	0.049	17	0.289	27	0.729
8	0.064	18	0.324	28	0.784
9	0.081	19	0.361	29	0.841
10	0.1	20	0.4	30	0.9

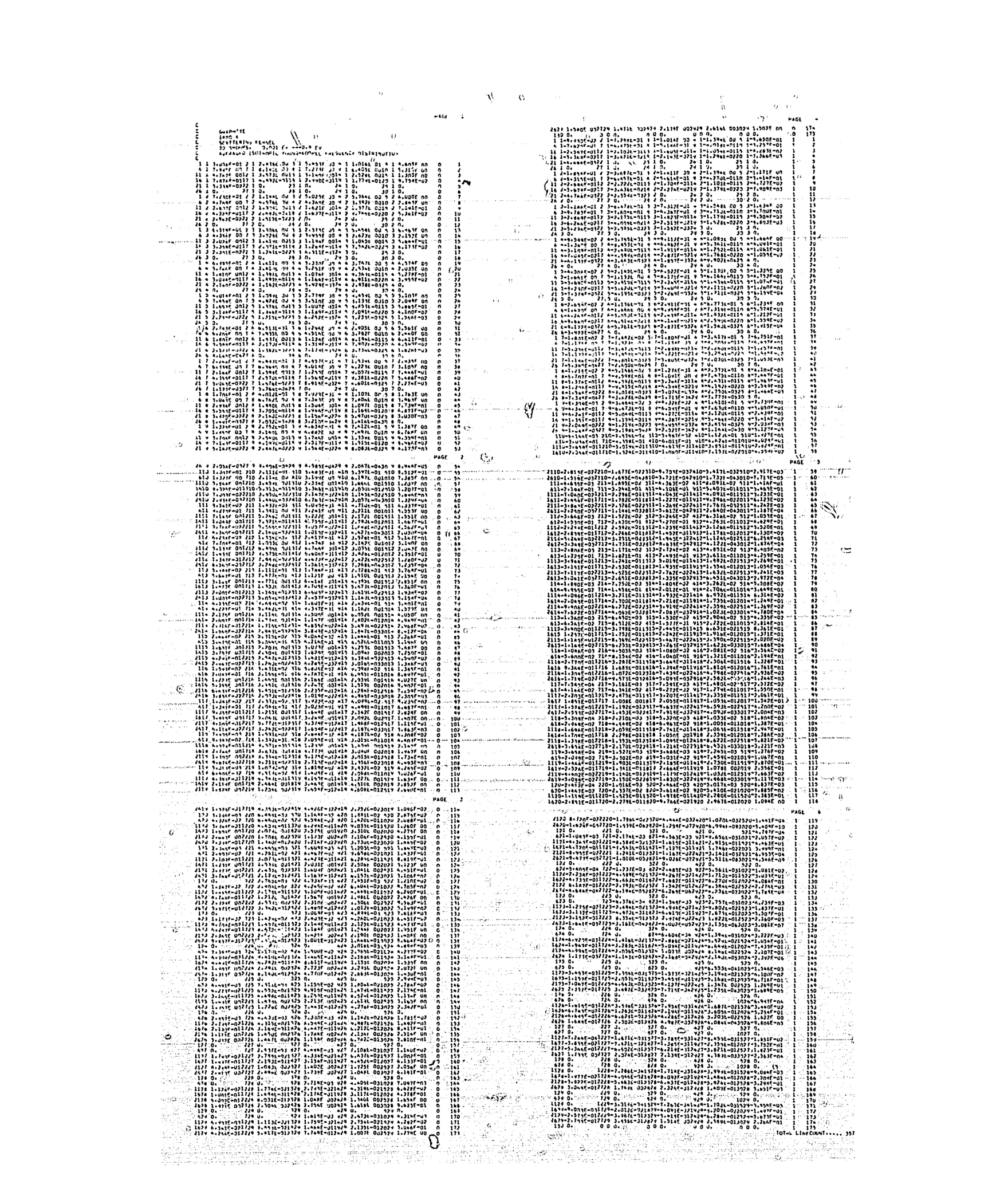

C
C GRAPHITE
C ROOM TEMPERATURE
C SCATTERING KERNEL
C 30 GROUPS. 0.001 EV ---0.9 EV
C CALCULATED FROM THE YOUNG-KOPPEL FREQUENCY DISTRIBUTION
C

1	1	1.029E-01	2	1	4.572E-01	3	1	8.365E-01	4	1	1.033E 00	5	1	1.030E 00	0	1
6	1	7.446E-01	7	1	5.972E-01	8	1	3.387E-01	9	1	2.153E-01	10	1	9.637E-02	0	2
11	1	4.493E-02	12	1	1.403E-02	13	1	6.593E-03	14	1	3.276E-03	15	1	2.268E-04	0	3
16	1	5.875E-05	17	1	0.	18	1	0.	19	1	0.	20	1	0.	0	4
21	1	0.	22	1	0.	23	1	0.	24	1	0.	25	1	0.	0	5
26	1	0.	27	1	0.	28	1	0.	29	1	0.	30	1	0.	0	6
1	2	1.355E-01	2	2	4.941E-01	3	2	8.330E-01	4	2	9.164E-01	5	2	8.020E-01	0	7
6	2	4.443E-01	7	2	3.592E-01	8	2	2.451E-01	9	2	1.174E-01	10	2	5.506E-02	0	8
11	2	3.057E-02	12	2	7.941E-03	13	2	3.353E-03	14	2	1.967E-03	15	2	1.410E-04	0	9
16	2	3.535E-05	17	2	7.659E-06	18	2	1.404E-06	19	2	0.	20	2	0.	0	10
21	2	0.	22	2	0.	23	2	0.	24	2	0.	25	2	0.	0	11
26	2	0.	27	2	0.	28	2	0.	29	2	0.	30	2	0.	0	12
1	3	1.219E-01	2	3	4.624E-01	3	3	8.827E-01	4	3	1.005E 00	5	3	1.103E 00	0	13
6	3	5.249E-01	7	3	3.501E-01	8	3	2.803E-01	9	3	1.016E-01	10	3	4.784E-02	0	14
11	3	2.411E-02	12	3	1.264E-02	13	3	2.949E-03	14	3	1.804E-03	15	3	1.353E-04	0	15
16	3	3.146E-05	17	3	7.767E-06	18	3	1.324E-06	19	3	2.794E-07	20	3	0.	0	16

[illegible]

[illegible]

[illegible]

[illegible]

[illegible]

[illegible]

TOTAL LINECOUNT